Charette Matthew, A. (Orcid ID: 0000-0003-3699-592X)
Kipp Lauren, Elizabeth (Orcid ID: 0000-0002-5111-9779)
Jensen Laramie (Orcid ID: 0000-0001-6358-1277)
Dabrowski Jessica, S (Orcid ID: 0000-0002-3196-4027)
Fitzsimmons Jessica, N (Orcid ID: 0000-0002-9829-2464)
Ulfsbo Adam (Orcid ID: 0000-0001-7550-7381)
Jones Elizabeth (Orcid ID: 0000-0001-7660-0238)
Bundy Randelle, M (Orcid ID: 0000-0002-0600-3953)
Vivancos Sebastián, M. (Orcid ID: 0000-0002-8057-5685)
John Seth, G (Orcid ID: 0000-0002-8257-626X)
Xiang Yang (Orcid ID: 0000-0003-1862-0948)
Petrova Mariia, V (Orcid ID: 0000-0001-9967-2197)
Bauch Dorothea (Orcid ID: 0000-0002-1419-9714)
Newton Robert (Orcid ID: 0000-0002-0480-3121)
Amon Rainer, M. W. (Orcid ID: 0000-0002-1437-4316)
Anderson Robert, F. (Orcid ID: 0000-0002-8472-2494)
Andersson Per, S (Orcid ID: 0000-0002-1752-6469)
Benner Ronald (Orcid ID: 0000-0002-1238-2777)
Gerringa Loes, J.A. (Orcid ID: 0000-0002-3139-8352)
Granskog Mats, Anders (Orcid ID: 0000-0002-5035-4347)
Haley Brian, Alexander (Orcid ID: 0000-0003-2879-8117)
Hammerschmidt Chad (Orcid ID: 0000-0003-1906-228X)
Hansell Dennis, A. (Orcid ID: 0000-0001-9275-3445)
Kadko David, Charles (Orcid ID: 0000-0003-4505-7011)
Kaiser Karl (Orcid ID: 0000-0002-4951-4665)
Lam Phoebe, J. (Orcid ID: 0000-0001-6609-698X)
Millero Frank, J. (Orcid ID: 0000-0001-8705-0542)
Moore Willard, S. (Orcid ID: 0000-0001-5930-5325)
Planquette Hélène (Orcid ID: 0000-0002-2235-5158)
Rabe Benjamin (Orcid ID: 0000-0001-5794-9856)
Reader Heather, E (Orcid ID: 0000-0002-9469-8838)
Rutgers van der Loeff Michiel (Orcid ID: 0000-0003-1393-3742)
Schlosser Peter (Orcid ID: 0000-0002-6514-4203)
Shiller Alan, M. (Orcid ID: 0000-0002-2068-7909)
Sonke Jeroen, E. (Orcid ID: 0000-0001-7146-3035)
Stedmon Colin, A (Orcid ID: 0000-0001-6642-9692)
Woosley Ryan, J. (Orcid ID: 0000-0002-2008-7751)
Valk Ole (Orcid ID: 0000-0003-1406-0701)

This article has been accepted for publication and undergone full peer review but has not been through the copyediting, typesetting, pagination and proofreading process which may lead to differences between this version and the Version of Record. Please cite this article as doi: 10.1029/2019JC015920

The Transpolar Drift as a Source of Riverine and Shelf-Derived Trace Elements to the Central Arctic Ocean

Matthew A. Charette[*1], Lauren E. Kipp[2,3], Laramie T. Jensen[4], Jessica S. Dabrowski[1], Laura M. Whitmore[5], Jessica N. Fitzsimmons[4], Tatiana Williford[4], Adam Ulfsbo[6], Elizabeth Jones[7], Randelle M. Bundy[1,8], Sebastian M. Vivancos[3,9], Katharina Pahnke[10], Seth G. John[11], Yang Xiang[12], Mariko Hatta[13], Mariia V. Petrova[14], Lars-Eric Heimbürger-Boavida[14], Dorothea Bauch[15], Robert Newton[3], Angelica Pasqualini[16], Alison M. Agather[17], Rainer M.W. Amon[4,18], Robert F. Anderson[3], Per S. Andersson[19], Ronald Benner[20], Katlin L. Bowman[12], R. Lawrence Edwards[21], Sandra Gdaniec[19,22,23], Loes J.A. Gerringa[24], Aridane G. González[25,26], Mats Granskog[27], Brian Haley[28], Chad R. Hammerschmidt[17], Dennis A. Hansell[29], Paul B. Henderson[1], David C. Kadko[30], Karl Kaiser[4,18], Patrick Laan[24], Phoebe J. Lam[12], Carl H. Lamborg[12], Martin Levier[23], Xianglei Li[21], Andrew R. Margolin[29,31], Chris Measures[13], Rob Middag[24], Frank J. Millero[29], Willard S. Moore[20], Ronja Paffrath[10], Hélène Planquette[25], Benjamin Rabe[32], Heather Reader[33,34], Robert Rember[35], Micha J.A., Rijkenberg[25], Matthieu Roy-Barman[24], Michiel Rutgers van der Loeff[32], Mak Saito[1], Ursula Schauer[32], Peter Schlosser[3,36,37], Robert M. Sherrell[38,39], Alan M. Shiller[5], Hans Slagter[23,40], Jeroen E. Sonke[41], Colin Stedmon[33], Ryan J. Woosley[29,42], Ole Valk[32], Jan van Ooijen[24], Ruifeng Zhang[11,43]

Submitted to: *Journal of Geophysical Research-Oceans*

Date: December 2, 2019

Revised version: March 31, 2020

*corresponding author, mcharette@whoi.edu, +001-508-289-3205

1. Woods Hole Oceanographic Institution, Woods Hole, MA USA
2. Dalhousie University, Halifax, NS, Canada
3. Lamont-Doherty Earth Observatory of Columbia University, Palisades, NY, USA
4. Department of Oceanography, Texas A&M University, College Station, TX, USA
5. School of Ocean Science and Engineering, University of Southern Mississippi, Stennis Space Center, MS, USA
6. Department of Marine Sciences, University of Gothenburg, Gothenburg, Sweden.
7. Institute of Marine Research, Fram Centre, Tromsø, Norway
8. School of Oceanography, University of Washington, Seattle, Washington, USA

9. Department of Earth and Environmental Sciences, Columbia University, New York, NY, USA
10. Institute for Chemistry and Biology of the Marine Environment (ICBM), University of Oldenburg, Carl-von-Ossietzky-Str. 9-11, 26129 Oldenburg, Germany
11. Department of Earth Sciences , University of Southern California, Los Angeles, CA USA
12. Department of Ocean Sciences, University of California, Santa Cruz, Santa Cruz, CA, USA
13. Department of Oceanography, University of Hawaii at Manoa, 1000 Pope Road, Honolulu, Hawaii, USA
14. Aix Marseille Université, CNRS/INSU, Université de Toulon, IRD, Mediterranean Institute of Oceanography (MIO), UM 110, F-13288 Marseille, France
15. GEOMAR Helmholtz Center for Ocean Research Kiel, 24148 Kiel, Germany
16. Department of Earth and Environmental Engineering, Columbia University, New York, NY, USA
17. Department of Earth and Environmental Sciences, Wright State University, Dayton, OH, USA
18. Department of Marine Science, Texas A&M University at Galveston, Texas, USA
19. Swedish Museum of Natural History, Department of Geosciences, Stockholm, Sweden
20. School of the Earth, Ocean and Environment, University of South Carolina, Columbia, SC, USA
21. Department of Earth and Environmental Sciences, University of Minnesota, Minneapolis, MN USA
22. Stockholm University, Department of Geological Sciences, Stockholm, Sweden
23. Laboratoire des Sciences du Climat et de l'Environnement, LSCE/IPSL, CEA-CNRS-UVSQ, Université Paris-Saclay, Gif-sur-Yvette, France
24. Department of Ocean Systems, NIOZ Royal Institute for Sea Research and Utrecht University, Den Burg, Netherlands
25. University of Brest, CNRS, IRD, Ifremer, LEMAR, F-29280 Plouzané, France
26. Instituto de Oceanografía y Cambio Global, IOCAG, Universidad de Las Palmas de Gran Canaria, ULPGC, Las Palmas de Gran Canaria (ULPGC), Las Palmas, Spain
27. Norwegian Polar Institute, Tromsø, Norway
28. College of Earth, Ocean, and Atmospheric Sciences, Oregon State University, Corvalis, OR, USA

29. Rosenstiel School of Marine and Atmospheric Science, University of Miami, Miami, FL, USA
30. Florida International University, Applied Research Center, Miami, FL, USA
31. Institute for the Oceans and Fisheries, University of British Columbia, Vancouver, British Columbia, Canada
32. Alfred-Wegener-Institut Helmholtz-Zentrum für Polar- und Meeresforschung, Bremerhaven, Germany
33. Technical University of Denmark, National Institute of Aquatic Resources, Lyngby Denmark
34. Department of Chemistry, Memorial University of Newfoundland, St John's, NL, Canada
35. International Arctic Research Center, University of Alaska, Fairbanks, Fairbanks, AK, USA
36. Arizona State University, School of Sustainability, Tempe, AZ, USA
37. The Earth Institute of Columbia University, New York, NY, USA
38. Department of Marine and Coastal Sciences, Rutgers University, New Brunswick, NJ, USA
39. Department of Earth and Planetary Sciences, Rutgers University, Piscataway, NJ, USA
40. Max Planck Institute for Chemistry, Mainz, Germany
41. Laboratoire Géosciences Environnement Toulouse, CNRS/Institute for Research and Development/Université Paul Sabatier–Toulouse III, 31400 Toulouse, France
42. Center for Global Change Science, Massachusetts Institute of Technology, Cambridge, MA, USA
43. School of Oceanography, Shanghai Jiao Tong University, Shanghai, China

Key Points

- The Transpolar Drift is a source of shelf- and river-derived elements to the central Arctic Ocean
- The TPD is rich in dissolved organic matter (DOM), which facilitates long-range transport of trace metals that form complexes with DOM
- Margin trace element fluxes may increase with future Arctic warming due to DOM release from permafrost thaw and increasing river discharge

Abstract

A major surface circulation feature of the Arctic Ocean is the Transpolar Drift (TPD), a current that transports river-influenced shelf water from the Laptev and East Siberian Seas toward the center of the basin and Fram Strait. In 2015, the international GEOTRACES program included a high-resolution pan-Arctic survey of carbon, nutrients, and a suite of trace elements and isotopes (TEIs). The cruises bisected the TPD at two locations in the central basin, which were defined by maxima in meteoric water and dissolved organic carbon concentrations that spanned 600 km horizontally and ~25-50 m vertically. Dissolved TEIs such as Fe, Co, Ni, Cu, Hg, Nd, and Th, which are generally particle-reactive but can be complexed by organic matter, were observed at concentrations much higher than expected for the open ocean setting. Other trace element concentrations such as Al, V, Ga, and Pb were lower than expected due to scavenging over the productive East Siberian and Laptev shelf seas. Using a combination of radionuclide tracers and ice drift modeling, the transport rate for the core of the TPD was estimated at 0.9 ± 0.4 Sv (10^6 m^3 s^{-1}). This rate was used to derive the mass flux for TEIs that were enriched in the TPD, revealing the importance of lateral transport in supplying materials beneath the ice to the central Arctic Ocean and potentially to the North Atlantic Ocean via Fram Strait. Continued intensification of the Arctic hydrologic cycle and permafrost degradation will likely lead to an increase in the flux of TEIs into the Arctic Ocean.

Index Terms

- 4875 Trace elements
- 4808 Chemical tracers
- 4805 Biogeochemical cycles, processes, and modeling
- 4572 Upper ocean and mixed layer processes
- 4207 Arctic and Antarctic oceanography

Keywords

[Arctic Ocean, Transpolar Drift, trace elements, carbon, nutrients, GEOTRACES]

Plain Language Summary

A major feature of the Arctic Ocean circulation is the Transpolar Drift (TPD), a surface current that carries ice and continental shelf-derived materials from Siberia across the North Pole to the North Atlantic Ocean. In 2015, an international team of oceanographers conducted a survey of trace elements in the Arctic Ocean, traversing the TPD. Near the North Pole, they observed much higher concentrations of trace elements in surface waters than in regions on either side of the current. These trace elements originated from land and their journey across the Arctic Ocean is made possible by chemical reactions with dissolved organic matter that originates mainly in Arctic rivers. This study reveals the importance of rivers and shelf processes combined with strong ocean currents in supplying trace elements to the central Arctic Ocean and onwards to the Atlantic. These trace element inputs are expected to increase as a result of permafrost thawing and increased river runoff in the Arctic, which is warming at a rate much faster than anywhere else on Earth. Since many of the trace elements are essential building blocks for ocean life, these processes could lead to significant changes in the marine ecosystems and fisheries of the Arctic Ocean.

1.0 Introduction

Of all the major oceans on Earth, the Arctic Ocean is the most heavily influenced by processes occurring over continental shelves, which cover over 50% of its area (Jakobsson, 2002). The Arctic Ocean also has the lowest salinity surface waters, a result of limited evaporation, high riverine inputs, the annual sea-ice freeze/melt cycle, and restricted exchange with other ocean basins (Serreze et al., 2007). These factors combine to impart a shelf-derived biogeochemical signature over much of the polar mixed layer, the low salinity surface layer influenced by sea-ice and freshwater, even in the central basin.

In the western Arctic's Canada Basin, hydrographic fronts serve as barriers to rapid shelf-basin exchange processes, thereby eddies and wind-induced upwelling or downwelling constitute the primary mechanisms for off-shelf water and material transport and exchange (Muench et al., 2000; Pickart et al., 2005, 2013). In the eastern Arctic, however, the Transpolar Drift (TPD) is a major current that directly transports Eurasian shelf water and sea ice directly from the Laptev and East Siberian Seas toward the central basin and Fram Strait, a major outlet for Arctic waters (Ekwurzel et al., 2001; McLaughlin et al., 1996; Rigor et al., 2002; Rudels, 2015; Schlosser et al., 1994). The timescale for the trans-Arctic crossing of this current is on the order of 1-3 years (Pfirman et al., 1997; Steele et al., 2004); as such, the TPD is currently a mechanism for the rapid transport of shelf-derived materials including

nutrients and carbon to the central Arctic Ocean (Kipp et al., 2018; Letscher et al., 2011; Opsahl et al., 1999; Wheeler et al., 1997), with potential biogeochemical impacts detected as far downstream as the North Atlantic Ocean (e.g. Amon et al., 2003; Gerringa et al., 2015; Noble et al., 2017; Torres-Valdés et al., 2013). At present, primary production in the largely ice-covered central Arctic is light limited; however, surface warming has led to reductions in ice cover, as well as increases in river discharge and permafrost thawing (Frey & McClelland, 2009; McClelland et al., 2004; Peterson et al., 2002; Schuur et al., 2015; Spencer et al., 2015). With reduced ice cover, the TPD-derived transport of ice-rafted materials might be interrupted (Krumpen et al., 2019), though Newton et al. (2017) have shown that in the near term (~several decades) long distance ice transport will accelerate as the ice thins and is more responsive to the winds. Together, these changes are expected to modify the ecosystem dynamics of the Arctic Ocean, with shelf-basin exchange processes playing a significant role.

In 2015, three nations led cruises to the Arctic Ocean as part of the international GEOTRACES program, a global survey of the distributions of oceanic trace element and isotopes (TEIs). The Arctic GEOTRACES program represented an unprecedented effort in sampling of the Arctic water column from a biogeochemical perspective. High-resolution coverage of waters above 84°N captured the TEI fingerprint of the TPD, and will serve as an important reference for future studies that focus on climate change impacts in the Arctic. Radium isotopes measured during the Arctic GEOTRACES cruises have already been used to show that the chemical composition of the TPD is modified during passage over the Laptev Shelf, and to suggest that potentially significant changes in the flux of nutrients and carbon from the Siberian shelves are already underway (Kadko et al., 2019; Kipp et al., 2018; Rutgers van der Loeff et al., 2018). Additionally, Rijkenberg et al (2018) found higher dissolved Fe and Slagter et al. (2017) found increased concentrations of Fe-binding organic ligands in the path of the TPD relative to adjacent sampling stations. These ligands and the associated Fe on the one hand were found to correlate strongly with terrestrial sources, which are projected to increase in a changing Arctic. On the other hand, Rijkenberg et al (2018) found a local occurrence of Fe limitation over the Nansen basin and hypothesized that retreating ice could further exacerbate this nutrient limitation.

This paper is a synthesis of the distributions of TEIs in the central Arctic Ocean associated with the TPD. We examine the origin and fate of TEIs in this important trans-Arctic conduit and provide a first estimate of the mass transport rate for the TPD, based on ice drift trajectories and radionuclide tracers. By combining the TPD mass transport estimate with the TEI inventories reported herein, fluxes of these elements to the central Arctic Ocean via the

TPD are estimated. Finally, we discuss the biogeochemical implications of the changing climate on TEI concentrations and fluxes to the Arctic and North Atlantic Oceans.

2.0 Study Area

The characteristics of water masses in the Arctic Ocean are controlled by bathymetry and inflows from the Atlantic and Pacific Oceans. The Arctic has two major basins, the Eurasian and Amerasian Basins, which are separated by the Lomonosov Ridge (Rudels, 2015). The Lomonosov Ridge is an underwater ridge of continental crust that emerges north of the Siberian shelves at approximately 140°E. Here we refer to the Amerasian Basin as the "western Arctic", while the Siberian shelves and Eurasian Basin are referred to as the "eastern Arctic". The Eurasian Basin is further divided into the Nansen and Amundsen Basins by the Gakkel Ridge, and the Amerasian Basin is divided by the Alpha-Mendeleev Ridge into the large Canada Basin and the Makarov Basin. Surrounding these basins are wide, shallow continental shelves that occupy over 50% of the Arctic Ocean's area (Jakobsson, 2002). Pacific water flows into the Arctic through the narrow and shallow Bering Strait, while Atlantic water enters through the Barents Sea and the Fram Strait (Rudels, 2009). The major outflows of Arctic waters are through the Canadian Arctic Archipelago and Fram Strait, on either side of Greenland, into the North Atlantic (Carmack et al., 2016) (Fig. 1).

Arctic Ocean sea surface pressure gradients are largely driven by water mass salinity differences in the basin. Between the (relatively fresh) North Pacific and the (salty) North Atlantic waters, there is a steric height gradient of about a meter, creating a pressure gradient across the Arctic from the Pacific down to the Atlantic. Large inputs of freshwater along the Arctic coastlines create a sea-surface height gradient from the coasts to the central basins, which drives a series of boundary currents in the coastal seas and over the continental slope that move water eastward (counter-clockwise) around the Arctic (Rudels et al., 1994; Rudels, 2015).

Overprinted on these perennial pressure gradients, the surface circulation is strongly impacted by winds. Predominant atmospheric circulation causes the average sea level pressure to be high over the Canada Basin and low over the Eurasian Basin, Barents Sea, and Nordic Seas (Hunkins & Whitehead, 1992; Serreze & Barrett, 2011). The resulting winds draw relatively fresh water over the Amerasian Basin, and set up the anti-cyclonic Beaufort Gyre, and a weaker cyclonic gyre in the Eurasian Basin (Alkire et al., 2015; Bauch et al., 2011; Carmack et al., 2016; Ekwurzel et al., 2001; Newton et al., 1974; Proshutinsky & Johnson, 1997).

These two circulation cells converge just north of Siberia to form the Transpolar Drift (Rudels, 2015). The TPD extends from the Siberian shelves to the Fram Strait, as inferred from ice motion (Rigor et al., 2002) and water mass characteristics (McLaughlin et al., 1996). The position of the TPD is determined by the Arctic Oscillation (AO), a large-scale Arctic climate pattern characterized by sea level pressure anomalies (Fig. 1). The AO is highly correlated with the North Atlantic Oscillation (NAO) (Mysak, 2001), sea level pressure over the central Arctic, and with sea surface height anomalies along the coastal Arctic (Newton et al., 2006). During a low or negative AO and NAO, a strong Arctic High exists over the Canada Basin, expanding the anticyclonic Beaufort Gyre. In this case, the TPD originates from the Laptev and East Siberian Seas and flows over the Lomonosov Ridge (Morison et al., 2006; Woodgate et al., 2005) (solid red arrows in Fig. 1). Positive AO and NAO indices produce a weak Arctic High, resulting in a smaller Beaufort Gyre (Mysak, 2001). In a persistently positive phase of the AO, the TPD shifts eastward towards the Bering Strait, entraining more Pacific water from the Chukchi Sea while still receiving a contribution from the East Siberian Shelf waters, which are transported farther east along the shelf before entering the TPD (Morison et al., 2012; Mysak, 2001) (dashed red arrows in Fig. 1). During the years preceding the 2015 Arctic GEOTRACES sampling, the annual average AO was neutral to negative, and thus during the expeditions the TPD was located over the Lomonosov Ridge (Kipp et al., 2018; Rutgers van der Loeff et al., 2018). Monitoring of atmospheric circulation (Morison et al., 2012; Proshutinsky et al., 2009) as well as biogeochemical and water mass properties on previous hydrographic transects (Falck et al., 2005; Morison et al., 2012; Steele et al., 2004) provide evidence that this position has remained relatively stable over the past ca. 30 years.

The TPD is associated with high concentrations of dissolved organic matter (DOM) and a distinct oxygen isotope fingerprint relative to the surrounding surface waters. The DOM enrichment is due to river runoff and marine productivity occurring over the shelf where the TPD originates (Kaiser, Benner, et al., 2017; Stedmon et al., 2011). For the stable oxygen isotopes of water ($\delta^{18}O$-H_2O), negative oxygen isotope ratio anomalies are present in the core of the TPD—perhaps the lowest of all surface waters over the deep Arctic basins, between -3 and -4 ‰ (Bauch et al., 2011). The $\delta^{18}O$ signal is a proxy for meteoric water (includes precipitation and runoff). In Arctic river deltas and estuaries the $\delta^{18}O$ values are between about -18 and -22 ‰ while source waters in the Atlantic and Pacific have $\delta^{18}O$ of approximately +0.3 and -1.1 ‰, respectively (Bauch et al., 2011; Ekwurzel et al., 2001; Newton et al., 2013). Salinity gradients across the TPD are smoother than $\delta^{18}O$ changes,

largely because the decrease in continental runoff outside the TPD is compensated by a rise in the amount of sea ice meltwater at the surface (Newton et al., 2013; Schlosser et al., 2002). These signals in DOM and $\delta^{18}O$ are carried with the TPD all the way to the Fram Strait (Granskog et al., 2012).

The characteristics of the upper water column differ on either side of the TPD because it generally acts as a boundary between Atlantic and Pacific contributions to the Arctic pycnocline. High nutrient, high DOM, low salinity Pacific water is typically observed as an "upper halocline" over the Canada and Makarov Basins, where it separates surface waters from the Atlantic boundary currents below about 200 meters. Sub-surface distributions of nitrate, phosphate and silicate indicate that a layer of nutrient-rich shelf-modified Bering Strait Inflow thins and shoals northward from the Chukchi continental slope and dissipates in the vicinity of the TPD. Pacific influence is dominant in the Canadian Arctic Archipelago (Jones et al., 2003; Jones & Anderson, 2008) and extends north of Greenland to the Fram Strait (Dmitrenko et al., 2019; de Steur et al., 2013). Over the Eurasian Basin, the Pacific-influenced layer is absent, with Atlantic waters occupying the entire water column (Bauch et al., 2011).

3.0 Methods

3.1 Sampling and Analyses of TEIs–The data presented herein was collected primarily during two cruises in 2015 associated with the Arctic GEOTRACES program. The U.S. GEOTRACES GN01 (HLY1502) cruise was held aboard the *USCGC Healy*, while the German GEOTRACES GN04 (PS94) cruise was on the *R/V Polarstern* (Fig. 1). All sampling and analyses were conducted according to pre-established GEOTRACES approved protocols (for TEIs) (Cutter et al., 2014) and/or GO-SHIP approved protocols (for non-TEIs) (Hood et al., 2010). To further ensure quality of TEI data across participating laboratories, extensive intercalibration efforts were taken in accordance with GEOTRACES protocols (Cutter, 2013). For example, the GN01 and GN04 cruises both occupied the same station within two weeks of each other (GN01 station 30 and GN04 station 101), which enabled investigators to intercompare results for their respective TEIs. CTD/rosette data and methodologies for PS94 are available via the PANGEA database (Ober et al., 2016a, 2016b; Rabe et al., 2016b, 2016a). The GN01 CTD/rosette procedures are stored on the BCO-DMO database (Landing et al., 2019a, 2019b). Detailed methodologies can be found in the publications where the original TEI data were first reported (Methods Appendix Table A1). Certain TEIs were analyzed by multiple laboratories using similar or independent methods. In these cases, we

used the average value for each station and depth. The methods and data appendices provide more specifics on data averaging and sources.

3.2 Linear Mixing Model–In order to study the provenance and pathways of TEIs carried by the TPD, we must quantitatively parse the fraction (f) of source waters in each collected GEOTRACES sample. To do so, we use the relatively well-studied distribution of salinity (S), $\delta^{18}O$-H_2O ratios, and the Arctic N-P tracer (ANP; see Newton et al., 2013). These can be used to identify fractions of Pacific (Pac)- and Atlantic (Atl)- sourced seawater, sea-ice melt (SIM), and meteoric water (Met). The latter includes runoff and net *in-situ* precipitation. Along the cruise transects, *in-situ* precipitation is expected to be small in comparison with the continental runoff; hence f_{Met} will be our primary proxy for determining the water masses most influenced by the TPD. The value for each in a sample is expressed as a linear combination of the values in its constituent water masses:

$$f_{Atl}[S_{Atl}] + f_{Pac}[S_{Pac}] + f_{Met}[S_{Met}] + f_{SIM}[S_{SIM}] = [S]_{Obs}$$

$$f_{Atl}[\delta^{18}O_{Atl}] + f_{Pac}[\delta^{18}O_{Pac}] + f_{Met}[\delta^{18}O_{Met}] + f_{SIM}[\delta^{18}O_{SIM}] = [\delta^{18}O]_{Obs}$$

$$f_{Atl}[ANP_{Atl}] + f_{Pac}[ANP_{Pac}] + f_{Met}[ANP_{Met}] + f_{SIM}[ANP_{SIM}] = [ANP]_{Obs}$$

$$f_{Atl} + f_{Pac} + f_{Met} + f_{SIM} = 1$$

This constitutes a 4-dimensional linear system that can be solved in matrix form:

$$[f] = \{C\}^{-1}[y] ,$$

where [f] is a vector of water-mass fractions, [y] is a vector of the parameter values in the sample, and {C} is a matrix of values in the 'end members', i.e. the source waters. The model assumes 4 end members (Table 1) and 4 equations, so will yield an exact solution.

There are several important sources of error, which are discussed in detail by Newton et al. (2013) in the context of the 2005 Arctic Ocean Section. Briefly, the least-constrained fractions are those of Pacific- and Atlantic- influenced ocean water, which suffer from the non-conservative nature of nutrients in the ocean, large scatter in the values in the source waters, and potentially from drift in the end-member means with time (Newton et al., 2013). Fortunately, our focus here is on the concentration of meteoric waters and this fraction is insensitive to nutrient concentrations. Rather, it depends on salinity and $\delta^{18}O$ with the error originating primarily from seasonal and geographical variability in the $\delta^{18}O$ endmember of

Arctic rivers (Cooper et al., 2008). Monte Carlo analysis across a reasonable range of estimated mean $\delta^{18}O$ values for runoff yielded (one-sigma) errors of about 1% (absolute value) on the meteoric fractions.

The relationship between each TEI and the meteoric water fraction was determined using a linear regression model. The slope, intercept, r^2 value, and p value for each relationship are reported in Table 2. The effective shelf endmember concentrations of the TEIs were calculated using their respective linear regressions at 20% meteoric water, assuming that this is the meteoric water fraction of the TPD when it leaves the shelf and that there was no significant TEI removal or addition during transport. Meteoric water fractions of 10 – 35% have been observed at the point of origin of the TPD in the Laptev Sea (Bauch et al., 2011) and its terminus at the Fram Strait (Dodd et al., 2012). During the 2015 GEOTRACES expeditions, fractions up to 25% were observed near the North Pole, thus 20% is a conservative estimate.

Initial estimates of river endmember concentrations were calculated by extrapolating the linear regression to 100% meteoric water (regression intercept). These estimates have a high statistical uncertainty associated with them due to the extrapolation beyond the measured range and other factors that violate the assumptions of the standard estuarine mixing model (Boyle et al., 1974; Shiller, 1996), but they still provide a first approximation to compare with sparse existing river and shelf sea data. There is some data on TEI concentrations in the Eurasian rivers that ultimately feed into the TPD. Most are derived from the Arctic Great Rivers Observatory (A-GRO), which began as the Pan-Arctic River Transport of Nutrients, Organic Matter and Suspended Sediments (PARTNERS) project (Holmes et al., 2019). The weighted averages reported by the A-GRO provide a useful comparison for many of the elements discussed in this manuscript, but could be improved with measurements of more TEIs in each of the Arctic rivers and knowledge of the relative influence of each river in the TPD at a given time. Due to the shelf circulation patterns (Fig. 1), the major Eurasian rivers (Lena, Ob', Yenisey, and Kolyma) will exert a stronger influence on the TPD than the North American rivers (Mackenzie and Yukon). As such, we report herein the discharge weighted average TEI concentrations for the Eurasian rivers only. Most importantly, any differences between the effective river endmember and the mean river concentrations should not be interpreted in a quantitative manner; rather, this analysis is meant only to give the reader a sense of the relative influence of rivers and/or estuarine removal/addition processes on the TEIs that are transported to the central Arctic Ocean via the TPD.

4.0 Results and Discussion

We define the lateral extent of the TPD as ~84°N (in the Canada Basin) to 87°N (in the Eurasian Basin) for waters in the top 50 m. These boundaries were chosen qualitatively based on the distributions of the meteoric water fraction and TPD-influenced TEIs (Fig. 2). For example, there is a sharp concentration gradient for chromophoric dissolved organic matter (CDOM), dissolved organic carbon (DOC), dissolved Fe, and ^{228}Ra at stations north of 84°N 150°W, which coincides with a front between high and intermediate meteoric water fractions (~250 km along the section distance in Fig. 2). On the Eurasian side of the transect, there is minimal meteoric water influence south of 87°N (~1100 km along the section distance in Fig. 2). The TPD can be characterized generally by this high meteoric water component, which is due to large river contributions to the Siberian Arctic shelves. However, the meteoric water fraction alone cannot be used to delineate the western boundary of the TPD because the Beaufort Gyre in the Canada Basin contains a significant and growing freshwater component sourced from eastern Arctic rivers (Giles et al., 2012; Morison et al., 2012; Rabe et al., 2011, 2014).

As a function of depth, the elevated TEI concentrations and meteoric water fractions are confined to the upper 50 m. The 50 m cutoff also serves to exclude the halocline from our analysis, which is rich in certain TEIs and nutrients like silicate (Fig. 2g), and is influenced by different ventilation processes and source water masses than the TPD (Aagaard et al., 1981). The data presented herein are shown mainly as a function of the meteoric water fraction and were collected in the upper 50 m of the water column for all stations north of 84°N, which includes the polar mixed layer and the TPD.

4.1 Trace Element and Isotope Distributions, Sources, and Sinks

4.1.1 Nutrients–Within the Transpolar Drift influenced stations, nitrate concentrations generally decrease with increasing meteoric water fraction, while phosphate and silicate displayed the opposite trend (Fig. 3a-c). This pattern is in contrast with the average Eurasian river nitrate of 4.2 µmol/L (Holmes et al., 2019) and suggests that nitrate is largely assimilated (Arrigo et al., 2008) or consumed by denitrification (Chang & Devol, 2009) over the shelf prior to entering the TPD, and acts as the limiting nutrient for primary production, leaving residual phosphate and silicate concentrations of ~0.75 and 12 µmol L^{-1}, respectively. A linear fit to the silicate data and extrapolation to 100% meteoric water suggests an apparent riverine endmember concentration of 47 µmol L^{-1}. This estimate can be compared to the average discharge weighted silicate concentration for the Eurasian rivers reported by the A-

GRO, 177 µmol L^{-1} (Holmes et al., 2019). The apparent silicate riverine endmember is less than a third of the A-GRO weighted average, suggesting removal in estuaries or over the shelf, although shelf sediments can also act as a source of additional silicate (Frings, 2017; Tréguer & De La Rocha, 2013).

Given the large phosphorous (P) fluxes through the Arctic gateways, rivers are thought to be of relatively minor importance in the Arctic Ocean P budget (Holmes et al., 2012). Their P relationship with meteoric water fraction was relatively weak, which precludes us from estimating the effective river endmember P concentration. For comparative purposes only, we note that the P concentration range at the highest observed meteoric water percentage (>20%) is ~0.6-0.7 µmol L^{-1}, which is about two times higher than the weighted Arctic Eurasian river phosphate average of 0.31 µmol L^{-1} (Holmes et al., 2019). This finding is consistent with the study by Torres-Valdes et al. (2013), which suggested that the Arctic Ocean P budget imbalance (excess) cannot be explained entirely by riverine inputs.

The Arctic Ocean is at present known to be a net exporter of Si and P to the North Atlantic Ocean, where the excess P is thought to be partly responsible for N-fixation (Torres-Valdés et al., 2013). Looking toward the future, it is unclear if additional terrestrial inputs of nutrients will lead to an additional flux of nutrients to the TPD (and beyond) because some fraction would be consumed over the productive shelves before being exported toward the central basin. Further, though the mass flux of nutrients from rivers is small relative to the influx of nutrients to the Arctic through the Pacific and Atlantic gateways (Holmes et al., 2012), the river-influenced TPD is a nutrient source to the surface ocean where it is immediately available for use by phytoplankton. Whether or not the TPD becomes a more significant source of nutrients to Arctic primary production will depend on changes in light availability (due to ice loss (Ji et al., 2013; Nicolaus et al., 2012)), stratification, and extent of denitrification in Arctic shelf sediments.

4.1.2 Dissolved inorganic carbon and alkalinity– The surface water (<50 m) concentrations of dissolved inorganic carbon (DIC;1920-2260 µmol L^{-1}) and total alkalinity (TA; TA;1990-2340 µmol L^{-1}; Fig. 3f-g) largely reflect the salinity distribution and gradient (27.2-34.4) north of 84°N. River water contributes to Arctic Ocean DIC and TA, while sea-ice meltwater will result in a dilution of these two species. Waters with the largest meteoric fraction (20-23%) are characterized by slightly higher concentrations of DIC and TA compared to corresponding salinity values of 28 in the southern Eurasian Basin that are beyond the influence of rivers.

There are negative linear correlations between the meteoric water fraction and concentrations of DIC (r^2=0.43, $p < 0.001$) and TA (r^2=0.53, $p < 0.001$) in the upper 50 m in samples north of 84°N. The lower DIC (1920-2230 µmol L^{-1}) and TA (2020-2100 µmol L^{-1}) and large fractions of meteoric water (> 20%) are associated with high concentrations of DOC (120-150 µmol L^{-1}), reflecting the input of Siberian shelf water and river runoff to the central basins. The effective river endmembers for DIC and TA based on extrapolation of the linear fit to 100% meteoric water are 1090 and 950 µmol L^{-1}, respectively. These fit well with the discharge weighted concentrations of these two parameters for the major Arctic rivers as reported by Tank et al. (2012; DIC = 1110 µmol kg^{-1}; TA = 1010 µmol kg^{-1}) or Eurasian rivers only (TA = 800 µmol kg^{-1}, Cooper et al., 2008; TA = 815 µmol kg^{-1}, Holmes et al., 2019).

Seasonally varying discharge from the major Siberian rivers drives much of the variation in the surface distribution of DIC and TA in the shallow shelf seas (Drake et al., 2018; Griffin et al., 2018). As the Arctic warms and the permafrost thaws, the hydrologic cycle is accelerating and the total river discharge is increasing (Griffin et al., 2018), resulting in increased river export of nutrients, DOC, DIC, and TA (Drake et al., 2018; Kaiser, Canedo-Oropeza, et al., 2017; Pokrovsky et al., 2015; Tank et al., 2016). The Siberian shelf seas experience increasingly ice-free conditions (e.g. Serreze et al., 2007) and are areas of extensive biogeochemical transformation of organic matter, of both marine and terrestrial origin. This extended ice-free condition, in combination with brine production from sea ice formation, results in a cold bottom water of relatively high salinity and partial pressure of carbon dioxide (pCO_2). This high-pCO_2 water is partly outgassed to the atmosphere, and partly distributed on the outer shelf, as well as into the central Arctic basins depending on season, sea ice conditions, and wind field (Anderson et al., 2009; Anderson, Björk, et al., 2017).

Degradation of terrestrial organic matter and substantial discharge of Arctic river water with elevated pCO_2 leads to persistently low pH in the Siberian shelf seas. This calcium carbonate corrosive water has been observed all along the continental margin and well out into the Makarov and Canada basins, though the effects are most pronounced below the terrestrially influenced upper layer, at depths between 50 m and 150 m (Anderson, Ek, et al., 2017; Cross et al., 2018). This feature coincides with high nutrient concentrations of the upper halocline waters, consistent with organic matter remineralization as described by, e.g., Jones and Anderson (1986). This layer also holds the highest levels of pCO_2 (up to 780 µatm) and, consequently, the lowest values of the saturation state of the calcium carbonate polymorph aragonite Ω_{AR} (down to 0.7). Hence, the TPD is an increasingly important feature in the

distribution of physical and biogeochemical properties in general, and in the seawater CO_2 system and ocean acidification in particular.

In the TPD north of 84°N, Ω_{AR} calculated from TA and pH_{SWS}^{25C} at *in-situ* temperature and pressure, is effectively at saturation (Ω_{AR} = 1.06 ± 0.07, *n* = 17). Increasing river discharge, shelf remineralization of organic matter, and shelf-basin interactions are expected to further decrease the saturation state in the surface layers of the central Arctic in the future (Anderson, Björk et al., 2017; Brown et al., 2016; Semiletov et al., 2016; Wynn et al., 2016).

4.1.3 Dissolved organic matter–The average DOC concentration of Atlantic water entering the Arctic Ocean is 60 μmol L^{-1} at the surface and less than 50 μmol L^{-1} in the intermediate and deep waters (Amon et al., 2003; Anderson & Amon, 2015). This Atlantic water dominates the water column in the central Arctic Ocean, with its core in the upper 500 m. In the western Arctic Ocean, Pacific water (70 μmol L^{-1}) prevails in the top 100 m. Both Pacific and Atlantic waters are characterized by low CDOM (Anderson & Amon, 2015). Primary production in the Arctic Ocean contributes to the DOM distribution in surface waters where a seasonal signal can be observed, especially in open water over the productive shelves (Davis & Benner, 2005; Mathis et al., 2007).

Of all the characterized sources of DOC to the Arctic Ocean, river runoff has the highest concentration of DOC (350 - 990 μmol L^{-1}; Amon et al., 2012) along with elevated levels of CDOM (Anderson & Amon, 2015; Stedmon et al., 2011). In the eastern Arctic Ocean, DOC and CDOM have larger components of terrigenous DOM (Amon, 2004; Amon et al., 2003; Benner et al., 2005; Kaiser, Benner, et al., 2017), whereas DOC and CDOM in the Canada Basin have lower concentrations of terrigenous relative to marine-derived DOM (Benner et al., 2005; Stedmon et al., 2011). Fluvial discharge entrained in the TPD is a major source of terrigenous DOC and CDOM to surface waters of the central Arctic (Amon, 2004; Kaiser, Canedo-Oropeza, et al., 2017; Letscher et al., 2011; Opsahl et al., 1999; Shen et al., 2016). Sea-ice processes add to the complexity of DOC, CDOM and meteoric water distributions in the surface waters of the Arctic Ocean. Ice melt into low DOM ocean waters can stimulate primary production of DOM or be a source of ice algae DOM, but would not add CDOM to surface waters (Anderson & Amon, 2015). In contrast, sea-ice melt results in a dilution of surface water DOM (Granskog et al., 2015), but can add meteoric water from snow and river water included in sea ice. Within the TPD, the relationship between the meteoric water fraction and the DOC concentration was stronger (r^2=0.88, $p < 0.001$) than the relationship between the meteoric water and CDOM (r^2= 0.59, $p < 0.001$) (Figs. 2c,e, 3d-e) supporting the

notion that DOC and CDOM are independently controlled by different processes. Biological processes influence DOC and CDOM to different degrees, primary production will increase DOC but not CDOM, microbial degradation will decrease DOC, but might actually increase CDOM. Physico-chemical processes like photobleaching and flocculation will affect CDOM but not necessarily DOC while freezing affects DOC and CDOM in a similar fashion (Guéguen et al., 2012; Kaiser, Canedo-Oropeza, et al., 2017; Moran et al., 2000; Sholkovitz, 1976; Uher et al., 2001).

The effective meteoric water endmember for the linear regression with DOC is 451 µmol L^{-1}, which is about half of the discharge weighted value for the major Eurasian Arctic rivers (800 µmol L^{-1}; Holmes et al., 2012, 2019). Similar losses were reported for CDOM (Granskog et al., 2012), and both reflect removal during estuarine mixing and passage over the shelf seas by flocculation, photo-mineralization or microbial degradation (see section 4.1.2) (Alling et al., 2010; Hansell et al., 2004; Kaiser, Canedo-Oropeza, et al., 2017; Letscher et al., 2011), or the influence of shelf-ice melt as described by Amon et al. (2012). Earlier studies have reported conservative mixing of DOC in Arctic river estuaries (Amon & Meon, 2004; Köhler et al., 2003), but they were based on late summer sampling and excluded the freshet period, which delivers more bio-labile DOM to the Arctic coast.

Regarding the marine production of DOC and CDOM, warming temperatures and a decrease in ice cover will result in increased primary productivity, since light is the major limiting factor for the production of organic carbon by phytoplankton in the Arctic Ocean (Vancoppenolle et al., 2013). An Arctic Ocean-wide annual 20% increase in net primary production has already been reported based on remote sensing ocean color products (Arrigo & van Dijken, 2011) and will translate into more DOM derived from decomposing planktonic sources. As CDOM absorbs ultraviolet and visible light, the expected higher fluvial CDOM fluxes along with increased marine CDOM might have a negative feedback effect on the light limitation in the shelf areas (Pavlov et al., 2015) but should facilitate TEI transport to the open Arctic Ocean for those particle-reactive trace elements that form stable complexes with DOM (e.g. Fe, Cu, Ni, and Co).

4.1.4 Particulate matter–In the upper 50 m of TPD-influenced stations, none of the particulate (p) trace elements and isotopes (pTEIs) examined here show linear correlations with the fraction meteoric water (Fig. 4). While the lithogenic elements such as pFe and pAl were sometimes enriched by over an order of magnitude relative to their dissolved

concentrations in the TPD (Fig. 4d-f), they were not statistically correlated with the meteoric water fraction (Fig. 4a-c).

The POC and biogenic silica (bSi; Figs. 4g-h) also did not show significant correlations with meteoric water. However, only surface data from GN01 are available for these variables. Since GN01 stations did not span a large dynamic range in meteoric water, it is unclear whether the TPD could be a source of riverine POC to the central basin in the same way as it is for DOC. The δ^{13}C-POC within the TPD is extremely depleted (Fig. 4i), potentially consistent with an influence of depleted (-30 ‰) riverine organic matter that is of terrestrial origin (Holmes et al., 2019; McClelland et al., 2016), but it could also be explained by the large isotope fractionation observed in slow growing phytoplankton (Brown et al., 2014). The residence time of small size fraction (SSF; 1-51 µm) POC in the upper 100 m within the TPD is about 300 days at 88°N (station 38), and even longer at the other TPD stations (Black, 2018). This extremely low rate of particle loss in the upper Arctic Ocean (Black, 2018) is of similar magnitude to the time-scale of TPD transport from the shelf to the central Arctic (Kipp et al., 2018), potentially allowing for riverine POC to survive transport to the central Arctic.

In the context of rapidly changing climate, as permafrost thaws, river flux and coastal erosion increases, higher concentrations of riverine POC could be transported into the central Arctic Basin. There, the POC may be subject to more intense microbial degradation due to the expected rise in ocean temperature (Kirchman et al., 2005; Middelboe & Lundsgaard, 2003). Furthermore, the TPD is transporting younger ice sea-ice that is subject to melting before it reaches Fram Strait, thereby increasing central Arctic accumulation of ice-rafted material, such as POC, and decreasing export to the Atlantic (Krumpen et al., 2019).

4.1.5 Radium isotopes and barium–Radium-228 ($t_{1/2}$ = 5.75 y) activities were high in the TPD and had a strong positive correlation with the fraction of meteoric water (r^2 = 0.81, $p<0.001$). Activities increased from < 5 dpm 100L^{-1} at meteoric water fractions <5% to 20 – 25 dpm 100L^{-1} at meteoric water fractions ~20% (Figure 3i). These high ^{228}Ra activities persisted over the upper 50 m of the water column. The correlation between ^{226}Ra ($t_{1/2}$ = 1600 y) and meteoric water (r^2 = 0.49, $p<0.001$) was not as strong as that for ^{228}Ra, but ^{226}Ra levels did increase from ~6 – 8 dpm 100L^{-1} at low meteoric water fractions to ~9 – 11 dpm 100L^{-1} in the core of the TPD (Figure 3j). Radium-226 activities of samples collected on the western side of the Lomonosov Ridge remained high even outside of the region influenced by the

TPD, due to the influence of high-^{226}Ra Pacific inflow in the Canada Basin. In contrast, activities decreased (<6 dpm 100L^{-1}) in the Atlantic-influenced Eurasian Basin.

The strong correlation between ^{228}Ra and the fraction of meteoric water reflects the shelf signal carried in the TPD. While ^{228}Ra does have a riverine source (Rutgers van der Loeff et al., 2003), shelf sediments supply over 80% of the ^{228}Ra in Arctic surface waters (Kipp et al., 2018). The weighted average annual ^{228}Ra activity of Arctic rivers is on the order of 24 ± 13 dpm 100L^{-1}; desorption of Ra from suspended particles in the estuarine mixing zone could add an additional 25% (Kipp et al., 2018). This combined riverine ^{228}Ra source is significantly lower than the effective river endmember (97 dpm 100L^{-1}) determined by its relationship with meteoric water. This correlation therefore results from the transport of river water over the shallow Eurasian shelves before the TPD carries this river- and shelf-influenced signal to the central Arctic. The activities of ^{228}Ra measured in the TPD were higher in 2015 compared to 2007 and 2011, indicating an increased flux of ^{228}Ra to the central Arctic (Kipp et al., 2018; Rutgers van der Loeff et al., 2018). This rise is likely driven by the loss of ice cover over Eurasian shelves, permitting increased wind-driven vertical mixing that can transport ^{228}Ra produced in shelf sediments into the overlying water column through enhanced sediment resuspension and porewater exchange (Kipp et al., 2018; Serreze et al., 2007; Williams & Carmack, 2015).

The weaker correlation between ^{226}Ra and meteoric water results from the larger surface water inventory and smaller shelf source of this isotope compared to ^{228}Ra. Once removed from shelf sediments (through diffusion or resuspension) ^{226}Ra will regenerate more slowly from decay of its Th parent than ^{228}Ra due to its longer half-life. The ratio of ^{228}Ra/^{226}Ra inputs from shelves is therefore typically greater than 1, and ratios as high as 3.9 have been observed on the Laptev Shelf (Rutgers van der Loeff et al., 2003). On the GN01 and GN04 transects, ^{228}Ra/^{226}Ra activity ratios were between 1 and 2 at meteoric water fractions >15%, reflecting the high shelf ratios of these isotopes carried in the TPD. While activities of ^{226}Ra in the TPD have increased from 2007 to 2015, this change was not as large as that for ^{228}Ra (Kipp et al., 2018; Rutgers van der Loeff et al., 2018). The longer half-life of ^{226}Ra compared to ^{228}Ra results in a larger surface water inventory, thus a substantial rise in inputs is required to increase surface water ^{226}Ra activities.

Barium is a chemical analogue of radium. The highest surface dBa concentrations (<25 m) are observed in the Canada Basin (67.7 ± 1.4 nmol L^{-1}; range: 64.4 – 69.1 nmol L^{-1}). Makarov Basin surface waters are slightly lower (62.5 ± 0.7 nmol L^{-1}; range: 53.4 – 63.3 nmol L^{-1}), but are still high relative to incoming Atlantic and Pacific seawater. These high

concentrations likely indicate the presence of accumulated river water circulating in the Amerasian Basin (Guay et al., 2009). Samples in the Nansen Basin and the Barents Sea are lower and representative of the Atlantic source (~40 nmol L^{-1}). However, data from the Amundsen Basin are more variable, with surface concentrations that range from 48.6 – 65.5 nmol L^{-1}. This variation appears to be driven by the composition of the water at each station: where there are high ice melt or Atlantic fractions, the concentrations are lower (< 60 nmol L^{-1}). Alternatively, where Pacific water or meteoric fractions are relatively high, the concentrations are higher (> 60 nmol L^{-1}).

There is a strong positive correlation between dBa concentration and % meteoric water in the TPD (r^2=0.68, $p < 0.001$; Fig. 3h), which is driven by high river Ba concentrations (Abrahamsen et al., 2009; Guay & Falkner, 1997, 1998). Scatter around the trend may result from non-conservative behavior of Ba such as removal from the dissolved phase in association with biological activity (Pyle et al., 2018, 2019), particularly over the productive Arctic shelf regions (Roeske et al., 2012). Further complicating matters, the shelf may also be a source of Ba, as was demonstrated for ^{228}Ra (Kipp et al., 2018).

The best fit trendline for the dBa versus meteoric water relationship suggests an effective river endmember concentration of 158 nmol L^{-1}, which is higher than the discharge weighted dBa concentrations from the Eurasian rivers (92 nmol L^{-1}) (Holmes et al., 2019). Importantly, the data available from the A-GRO network are direct measurements of dBa in surface freshwater (S < 1) and since Ba is known to undergo desorption from suspended particulate matter (SPM) in the estuarine zone as salinity increases (e.g. Coffey et al., 1997), these measurements may not be representative of the effective endmember for riverine dBa. Accounting for desorption of Ba from SPM, Guay et al. (2009) reported effective endmembers between 100 and 130 nmol L^{-1} dBa in Eurasian rivers, which is closer to the value we determined from the linear regression with meteoric water fraction in the TPD. Supply of Ba from multiple rivers to the eastern Arctic shelves may also explain the slightly lower r^2 for the fit to meteoric water fraction as compared to other TEIs reported herein. Additionally, submarine groundwater discharge (SGD) can be a source of Ba to the marine environment as it generally contains high dBa (e.g., Shaw et al., 1998); at present, there are no constrained SGD dBa endmember concentrations available for the Arctic, but recent groundwater dBa measurements by Kipp et al. (2020) of 610-970 nmol L^{-1} suggest that this source may need to be taken into account for Arctic Ba geochemical budgets moving forward.

As Arctic temperatures continue to rise, Ra and Ba inputs to Arctic surface waters will also be amplified by permafrost degradation, increased river discharge, and increased coastal erosion. As permafrost thaws, SGD is likely to become a more important part of the Arctic hydrologic cycle (Walvoord et al., 2012), and will serve as an additional source of these TEIs (Charkin et al., 2017). The combination of thermal erosion of permafrost and physical erosion from more turbulent shelf seas will also result in more coastal sediment delivery to Arctic shelf seas, which can release Ra isotopes and Ba through desorption.

Notably, dBa (and ^{226}Ra to a lesser degree) can be influenced biologically and may be removed as barite precipitates, scavenged by particle surfaces, or taken up to some degree by phytoplankton cells (Bishop, 1988; Dehairs et al., 1980; Roeske et al., 2012). This non-conservative behavior complicates the element's utility as a tracer. As such, the influence of higher biological/particle interactions on Ba cycling in the Arctic as the central basins lose ice cover is difficult to anticipate.

4.1.6 Dissolved trace metals and metal isotopes– Along GN01, eleven dissolved (< 0.2 µm) trace metals (Al, V, Mn, Fe, Co, Ni, Cu, Zn, Ga, Cd, and Pb) were evaluated, as well as the size partitioning of dissolved Fe (dFe) into soluble (sFe < 0.02 µm) and colloidal (0.02 µm < cFe < 0.20 µm) size fractions. The fraction of the total dCo that was chemically labile (LCo) versus strongly organically complexed was also quantified. Several metals displayed a concentration enrichment associated with the TPD in the central Arctic, as well as a significant relationship (95% confidence interval) with meteoric water north of 84°N and within the upper 50 m. Based on the r^2 values for a linear fit to the data, changes in meteoric water loadings explained >50% of the dFe, dCo, LCo, dNi, dCu, dCd, dGa, and dPb concentration variability and >40% of dMn variability (Fig. 5a, f-h, k-l 6d-e). Dissolved Zn had a significant relationship (p=0.001) with meteoric water in the TPD, but a comparatively lower r^2 (0.36; Fig. 5j), while dissolved Al with meteoric water displayed no statistical significance at all (Fig. 6a). Dissolved V displayed a strong negative correlation with meteoric water (Fig. 6b; r^2=0.65, p=0.001).

The measured dissolved metal concentrations are consistent with previous, albeit limited, literature on trace metals from the Arctic Ocean. Early studies of some trace metals such as Mn, Fe, Ni, Cu, Zn and Cd demonstrated low surface concentrations, with enrichments between 100 and 200 m in the halocline, and low but uniform values in the deep ocean (Danielsson & Westerlund, 1983; Moore, 1981; Yeats, 1988; Yeats & Westerlund, 1991). More recent studies focused primarily on the Chukchi Shelf (Aguilar-Islas et al., 2013; Cid et

al., 2012; Kondo et al., 2016; Nishimura et al., 2012) or on the Eurasian Basin (Klunder, Bauch, et al., 2012; Klunder, Laan, et al., 2012; Middag et al., 2011), but again show very similar patterns, particularly with regard to the Canada Basin halocline feature that dominates many of the trace metal distributions. Within the TPD region, dFe and dMn concentrations compare well to those measured previously in studies focused on the Eurasian side of the Arctic Ocean (Klunder, Bauch, et al., 2012; Klunder, Laan, et al., 2012; Middag et al., 2011). Compared to other global ocean surface waters in the 2017 GEOTRACES Intermediate Data Product (Schlitzer et al., 2018), Arctic Ocean surface waters have anomalously high concentrations of dissolved trace metals such as Fe, Co, Zn, Ni, Cu, and Cd, likely due to a combination of larger external sources and less biological uptake and/or scavenging removal under the sea ice (Fig. 7). This surface enrichment can be seen for dFe (0.2 to 4 nmol L^{-1}) and dCu (3.9 to 7.4 nmol L^{-1}) in comparison to measurements from the Atlantic Ocean at a similar distance from the continental margin (Fig. 7). While the wide continental shelves, sea ice, dust, and incoming Pacific and Atlantic waters are all potential sources of trace metals to surface Arctic waters, the strong correlation between meteoric water and dFe, dCo, dCu, and dNi north of 84°N point to a riverine source that originated in the eastern Arctic Ocean. However, since the meteoric water signal of the TPD is significantly modified and transformed in the Laptev Sea (Kadko et al., 2019; Kipp et al., 2018), concentrations of certain dissolved metals in TPD waters over the North Pole can only be interpreted when high-particle shelf and estuarine reactions are considered. For example, scavenging-prone metals had an inverse (dGa, dPb) or very poor relationship (dAl) with meteoric water over the central Arctic, despite high concentrations of these trace metals in Arctic rivers (e.g. Pb of up to 480 pmol L^{-1} in the Lena River; Colombo et al., 2019; Hölemann et al., 2005). In Kadko et al. (2019), it is suggested that scavenging on the continental shelves may be a major sink of dissolved Pb from the Arctic Ocean. These lines of evidence suggest that removal of these TEIs by flocculation in estuaries and/or by scavenging onto the abundant particles over the Laptev Sea continental margin are important processes that greatly limit their being transported with the TPD into the central Arctic.

Dissolved Fe and Mn are expected to undergo similar scavenging and flocculation processes as dAl, and so despite their extremely high concentrations in the Eurasian Arctic rivers (averages of 2300 and 470 nmol L^{-1}, respectively; Holmes et al., 2019), one would expect lower concentrations downstream in the TPD. Indeed, concentrations of dFe and dMn in the TPD were between two and three orders of magnitude lower than river concentrations (2.90 ± 1.0 nmol L^{-1} and 4.2 ± 1.4 nmol L^{-1}, respectively). Dissolved Mn had a lower degree of

correlation with meteoric water and was present at concentrations similar to the central Atlantic (Fig. 7b), suggesting that it was oxidized continually to the particulate phase and/or scavenged during transit across the Arctic. In contrast, dFe maintained a strong linear relationship with meteoric water despite the massive loss of Fe between rivers and the central Arctic. Notably for dissolved Fe, both smaller sFe and larger cFe had strong relationships with the fraction of meteoric water (Fig. 5b-c; r^2= 0.79 and 0.88, respectively), suggesting that both sFe and cFe contributed significantly to the TPD meteoric water dFe source. However, the slope of the sFe vs. %MET regression was ~90% that of the corresponding dFe slope (cFe slope was only 47% that of dFe), suggesting that the dFe that persists from meteoric water fluxes is rich in smaller organically-chelated Fe species and is not predominantly composed of colloidal-sized inorganic Fe oxyhydroxides. This makes sense since larger colloidal-sized species such as weathered Fe nanoparticles present in river water and Fe oxyhydroxides formed during Fe precipitation within the Siberian estuaries were likely removed from the water column via scavenging and/or aggregation. In contrast, smaller soluble-sized species are more likely to persist as Fe is bound to organic ligands, which have recently been found to be dominated by humic substances that stabilize Fe and account for its high solubility in the TPD (Laglera et al., 2019; Slagter et al., 2017, 2019). Other strong organic Fe-binding ligands may also contribute to the stabilized sFe pool, as Fe bound to strong organic ligands have been found to be resistant to flocculation in estuaries (Bundy et al., 2015).

Fe stable isotope ratios (δ^{56}Fe) support a riverine source for dFe in the TPD (Fig. 5d). If reducing shelf sediments were a source of dFe to the TPD, then the dFe δ^{56}Fe signature would be expected to be low (-2 to -4 ‰; Conway & John, 2014; John et al., 2012; Severmann et al., 2006, 2010). Instead, TPD δ^{56}Fe values are much closer to continental values around 0 ‰ (ranging from -0.4 ‰ to +0.5 ‰ in waters with >5% meteoric water), consistent with those found in other Arctic rivers (Ilina et al., 2013; Stevenson et al., 2017; R. Zhang et al., 2015). Indeed, the values are very similar to the range in δ^{56}Fe for particulate and colloidal Fe in the Lena River Estuary (-0.4 ‰ to +0.1‰), though dissolved δ^{56}Fe was not measured in that study (Conrad et al., 2019).

Dissolved Fe, Co, Ni, and Cu had the most statistically-significant correlations with meteoric water fraction (Figs. 5,6), and these metals are likely to be substantially organically-complexed in seawater (Constant M.G. van den Berg, 1995; Bruland et al., 2013; Millero et al., 2009; Yang & Van Den Berg, 2009). These results are consistent with the high apparent residence times of Fe, Ni and Cu determined within TPD-influenced water of the GN01 study

(Kadko et al., 2019) and supports the conclusion that organic chelation is required for efficient transport of riverine dissolved metals into the central Arctic. For example, the majority of the dCo in samples with the highest fraction meteoric water was strongly organically complexed (up to 90%) compared to an average of ~70% organically complexed in the remainder of the GN01 transect.

Dissolved Fe, with its apparent and measured Eurasian river endmember of 19 nmol L^{-1} and 2300 nmol L^{-1} (Holmes et al., 2019), respectively, was largely scavenged/aggregated in the estuary and/or over the shelf before being transported offshore. In contrast, the apparent riverine endmembers for dCu (30 nmol L^{-1}) and dNi (31 nmol L^{-1}) are within less than one order of magnitude of their Eurasian Arctic river averages (dCu = 22 nmol L^{-1}; dNi = 17 nmol L^{-1}; Holmes et al., 2019), suggesting that they were organically-chelated before leaving the river and were not scavenged or taken up biologically in the estuary or on the shelf to any significant extent (C.M.G. Van Den Berg & Nimmo, 1987; Donat & van den Berg, 1992) The 100% meteoric water endmember yields dissolved and labile Co apparent endmembers of 854 and 243 pmol L^{-1}, respectively. The dCo apparent riverine endmember is largely consistent with the Arctic rivers average of 1280 pmol L^{-1} (Holmes et al., 2019), suggesting that rivers are the primary source of dCo in the TPD and that this riverine dCo signature is preserved by organic matter complexation (e.g. Ellwood & Van den Berg, 2001) and mainly affected by dilution over the timescale of transport from the shelf to the sampling region in the vicinity of the North Pole (~6-12 months, Kipp et al., 2018). As was observed for dNi and dCu, these data suggest that organic complexation from the high DOM riverine waters plays an important role in stabilizing scavenging-prone metals in the TPD.

Dissolved Zn is also elevated in Eurasian Arctic rivers (59 nmol L^{-1}; Holmes et al., 2019), but compared to other metals there was only a weak, but positive relationship between dZn and meteoric water to link the central Arctic Zn to a riverine source (Jensen et al., 2019). Dissolved Zn concentrations are highest in halocline waters of the western Arctic (~1-6 nmol L^{-1}; 50-250 m) due to a large source of Zn from remineralization in Chukchi Shelf porewaters (Jensen et al., 2019), while they decrease to sub-nanomolar concentrations in the uppermost 50 m of the Arctic under the ice. Because the concentrations of Zn in Arctic melt pond waters (Marsay et al., 2018) and the Lena River (Guieu et al., 1996) are also around 1 nmol L^{-1}, it is difficult to distinguish the source of Zn in the TPD waters from concentrations alone. Zinc stable isotopes ($\delta^{66}Zn$) range between +0.2 ‰ and +0.8 ‰ in TPD waters with a significant meteoric water component (>10%), a range that is consistent both with the isotope composition of meltwaters (-0.11 ‰ to +0.75 ‰; Marsay et al., 2018) and with the variability

found in global rivers (-0.12 ‰ to +0.88 ‰; Little et al., 2014). Thus, the lower δ^{66}Zn signatures observed in the core of the TPD compared to surface waters further south in the Arctic (Fig. 5k) may reflect either background seawater variability, sea ice input, or river/shelf input from the TPD, though the positive slope between dZn and meteoric water does suggest that the latter source is most likely (Bruland, 1989; Murray et al., 2014). Further research will be needed to determine the relative importance of these sources, though it has been suggested that aerosol input is likely the most significant source of Zn to the open Arctic with some riverine input as well (Kadko et al., 2019).

Dissolved Cd concentrations in Eurasian Arctic rivers (68 pmol L^{-1}; Holmes et al., 2019) are lower than those in the central Arctic, meaning that both dCd concentrations and Cd stable isotopes (δ^{114}Cd) in the TPD are heavily influenced by a marine source (Fig. 5i). Additionally, δ^{114}Cd in both melt ponds and Arctic rivers is similar to seawater values, making it difficult to know whether the lower δ^{114}Cd values seen in the TPD are caused by river/shelf input, or are simply the result of the mixing between Atlantic and Pacific waters in the Arctic (Zhang et al., 2019).

Dissolved Al did not trend significantly with the meteoric fraction, while dGa did, but with an inverse relationship. Gallium and Al have similar oceanic sources (rivers and atmospheric deposition) and sinks (scavenging), although Ga is less particle reactive and thus has a longer residence time in seawater (Orians & Bruland, 1988; Shiller, 1998). Surface dAl and dGa concentrations are both low in the Arctic Ocean, including the TPD, suggesting that there is little or no input from shelf waters (Fig. 6a,c). The dAl concentrations are also much lower than those typically observed in the open ocean where dust deposition can lead to surface enrichment of this TEI (e.g. the Atlantic Ocean; Fig. 7c). There was no evidence of ice rafted sediment adding trace elements to the surface waters, which is consistent with the lack of any visual identification reports of this material during the GN01 cruise. Dissolved Al during the 2007 GIPY11 cruise was 0.3-1.4 nmol L^{-1} in surface waters of the eastern Arctic (Schlitzer et al., 2018), which is very similar to the range of data reported herein (0.9-1.8 nmol L^{-1}). In contrast, the 1994 Trans Arctic cruise (Measures, 1999) showed highly variable concentrations of dissolved Al, with the highest values corresponding to regions where significant levels of ice rafted sediment were observed. Furthermore, though the fluvial dAl load in Arctic rivers is known to be substantial (Stoffyn & Mackenzie, 1982), export of riverine Al to the open ocean, including in the TPD, is negligible because of estuarine removal processes (Mackin & Aller, 1984; Tria et al., 2007). In support of the estuarine/coastal removal argument, previous data (Middag et al., 2009) showed that dAl

values are as low as 2.3 nmol L^{-1} in the Laptev Sea, which is strongly influenced by the outflow of the Lena River. While fluvial dGa data are limited, most reports suggest typical concentrations in the 10-100 pmol L^{-1} range (Colombo et al., 2019; Gaillardet et al., 2014; Shiller & Frilot, 1996). Additionally, McAlister & Orians (2012) demonstrated that dGa behaves non-conservatively in the Columbia River plume, showing apparent scavenging removal. Likewise, McAlister and Orians (2015) indicate that interactions with Arctic shelf sediments may be a dGa sink due to scavenging onto particle surfaces, which is supported by the negative slope and 100% meteoric water intercept of -24 pmol L^{-1} reported herein.

Non-conservative behavior is observed in the global ocean vanadium cycle as a result of biological uptake, particle scavenging, and reduction to an insoluble phase (Brinza et al., 2008; Crans et al., 2004; Wehrli & Stumm, 1989). However, V in surface water may also be diluted by sea ice melt and/or riverine input (Marsay et al., 2018). The Arctic riverine endmember ranges between 1.7 – 22 nmol L^{-1}; the discharge-weighted mean of Eurasian rivers is 11 nmol L^{-1} (Holmes et al., 2019). Like dGa, the dV and meteoric water correlation in the TPD has a negative slope and is significant (r^2=0.65, p=0.001; Fig. 6b), with an extrapolated dV river endmember concentration of -35 nmol L^{-1}. This negative zero-salinity intercept requires a removal process at lower salinities, likely related to coupled particle scavenging and reduction in shelf waters and sediments (Kadko et al., 2019; Morford & Emerson, 1999; Whitmore et al., 2019). Specifically, release of dissolved Fe from reducing sediments leads to precipitation of Fe oxyhydroxides in the water column which then scavenge dV (Trefry & Metz, 1989), delivering the sorbed V to the sediments with the settling Fe particles. In the reducing sediments, the Fe can then be dissolved and released to the water again, while reduced V can be more permanently incorporated into the sediments (Scholz et al., 2011). This cycling of the Fe between sediments and water column creates an "Fe shuttle" that can lower the dV of the water column (Scholz et al., 2011, 2017). As noted in Section 4.1.5, the changing ^{228}Ra distribution implies increased sediment-water exchange on the Arctic shelves (Kipp et al., 2018; Rutgers van der Loeff et al., 2018). How this impacts the Fe shuttle and the resulting effect on dV is unclear since increased sediment-water exchange could increase sediment efflux of reduced Fe or diminish it through sediment oxygenation.

The projected future increases in Arctic riverine discharge and thawing permafrost are likely to enhance fluxes of bioactive trace elements such as Fe, Co, Ni, and Cu, which are high in

rivers and sediments, as well as fluxes of DOM-derived organic ligands that stabilize these metals in the dissolved phase. A future Arctic with higher concentrations of DOM might serve to further enhance some of these metal fluxes, as organic chelation appears to be critical in selecting the dissolved metals that are stably transported via the TPD (Slagter et al., 2017; Laglera et al., 2019). Thus, future increases in meteoric water in the Arctic may disproportionately impact certain trace metals over others, with implications for organisms that use those metals as cofactors in essential metabolic processes. For example, some phytoplankton use Co instead of Zn in carbonic anhydrase, despite that concentrations of Zn greatly exceed those of dCo in surface waters of most regions (Saito & Goepfert, 2008). However, the Arctic is unique in that surface Co/Zn ratios are much higher than in other ocean basins (Fig. 5j). Higher inputs of Co to the TPD may also affect biological communities downstream of the Arctic, as TPD waters exit the Arctic through Fram Strait into the North Atlantic Ocean. Evidence of this elevated Co signature has been observed in the North Atlantic (Noble et al., 2017). Increases in these metal sources in a future warming Arctic may therefore impact not only Arctic biological community structure, but potentially North Atlantic ecosystems as well.

Additionally, with more open water from ice cover decline, atmospheric deposition of Al and Ga may become more important sources of these two TEIs to the surface Arctic. However, this may be offset in part by scavenging loss due to increased shelf sediment-water interactions (Kipp et al., 2018; McAlister & Orians, 2012, 2015). The contrast in the residence times for dGa and dAl suggests that comparison of the distributions of the two elements in a changing Arctic Ocean may reveal changes in scavenging and resuspension impacts on Al and other elements. Lastly, shelf conditions that promote hypoxia may influence the V cycle by increasing V removal by the reducing sedimentary environment.

4.1.7 Mercury–Among all stations located north of 84°N and shallower than 50 m, total mercury (tHg) ranged from ~0.5-2.5 pmol L^{-1}, methyl-mercury (MeHg, the sum of mono- and dimethyl-mercury) ranged from <0.05-0.22 pmol L^{-1}, monomethyl-mercury (MMHg) ranged from <0.05-0.20 pmol L^{-1}, and dimethyl-mercury (DMHg) ranged from <0.05-0.12 pmol L^{-1} (Fig. 6f-g) (Agather et al., 2019). Contrary to all other open ocean basins, total Hg concentrations were enriched in surface waters. Total Hg and MeHg correspond well to the few previous observations available in the central Arctic Ocean (Heimbürger et al., 2015) and the Canadian Arctic Archipelago (F. Wang et al., 2012; K. Wang et al., 2018): tHg surface

enrichment followed by a shallow MeHg peak at the halocline and in the Atlantic waters below. Prior to the 2015 GEOTRACES campaign, there were no MMHg and DMHg data for the central Arctic Ocean. Similar to other open ocean basins, MeHg concentrations were depleted in surface waters, likely due to a combination of MeHg photodemethylation, MMHg uptake into phytoplankton and DMHg evasion to the atmosphere. Although ice can act as a barrier to air-sea gas exchange and hinder elemental Hg (Hg^0) evasion (DiMento et al., 2019), no significant differences were observed between the MeHg concentrations at ice covered versus non-ice covered stations. Looking forward, ice thinning and melting in the central Arctic (Krumpen et al., 2019) may reduce this barrier.

Samples with elevated meteoric water fractions (>15%) were characterized by higher tHg concentrations (up to ~2 pmol L^{-1}), though there was no significant correlation between the two variables. This might be because rivers are not the only source of tHg to the water column. Mercury also enters the Arctic Ocean via atmospheric deposition and oceanic inputs, mostly from the Atlantic Ocean (Cossa et al., 2018; Outridge et al., 2008; Soerensen et al., 2016; Sonke et al., 2018). However, the lack of correlation between total Hg and meteoric water input in the TPD is surprising given the substantial input flux predicted from measurements of Hg in Arctic rivers. Sonke et al. (2018) derived a discharge-weighted tHg concentration of 46 pmol L^{-1} for the monitored Eurasian rivers, with values of up to 191 pmol L^{-1} in the spring freshet (Yenisei River). This result implies a large loss of Hg in estuaries and shelves, which may be the result of atmospheric evasion (Fisher et al., 2012; Sonke & Heimbürger, 2012). A more recent box model study reveals that a portion of the evading Hg is in the form of DMHg (Soerensen et al., 2016). Estuarine and shelf sediments might also act as sinks for Hg entering from pan-Arctic rivers (e.g., Amos et al., 2014), but this idea remains to be tested for this basin.

The MeHg species had no significant correlation to meteoric water fraction above 84°N. Since shelf sediments can be sources of MeHg (e.g., Hammerschmidt & Fitzgerald, 2006; Hollweg et al., 2010), we might expect a correlation to meteoric water inputs. The lack of such a correlation suggests that either MeHg produced on the Eurasian shelves was lost to demethylation processes during the ~6-18 month transit from the shelf-break to the central Arctic Ocean, or that production in the mixed layer is a stronger source than the shelves. Large subsurface maxima in methylated Hg species (Agather et al., 2019; Heimbürger et al., 2015) suggests a third source for MeHg in the TPD could be diffusion from the MeHg species-rich halocline (Soerensen et al., 2016).

In the future, climate warming is expected to increase Hg inputs to the Arctic drastically as permafrost contains large Hg stocks (Schuster et al., 2018). The Arctic reservoir with the highest relative proportion of MeHg, often representing more than 40%, is generally open ocean seawater (Heimbürger et al., 2015). It is primarily the ocean-sourced MeHg that bioamplifies to harmful levels, putting Arctic wildlife and human health at risk. The additional input of Hg and DOC might further stimulate MeHg production in the Arctic Ocean. Future coupled ocean-atmosphere numerical models (e.g. Fisher et al., 2012; Zhang et al., 2015) and box model assessments (e.g. Soerensen et al., 2016) designed to constrain Arctic Hg cycling will need to consider Hg cycling and transport associated with the TPD.

4.1.8 Rare earth elements–North of 84°N, dNd and dEr concentrations in the upper 50 m ranged between 16.8 and 48.6 pmol L^{-1} and 4.5 and 13.8 pmol L^{-1}, respectively. Surface concentrations of both rare earth elements (REEs) are highest within the TPD, a factor of at least 2 higher than outside the TPD influence (Fig 6h-i). The spatial and vertical REE distributions seen in this new dataset are in agreement with previous REE distributions from the central Arctic, including extremely high concentrations within the TPD (Fig. 2h; Andersson et al., 2008; Porcelli et al., 2009; Zimmermann et al., 2009), exceeded only by REE concentrations in the Laptev Sea close to the Lena Delta (Laukert et al., 2017). The elevated surface REE concentrations in the central Arctic, and in particular within the TPD, are supportive of a substantial terrestrial input mainly via rivers. This inference is reinforced by the correlation of dNd and dEr with the fraction of meteoric water (Fig. 6h-i; r^2 = 0.54 and 0.49 for Nd and Er, respectively; p<0.001 for both) and with DOC (Fig. 3d). Together with a lack of systematic changes in Er/Nd ratios in the TPD, this suggests little to no particle-seawater interactions in the central Arctic. This is in contrast to other open ocean settings, where scavenging removes REEs with a preferential removal of the light over the heavy REE and therefore the Er/Nd ratio (e.g. Elderfield, 1988).

The mean discharge weighted Eurasian river dNd concentration is 1300 nmol L^{-1} (Holmes et al., 2019), though there is variability among the Siberian rivers as discussed by Zimmerman et al. (2009) for the summer high discharge season (Ob: 2152 pmol L^{-1}; Lena: 826 pmol L^{-1}; Yenisei: 154 pmol L^{-1}). This variability may in part explain some of the scatter in the REE vs. meteoric water fraction correlation, especially at high values. The apparent river endmember REE concentrations that were estimated by extrapolating the REE concentrations to 100% meteoric water (Nd = 120 pmol L^{-1}, Er = 32.3 pmol L^{-1}) are therefore difficult to compare to known river REE compositions. If the weighted river Nd concentration of 1300 pmol L^{-1} is

combined with an estuarine removal of 75% Nd (Laukert et al., 2017), the river endmember Nd concentration reaching the shelf would be ~325 pmol L^{-1}, nearly a factor of three higher than the extrapolation of the REEs to 100% meteoric water. This discrepancy would therefore imply greater estuarine REE removal, substantial REE removal over the shelf, and/or removal along the flow path of surface waters from the shelves to the central Arctic. Removal over the shelf or along the TPD is, however, not reflected in the heavy over light dissolved REE ratios (Er/Nd = 3-4) that otherwise should be elevated by scavenging due to preferential removal of the light relative to the heavy REEs (Elderfield, 1988), but are similar to those in the Laptev Sea outside the direct river influence i.e., at high salinity. Therefore, the extrapolated river endmember Nd concentration approach must be hampered by the large differences in river REE concentrations, seasonal variability in the river endmembers and/or discharge and the unknown relative contributions of the rivers to the REE signal in the TPD.

Unlike the radium isotope increase that has been attributed to enhanced input from the Siberian shelves in response to decreasing sea ice cover (Kipp et al., 2018; Rutgers van der Loeff et al., 2018), there are no systematic REE changes seen in the central Arctic from 2003 to 2015 (Andersson et al., 2008; Porcelli et al., 2009; Zimmermann et al., 2009). Hence, a recent increase in REE input from the shelves or the rivers is not observed based on the limited dataset currently available.

4.1.9 Thorium-232– Thorium-232, with a half-life of 14.01 Gyr, is the only primordial nuclide of thorium and is abundant in the continental crust (Rudnick & Gao, 2003). The dissolved ^{232}Th concentrations in the TPD are an order of magnitude higher than those observed in deep waters at the same stations. Surface dissolved ^{232}Th concentrations at Arctic TPD stations are a factor of three higher than those observed in the open North Atlantic Ocean, with similar concentrations at 500 meters where the Arctic is dominated by Atlantic water (Jones, 2001) (Fig. 7e).

A strong positive correlation between dissolved ^{232}Th and meteoric water fraction is observed in upper ocean waters (<50 m) at all TPD stations (r^2 = 0.83, p < 0.001) (Fig. 3k). An associated strong positive correlation is also observed in these waters between dissolved ^{232}Th and DOC. These strong positive correlations taken together with low surface ^{232}Th concentrations at margin stations suggest that the source of the Th-enriched TPD surface waters is Siberian rivers and not diagenetic release of Th from eastern Arctic shelf sediments. Further, similar to many of the transition metals described above, these correlations suggest

that ^{232}Th is complexed by organic ligands that prevent it from being scavenged during transport (Hirose & Tanoue, 2001; Slagter et al., 2017; R. Zhang et al., 2015).

4.2 TPD Transport Rates and Fluxes

As discussed in the introduction, there are a number of studies that have documented and modeled the circulation pathways and seasonal to interannual dynamics of the Transpolar Drift (Ekwurzel et al., 2001; McLaughlin et al., 1996; Rigor et al., 2002; Rudels, 2015; Schlosser et al., 1994). However, to the best of our knowledge, there are no published estimates of the mass transport associated with the TPD. Fortunately, Kipp et al. (2018) reported two independent estimates of the transport time scale of the TPD in 2015 from the eastern Arctic shelf break (78°N) to ~88°N. Using radionuclide tracers (^{228}Th/^{228}Ra), transport was in the range of 6-12 months or 0.04-0.08 m/s. Ice back trajectory analysis suggested a time scale of 8 to 18 months for the GEOTRACES stations within the TPD; assuming a transport distance of 1200 km, mean current speeds would be in the range of 0.03-0.06 m/s. Separately, Kadko et al. (2016) modeled the decay of atmospherically-derived ^{7}Be during transport under the ice to derive an average TPD current speed of 0.10 m/s. Combined, the average current speed for the TPD is thus 0.059 ± 0.030 m/s, which is equivalent to a mass transport of 0.9 ± 0.4 Sv if we assume the width and depth of the current are 600 km and 25 m, respectively (see Methods for details on how the horizontal extent of the TPD was defined). Considering that this current is approximately 20% meteoric water, the lower bound of this flux estimate (0.5 Sv x 0.2 = 0.10 Sv) compares well with the total Eurasian river runoff estimates of 2800 km^3/y or 0.09 Sv (Lammers et al., 2001) and 3264 km^3/y or 0.10 Sv (Sonke et al., 2018). This ground-truthing exercise does not account for direct precipitation to Arctic Ocean surface waters, which is of the same order of magnitude as river runoff on a basin-wide scale (Serreze et al., 2006). However, the fact that the Eurasian river runoff is more closely aligned with the lower bound of our meteoric water-corrected mass transport estimate may also be owed to (1) an overestimate in our TPD cross sectional area or (2) a larger contribution of North American rivers to the freshwater component of the TPD. This latter point might be a further explanation for the scatter in some of our TEI/meteoric water relationships.

Fluxes of TEIs with strong linear correlations to meteoric water can be reasonably estimated because we can assume they are approximately conserved away from the shelves. These include dFe, dCu, dNi, d^{232}Th, dNd, and DOC. For the purposes of these flux calculations, we assume that the TPD source waters leaving the Siberian shelves consist of 20% meteoric

water. Dissolved Fe (r^2 = 0.67) had a concentration equal to 3.6 nmol L^{-1} at 20% meteoric water. With a mass transport of 0.9 Sv, the shelf derived Fe flux in the TPD is 1.0 ± 0.5 x 10^8 mol y^{-1} (Table 3). Kadko et al. (2019) quantified the atmospheric deposition of soluble Fe to the GEOTRACES TPD stations as 0.61±0.17 nmol/m^2/d. Scaling this estimate up to the Arctic Ocean basin (9.5x10^{12} m^2; Jakobsson, 2002) produces a total atmospheric deposition flux of 2.1 ± 0.6 x 10^6 mol y^{-1}, which is only 2% of the shelf-basin flux of Fe derived from the TPD. Kadko et al (2019), using an approach that is independent to our own, arrived at a similar conclusion that the atmospheric input is dwarfed by that delivered through the TPD. By comparison, the shelf-basin flux of dissolved Fe from the Chukchi Sea has been estimated at 9.1-22 x 10^6 mol y^{-1} (Vieira et al., 2019); hence, the Siberian shelves and the TPD are much more efficient transporters of continental margin-derived dissolved Fe to the central Arctic basins than dust. A similar picture emerges for both Cu (2.0 ± 1.0 x 10^8 mol y^{-1}; Table 3), for which atmospheric deposition is only 4% of the shelf input, and Ni (2.4 ± 1.2 x 10^8 mol y^{-1}; Table 3), with a TPD flux that rivals global riverine Ni inputs (3.6 x 10^8 mol y^{-1}; Cameron & Vance, 2014). These disparities highlight the relative importance of boundary TEI inputs in this shelf-dominated and relatively small ocean basin.

Given the highly particle reactive nature of thorium, the dissolved ^{232}Th concentrations observed within the TPD were somewhat surprising. In terms of flux, the TPD is estimated to carry 3.5 ± 1.8 x 10^4 mol y^{-1} of ^{232}Th. If the dust input and solubility of ^{232}Th are ~50 µg/m^2/y (Kienast et al., 2016) and 1% (Hsieh et al., 2011), respectively, then the dissolved input to the Arctic Ocean (assuming no ice cover) would be on the order of 2.1 x 10^4 mol y^{-1}. Such a strong lateral input of ^{232}Th relative to atmospheric deposition would complicate the use of dissolved ^{232}Th as a dust flux proxy in this basin and potentially others where fluvial inputs rich in DOM are entering the ocean (Anderson et al., 2016; Hayes et al., 2013; Kienast et al., 2016; Robinson et al., 2008).

The riverine input of Nd to the Arctic Ocean has not been well constrained owing to the relatively few measurements of Nd concentrations in eastern Arctic rivers and of Nd removal in the estuarine mixing zone. That said, the TPD flux of Nd is 1.2 ± 0.6 x 10^6 mol y^{-1}, which is on par with the global riverine Nd flux (1.8 x 10^6 mol y^{-1}; Arsouze et al., 2009). From recent work we know that sedimentary fluxes of Nd to the ocean may far exceed those from rivers (18-110 x 10^6 mol y^{-1}; Abbott et al., 2015) Yet, the Nd carried in the TPD is lower than expected from a combined discharge-weighted river contribution and hence rather suggests a Nd deficit, providing no evidence for Nd contributions from shelf sediments in the Arctic. Rather, the lower than expected REE concentrations point to the large range in river

endmember REE concentrations, the likelihood of substantial REE removal in the estuaries, and their unknown relative contributions to the TPD. For DOC, the flux carried by the TPD is $3.7 \pm 1.9 \times 10^{12}$ mol y^{-1}, as compared to a total DOC flux from the major Arctic rivers of 2.1-3.0×10^{12} mol y^{-1} (Raymond et al., 2007) indicating a major contribution of terrigenous DOC to the total TPD DOM flux.

5. Conclusions

Intensification of the hydrologic cycle and permafrost degradation may result in the release of about 25% of the carbon stored in Arctic soils in the next 100 years (Gruber et al., 2004). According to the NOAA Arctic report card (Osborne et al., 2018), the 2018 summer/autumn discharge for the largest rivers flowing into the Arctic was 20% greater than in the 1980-89 period and will continue to increase. These changes will have a substantial effect on the riverine supply of DOM into the Arctic Ocean, as well as the long-distance transport of TEIs within the Transpolar Drift that are likely complexed by this organic matter, including Fe, Co, Ni, Cu, Th, and possibly the REEs.

While the halocline contains ample nutrient concentrations, the increased freshwater inputs are strengthening water column stratification, which could further limit nutrient inputs via vertical mixing processes (Rudels et al., 1991). Hence, increased macro- and micro-nutrient concentrations delivered to the central Arctic Ocean via the TPD may play an important role in upper ocean productivity in the coming decades, since, for example, nitrate already limits primary production in some Arctic locations (Tremblay & Gagnon, 2009), as did Fe in the case of one large under ice bloom, though this was located outside of the TPD (Rijkenberg et al., 2018). In the case of Fe, whether limitation will occur in the changing Arctic will depend on the interplay between nutrient utilization ratios (Rijkenberg et al., 2018) and projected increases of ligand-borne, specifically humic-borne, terrestrial dFe (Slagter et al., 2017, 2019).

The complexity of physical and biochemical factors and their interplay, such as the effect of increased river runoff and stratification on the saturation state of aragonite (Yamamoto-Kawai et al., 2009), combine with scarcity of data to make future effects of TPD influence on the central Arctic difficult to predict (Carmack & McLaughlin, 2011). However, DOM is strongly related to hydrographic parameters and biogeochemical cycles in the shelf seas and TPD (Amon et al., 2003; Granskog et al., 2012), but has the advantage of relatively simple measurement via remote sensing in ice-free waters (Fichot et al., 2013; Juhls et al., 2019; Matsuoka et al., 2017) or *in-situ* instrumentation capable of high vertical resolution such as

the fluorometers deployed on these cruises. Looking to the future, this makes CDOM a powerful tracer of climate change impacts on a multitude of Arctic system processes (e.g. Stedmon et al., 2015).

For some TEIs, the sediments within the broad and shallow eastern Arctic shelves play a dominant role in their cycling and signature within the TPD. Radium isotopic ratios and a mass balance calculation point to shelf sediments as the dominant source of ^{228}Ra carried by the TPD (Kipp et al., 2018). While ^{228}Ra is not a biologically important TEI, it acts as a quasi-conservative tracer of other shelf-derived materials like Ba, which has TPD concentrations that cannot be fully explained by a river source. The Ra-derived evidence of active sediment-water exchange processes in the eastern Arctic coastal zone supports the apparent strong sinks for Pb and V, which are known to be removed by particle scavenging and/or reduction processes in shelf sediments. Increased ^{228}Ra levels in the TPD therefore suggest that the concentrations of these other TEIs may be affected both positively (Ba) or negatively (Pb, Al, Ga, and V) under a changing climate where shelf sediments are exposed to wind-driven mixing under reduced ice cover. This ice loss and its potential impacts on TEI cycling will be exacerbated not only by atmospheric forcing, but also by penetration of warmer Atlantic Ocean waters into the Arctic (e.g. Polyakov et al., 2017).

The TEIs that have the strongest correlation with meteoric water fraction are those that are known to form complexes with organic matter. As a result, other than dilution via mixing, their concentrations, which are significantly elevated relative to other ocean basins, are preserved in the TPD over distances >1000 km and timescales of up to 18 months. It is therefore reasonable to expect that this TEI "fingerprint" of the TPD would be carried beyond the ice covered central Arctic Ocean, through Fram Strait, and into the ice-free surface waters of the North Atlantic Ocean as seen for Arctic river DOM (Amon et al., 2003; Benner et al., 2005; Gerringa et al., 2015; Granskog et al., 2012). In the present day, the TEIs transported in the TPD may become participants in biogeochemical processes of this ocean basin, or in the future be utilized closer to their source as the pan-Arctic ice cover is reduced with warming temperatures. This new utilization would apply to an increasingly ice-free Arctic Ocean including the Canada Basin, where the Beaufort Gyre (Fig. 1) is known to entrain and store an increasing amount of freshwater sourced from eastern Arctic rivers (Giles et al., 2012; Morison et al., 2012; Rabe et al., 2011, 2014).

Lastly, our understanding of the effects of the changing climate on Arctic Ocean TEI concentrations and fluxes has been greatly hampered by a lack of data, mainly due to the logistics and expense of conducting oceanography at high-latitudes where icebreakers are

required for sampling. Geopolitical issues have resulted in large data gaps for the eastern Arctic shelf seas. In the near future, international collaboration through long term observatories at key locations and Arctic gateways, synoptic surveys (e.g. http://www.synopticarcticsurvey.info) and advances in technology (e.g. floats, gliders, ice tethered sensors and samplers) may provide the temporal and spatial coverage needed to address some of the pressing unanswered questions posed herein.

Acknowledgements

The authors thank the editor and two anonymous reviewers for their constructive comments and feedback. This study would not have been possible without the dedication of the captains and crews of the *USCGC Healy* and *R/V Polarstern*. The authors also thank the many members of the shipboard scientific parties, including the chief scientists, who enabled sample collection via the various CTD rosette and *in situ* pumping systems, as well as the sample analyses on the ship and back in their home laboratories. Funding for Arctic GEOTRACES was provided by the U.S. National Science Foundation, Swedish Research Council Formas, French Agence Nationale de la Recherche and LabexMER, Netherlands Organization for Scientific Research, and Independent Research Fund Denmark.

Data from GEOTRACES cruises GN01 (HLY1502) and GN04 (PS94) have been archived at the Biological & Chemical Oceanography Data Management Office (BCO-DMO; https://www.bco-dmo.org/deployment/638807) and PANGAEA (https://www.pangaea.de/?q=PS94&f.campaign%5B%5D=PS94) websites, respectively. The inorganic carbon data are available at the NOAA Ocean Carbon Data System (OCADS; doi:10.3334/CDIAC/OTG.CLIVAR_ARC01_33HQ20150809). In addition to these national data archives, the data used in this paper is available as a supplementary downloadable excel file.

References

Aagaard, K., Coachman, L. K., & Carmack, E. (1981). On the halocline of the Arctic Ocean. *Deep Sea Research Part A, Oceanographic Research Papers*, *28*(6), 529–545. https://doi.org/10.1016/0198-0149(81)90115-1

Abbott, A. N., Haley, B. A., McManus, J., & Reimers, C. E. (2015). The sedimentary flux of dissolved rare earth elements to the ocean. *Geochimica et Cosmochimica Acta*, *154*, 186–200. https://doi.org/10.1016/j.gca.2015.01.010

Abrahamsen, E. P., Meredith, M. P., Falkner, K. K., Torres-Valdes, S., Leng, M. J., Alkire, M. B., et al. (2009). Tracer-derived freshwater composition of the Siberian continental shelf and slope following the extreme Arctic summer of 2007. *Geophysical Research Letters*, *36*(7), L07602. https://doi.org/10.1029/2009GL037341

Agather, A. M., Bowman, K. L., Lamborg, C. H., & Hammerschmidt, C. R. (2019). Distribution of mercury species in the Western Arctic Ocean (U.S. GEOTRACES GN01). *Marine Chemistry*, *216*, 103686. https://doi.org/10.1016/j.marchem.2019.103686

Aguilar-Islas, A. M., Rember, R., Nishino, S., Kikuchi, T., & Itoh, M. (2013). Partitioning and lateral transport of iron to the Canada Basin. *Polar Science*, *7*(2), 82–99. https://doi.org/10.1016/J.POLAR.2012.11.001

Alkire, M. B., Morison, J., & Andersen, R. (2015). Variability in the meteoric water, sea-ice melt, and Pacific water contributions to the central Arctic Ocean, 2000-2014. *Journal of Geophysical Research: Oceans*, *120*(3), 1573–1598. https://doi.org/10.1002/2014JC010023

Alling, V., Sanchez-Garcia, L., Porcelli, D., Pugach, S., Vonk, J. E., van Dongen, B., et al. (2010). Nonconservative behavior of dissolved organic carbon across the Laptev and East Siberian seas. *Global Biogeochemical Cycles*, *24*(4), GB4033. https://doi.org/10.1029/2010GB003834

Amon, R. M. W. (2004). The Role of Dissolved Organic Matter for the Organic Carbon Cycle in the Arctic Ocean. In *The Organic Carbon Cycle in the Arctic Ocean* (pp. 83–99). Berlin, Heidelberg: Springer Berlin Heidelberg. https://doi.org/10.1007/978-3-642-18912-8_4

Amon, R. M. W., & Meon, B. (2004). The biogeochemistry of dissolved organic matter and nutrients in two large Arctic estuaries and potential implications for our understanding of the Arctic Ocean system. *Marine Chemistry*, *92*, 311–330. https://doi.org/10.1016/j.marchem.2004.06.034

Amon, R. M. W., Budéus, G., & Meon, B. (2003). Dissolved organic carbon distribution and origin in the Nordic Seas: Exchanges with the Arctic Oean and the North Atlantic. *Journal of Geophysical Research C: Oceans*, *108*(C7), 1–17. https://doi.org/10.1029/2002jc001594

Amon, R. M. W., Rinehart, A. J., Duan, S., Louchouarn, P., Prokushkin, A., Guggenberger, G., et al. (2012). Dissolved organic matter sources in large Arctic rivers. *Geochimica et Cosmochimica Acta*, *94*, 217–237. https://doi.org/10.1016/J.GCA.2012.07.015

Amos, H. M., Jacob, D. J., Kocman, D., Horowitz, H. M., Zhang, Y., Dutkiewicz, S., et al. (2014). Global biogeochemical implications of mercury discharges from rivers and sediment burial. *Environmental Science and Technology*, *48*(16), 9514–9522. https://doi.org/10.1021/es502134t

Anderson, L. G., & Amon, R. M. W. (2014). DOM in the Arctic Ocean. In *Biogeochemistry of Marine Dissolved Organic Matter: Second Edition* (pp. 609–633). Academic Press. https://doi.org/10.1016/B978-0-12-405940-5.00014-5

Anderson, L. G., Jutterström, S., Hjalmarsson, S., Wåhlström, I., & Semiletov, I. P. (2009). Out-gassing of CO2 from Siberian Shelf seas by terrestrial organic matter decomposition. *Geophysical Research Letters*, *36*(20), L20601. https://doi.org/10.1029/2009GL040046

Anderson, L. G., Ek, J., Ericson, Y., Humborg, C., Semiletov, I., Sundbom, M., & Ulfsbo, A. (2017). Export of calcium carbonate corrosive waters from the East Siberian Sea. *Biogeosciences*, *14*(7), 1811–1823. https://doi.org/10.5194/bg-14-1811-2017

Anderson, L. G., Björk, G., Holby, O., Jutterström, S., Magnus Mörth, C., O'Regan, M., et al. (2017). Shelf-Basin interaction along the East Siberian Sea. *Ocean Science*, *13*(2), 349–363. https://doi.org/10.5194/os-13-349-2017

Anderson, R. F., Fleisher, M. Q., Robinson, L. F., Edwards, R. L., Hoff, J. A., Moran, S. B., et al. (2012). GEOTRACES intercalibration of 230Th, 232Th, 231Pa, and prospects for 10Be. *Limnology and Oceanography: Methods*, *10*, 179–213. https://doi.org/10.4319/lom.2012.10.179

Anderson, R. F., Cheng, H., Edwards, R. L., Fleisher, M. Q., Hayes, C. T., Huang, K. F., et al. (2016). How well can we quantify dust deposition to the ocean? *Philosophical Transactions of the Royal Society A: Mathematical, Physical and Engineering Sciences*, *374*(2081), 20150285. https://doi.org/10.1098/rsta.2015.0285

Andersson, P. S., Porcelli, D., Frank, M., Björk, G., Dahlqvist, R., & Gustafsson, Ö. (2008). Neodymium isotopes in seawater from the Barents Sea and Fram Strait Arctic-Atlantic

gateways. *Geochimica et Cosmochimica Acta*, *72*(12), 2854–2867. https://doi.org/10.1016/j.gca.2008.04.008

Arrigo, K. R., & van Dijken, G. L. (2011). Secular trends in Arctic Ocean net primary production. *Journal of Geophysical Research*, *116*(C9), C09011. https://doi.org/10.1029/2011JC007151

Arrigo, K. R., van Dijken, G., & Pabi, S. (2008). Impact of a shrinking Arctic ice cover on marine primary production. *Geophysical Research Letters*, *35*(19), L19603. https://doi.org/10.1029/2008GL035028

Arsouze, T., Dutay, J.-C., Lacan, F., & Jeandel, C. (2009). Reconstructing the Nd oceanic cycle using a coupled dynamical – biogeochemical model. *Biogeosciences*, *6*(12), 2829–2846. https://doi.org/10.5194/bg-6-2829-2009

Bauch, D., van der Loeff, M. R., Andersen, N., Torres-Valdes, S., Bakker, K., & Abrahamsen, E. P. (2011). Origin of freshwater and polynya water in the Arctic Ocean halocline in summer 2007. *Progress in Oceanography*, *91*(4), 482–495. https://doi.org/10.1016/J.POCEAN.2011.07.017

Behrens, M. K., Muratli, J., Pradoux, C., Wu, Y., Böning, P., Brumsack, H. J., et al. (2016). Rapid and precise analysis of rare earth elements in small volumes of seawater - Method and intercomparison. *Marine Chemistry*, *186*, 110–120. https://doi.org/10.1016/j.marchem.2016.08.006

Benner, R., Louchouarn, P., & Amon, R. M. W. (2005). Terrigenous dissolved organic matter in the Arctic Ocean and its transport to surface and deep waters of the North Atlantic. *Global Biogeochemical Cycles*, *19*(2), 1–11. https://doi.org/10.1029/2004GB002398

Van Den Berg, C.M.G., & Nimmo, M. (1987). Determination of interactions of nickel with dissolved organic material in seawater using cathodic stripping voltammetry. *Science of The Total Environment*, *60*(C), 185–195. https://doi.org/10.1016/0048-9697(87)90415-3

van den Berg, Constant M.G. (1995). Evidence for organic complexation of iron in seawater. *Marine Chemistry*, *50*(1–4), 139–157. https://doi.org/10.1016/0304-4203(95)00032-M

Bishop, J. K. B. (1988). The barite-opal-organic carbon association in oceanic particulate matter. *Nature*, *332*(6162), 341–343. https://doi.org/10.1038/332341a0

Black, E. E. (2018). An investigation of basin-scale controls on upper ocean export and remineralization. *Thesis*. Massachusetts Institute of Technology. https://doi.org/10.1575/1912/9576

Boyle, E., Collier, R., Dengler, A. T., Edmond, J. M., Ng, A. C., & Stallard, R. F. (1974). On the chemical mass-balance in estuaries. *Geochimica et Cosmochimica Acta*, *38*(11),

1719–1728. https://doi.org/10.1016/0016-7037(74)90188-4

Brinza, L., Benning, L. G., & Statham, P. J. (2008). Adsorption studies of Mo and Vonto ferrihydrite. *Mineralogical Magazine*, *72*(1), 385–388. https://doi.org/10.1180/minmag.2008.072.1.385

Brown, K. A., McLaughlin, F., Tortell, P. D., Varela, D. E., Yamamoto-Kawai, M., Hunt, B., & Francois, R. (2014). Determination of particulate organic carbon sources to the surface mixed layer of the Canada Basin, Arctic Ocean. *Journal of Geophysical Research: Oceans*, *119*(2), 1084–1102. https://doi.org/10.1002/2013JC009197

Brown, K. A., McLaughlin, F., Tortell, P. D., Yamamoto-Kawai, M., & Francois, R. (2016). Sources of dissolved inorganic carbon to the Canada Basin halocline: A multitracer study. *Journal of Geophysical Research: Oceans*, *121*(5), 2918–2936. https://doi.org/10.1002/2015JC011535

Bruland, K. W. (1989). Complexation of zinc by natural organic ligands in the central North Pacific. *Limnology and Oceanography*, *34*(2), 269–285. https://doi.org/10.4319/lo.1989.34.2.0269

Bruland, K. W., Middag, R., & Lohan, M. C. (2013). Controls of Trace Metals in Seawater. In *Treatise on Geochemistry: Second Edition* (Vol. 8, pp. 19–51). Elsevier Inc. https://doi.org/10.1016/B978-0-08-095975-7.00602-1

Bundy, R. M., Abdulla, H. A. N., Hatcher, P. G., Biller, D. V, Buck, K. N., & Barbeau, K. A. (2015). Iron-binding ligands and humic substances in the San Francisco Bay estuary and estuarine-influenced shelf regions of coastal California. *Marine Chemistry*, *173*, 183–194. https://doi.org/10.1016/j.marchem.2014.11.005

Cameron, V., & Vance, D. (2014). Heavy nickel isotope compositions in rivers and the oceans. *Geochimica et Cosmochimica Acta*, *128*, 195–211. https://doi.org/10.1016/j.gca.2013.12.007

Carmack, E. C., & McLaughlin, F. (2011). Towards recognition of physical and geochemical change in Subarctic and Arctic Seas. *Progress in Oceanography*, *90*(1–4), 90–104. https://doi.org/10.1016/j.pocean.2011.02.007

Carmack, E. C., Yamamoto-Kawai, M., Haine, T. W. N., Bacon, S., Bluhm, B. A., Lique, C., et al. (2016). Freshwater and its role in the Arctic Marine System: Sources, disposition, storage, export, and physical and biogeochemical consequences in the Arctic and global oceans. *Journal of Geophysical Research G: Biogeosciences*, *121*(3), 675–717. https://doi.org/10.1002/2015JG003140

Chang, B. X., & Devol, A. H. (2009). Seasonal and spatial patterns of sedimentary

denitrification rates in the Chukchi sea. *Deep Sea Research Part II: Topical Studies in Oceanography*, *56*(17), 1339–1350. https://doi.org/10.1016/J.DSR2.2008.10.024

Charkin, A. N., Rutgers van der Loeff, M., Shakhova, N. E., Gustafsson, Ö., Dudarev, O. V., Cherepnev, M. S., et al. (2017). Discovery and characterization of submarine groundwater discharge in the Siberian Arctic seas: a case study in the Buor-Khaya Gulf, Laptev Sea. *The Cryosphere*, *11*(5), 2305–2327. https://doi.org/10.5194/tc-11-2305-2017

Cid, A. P., Nakatsuka, S., & Sohrin, Y. (2012). Stoichiometry among bioactive trace metals in the Chukchi and Beaufort Seas. *Journal of Oceanography*, *68*(6), 985–1001. https://doi.org/10.1007/s10872-012-0150-8

Coffey, M., Dehairs, F., Collette, O., Luther, G., Church, T., & Jickells, T. (1997). The Behaviour of Dissolved Barium in Estuaries. *Estuarine, Coastal and Shelf Science*, *45*(1), 113–121. https://doi.org/10.1006/ecss.1996.0157

Colombo, M., Brown, K. A., De Vera, J., Bergquist, B. A., & Orians, K. J. (2019). Trace metal geochemistry of remote rivers in the Canadian Arctic Archipelago. *Chemical Geology*, *525*, 479–491. https://doi.org/10.1016/j.chemgeo.2019.08.006

Conrad, S., Ingri, J., Gelting, J., Nordblad, F., Engström, E., Rodushkin, I., et al. (2019). Distribution of Fe isotopes in particles and colloids in the salinity gradient along the Lena River plume, Laptev Sea. *Biogeosciences*, *16*(6), 1305–1319. https://doi.org/10.5194/bg-16-1305-2019

Conway, T. M., & John, S. G. (2014). Quantification of dissolved iron sources to the North Atlantic Ocean. *Nature*, *511*(7508), 212–215. https://doi.org/10.1038/nature13482

Conway, T. M., Rosenberg, A. D., Adkins, J. F., & John, S. G. (2013). A new method for precise determination of iron, zinc and cadmium stable isotope ratios in seawater by double-spike mass spectrometry. *Analytica Chimica Acta*, *793*, 44–52. https://doi.org/10.1016/j.aca.2013.07.025

Cooper, L. W., McClelland, J. W., Holmes, R. M., Raymond, P. A., Gibson, J. J., Guay, C. K., & Peterson, B. J. (2008). Flow-weighted values of runoff tracers (δ18O, DOC, Ba, alkalinity) from the six largest Arctic rivers. *Geophysical Research Letters*, *35*(18), L18606. https://doi.org/10.1029/2008GL035007

Cossa, D., Heimbürger, L. E., Pérez, F. F., García-Ibáñez, M. I., Sonke, J. E., Planquette, H., et al. (2018). Mercury distribution and transport in the North Atlantic Ocean along the GEOTRACES-GA01 transect. *Biogeosciences*, *15*(8), 2309–2323. https://doi.org/10.5194/bg-15-2309-2018

Crans, D. C., Smee, J. J., Gaidamauskas, E., & Yang, L. (2004). The Chemistry and Biochemistry of Vanadium and the Biological Activities Exerted by Vanadium Compounds. *Chemical Reviews*. American Chemical Society. https://doi.org/10.1021/cr020607t

Cross, J. N., Mathis, J. T., Pickart, R. S., & Bates, N. R. (2018). Formation and transport of corrosive water in the Pacific Arctic region. *Deep-Sea Research Part II: Topical Studies in Oceanography*, *152*, 67–81. https://doi.org/10.1016/j.dsr2.2018.05.020

Cutter, G. A. (2013). Intercalibration in chemical oceanography-Getting the right number. *Limnology and Oceanography: Methods*, *11*(JULY), 418–424. https://doi.org/10.4319/lom.2013.11.418

Cutter, G. A., Andersson, P. S., Codispoti, L., Croot, P. L., Francois, R., Lohan, M. C., et al. (2014). *Sampling and Sample-handing Protocols for GEOTRACES Cruises*. Retrieved from http://www.geotraces.org/images/stories/documents/intercalibration/Cookbook_v2.pdf

Danielsson, L.-G., & Westerlund, S. (1983). Trace Metals in the Arctic Ocean. In *Trace Metals in Sea Water* (pp. 85–95). Boston, MA: Springer US. https://doi.org/10.1007/978-1-4757-6864-0_5

Davis, J., & Benner, R. (2005). Seasonal trends in the abundance, composition and bioavailability of particulate and dissolved organic matter in the Chukchi/Beaufort Seas and western Canada Basin. *Deep-Sea Research Part II: Topical Studies in Oceanography*, *52*(24–26), 3396–3410. https://doi.org/10.1016/j.dsr2.2005.09.006

Dehairs, F., Chesselet, R., & Jedwab, J. (1980). Discrete suspended particles of barite and the barium cycle in the open ocean. *Earth and Planetary Science Letters*, *49*(2), 528–550. https://doi.org/10.1016/0012-821X(80)90094-1

Dickson, A. G., Sabine, C. L., & Christian, J. R. (Eds). (2007). *Guide to best practices for ocean CO2 measurements, PICES Special Publication 3*. IOCCP REPORT No. 8. Retrieved from https://cdiac.ess-dive.lbl.gov/ftp/oceans/Handbook_2007/Guide_all_in_one.pdf

DiMento, B. P., Mason, R. P., Brooks, S., & Moore, C. (2019). The impact of sea ice on the air-sea exchange of mercury in the Arctic Ocean. *Deep-Sea Research Part I: Oceanographic Research Papers*, *144*, 28–38. https://doi.org/10.1016/j.dsr.2018.12.001

Dmitrenko, I. A., Kirillov, S. A., Rudels, B., Babb, D. G., Myers, P. G., Stedmon, C. A., et al. (2019). Variability of the Pacific-Derived Arctic Water Over the Southeastern Wandel Sea Shelf (Northeast Greenland) in 2015–2016. *Journal of Geophysical Research:*

Oceans, *124*(1), 349–373. https://doi.org/10.1029/2018JC014567

Dodd, P. A., Rabe, B., Hansen, E., Falck, E., MacKensen, A., Rohling, E., et al. (2012). The freshwater composition of the Fram Strait outflow derived from a decade of tracer measurements. *Journal of Geophysical Research: Oceans*, *117*(11), C11005. https://doi.org/10.1029/2012JC008011

Donat, J. R., & van den Berg, C. M. G. (1992). A new cathodic stripping voltammetric method for determining organic copper complexation in seawater. *Marine Chemistry*, *38*(1–2), 69–90. https://doi.org/10.1016/0304-4203(92)90068-L

Drake, T. W., Tank, S. E., Zhulidov, A. V., Holmes, R. M., Gurtovaya, T., & Spencer, R. G. M. (2018). Increasing Alkalinity Export from Large Russian Arctic Rivers. *Environmental Science & Technology*, *52*(15), 8302–8308. https://doi.org/10.1021/acs.est.8b01051

Ekwurzel, B., Schlosser, P., Mortlock, R. A., Fairbanks, R. G., & Swift, J. H. (2001). River runoff, sea ice meltwater, and Pacific water distribution and mean residence times in the Arctic Ocean. *Journal of Geophysical Research: Oceans*, *106*(C5), 9075–9092. https://doi.org/10.1029/1999JC000024

Elderfield, H. (1988). The Oceanic Chemistry of the Rare-Earth Elements. *Philosophical Transactions of the Royal Society A: Mathematical, Physical and Engineering Sciences*, *325*(1583), 105–126. https://doi.org/10.1098/rsta.1988.0046

Ellwood, M. J., & Van den Berg, C. M. G. (2001). Determination of organic complexation of cobalt in seawater by cathodic stripping voltammetry. *Marine Chemistry*, *75*(1–2), 33–47. https://doi.org/10.1016/S0304-4203(01)00024-X

Falck, E., Kattner, G., & Budéus, G. (2005). Disappearance of Pacific Water in the northwestern Fram Strait. *Geophysical Research Letters*, *32*(14), 1–4. https://doi.org/10.1029/2005GL023400

Fichot, C. G., Kaiser, K., Hooker, S. B., Amon, R. M. W., Babin, M., Bélanger, S., et al. (2013). Pan-Arctic distributions of continental runoff in the Arctic Ocean. *Scientific Reports*, *3*(1053), 1–6. https://doi.org/10.1038/srep01053

Fisher, J. A., Jacob, D. J., Soerensen, A. L., Amos, H. M., Steffen, A., & Sunderland, E. M. (2012). Riverine source of Arctic Ocean mercury inferred from atmospheric observations. *Nature Geoscience*, *5*(7), 499–504. https://doi.org/10.1038/ngeo1478

Fitzsimmons, J. N., & Boyle, E. A. (2014). Assessment and comparison of Anopore and cross flow filtration methods for the determination of dissolved iron size fractionation into soluble and colloidal phases in seawater. *Limnology and Oceanography: Methods*, *12*,

246–263. https://doi.org/10.4319/lom.2014.12.246

Frey, K. E., & McClelland, J. W. (2009). Impacts of permafrost degradation on arctic river biogeochemistry. *Hydrological Processes*, *23*(1), 169–182. https://doi.org/10.1002/hyp.7196

Frings, P. (2017). Revisiting the dissolution of biogenic Si in marine sediments: a key term in the ocean Si budget. *Acta Geochimica*, *36*(3), 429–432. https://doi.org/10.1007/s11631-017-0183-1

Gaillardet, J., Viers, J., & Dupré, B. (2014). Trace Elements in River Waters. In *Treatise on Geochemistry: Second Edition* (Vol. 7, pp. 195–235). Elsevier Inc. https://doi.org/10.1016/B978-0-08-095975-7.00507-6

Gdaniec, S., Roy-Barman, M., Levier, M., Valk, O., van der Loeff, M. R., Foliot, L., et al. (2020). 231Pa and 230Th in the Arctic Ocean: Implications for boundary scavenging and 231Pa-230Th fractionation in the Eurasian Basin. *Chemical Geology*, *532*. https://doi.org/10.1016/j.chemgeo.2019.119380

Gerringa, L. J. A., Rijkenberg, M. J. A., Schoemann, V., Laan, P., & de Baar, H. J. W. (2015). Organic complexation of iron in the West Atlantic Ocean. *Marine Chemistry*, *177*, 434–446. https://doi.org/10.1016/j.marchem.2015.04.007

Giles, K. A., Laxon, S. W., Ridout, A. L., Wingham, D. J., & Bacon, S. (2012). Western Arctic Ocean freshwater storage increased by wind-driven spin-up of the Beaufort Gyre. *Nature Geoscience*, *5*(3), 194–197. https://doi.org/10.1038/ngeo1379

Granskog, M. A., Stedmon, C. A., Dodd, P. A., Amon, R. M. W., Pavlov, A. K., De Steur, L., & Hansen, E. (2012). Characteristics of colored dissolved organic matter (CDOM) in the Arctic outflow in the Fram Strait: Assessing the changes and fate of terrigenous CDOM in the Arctic Ocean. *Journal of Geophysical Research: Oceans*, *117*(12), C12021. https://doi.org/10.1029/2012JC008075

Granskog, M. A., Pavlov, A. K., Sagan, S., Kowalczuk, P., Raczkowska, A., & Stedmon, C. A. (2015). Effect of sea-ice melt on inherent optical properties and vertical distribution of solar radiant heating in Arctic surface waters. *Journal of Geophysical Research: Oceans*, *120*(10), 7028–7039. https://doi.org/10.1002/2015JC011087

Griffin, C. G., McClelland, J. W., Frey, K. E., Fiske, G., & Holmes, R. M. (2018). Quantifying CDOM and DOC in major Arctic rivers during ice-free conditions using Landsat TM and ETM+ data. *Remote Sensing of Environment*, *209*, 395–409. https://doi.org/10.1016/J.RSE.2018.02.060

Gruber, N., Friedlingstein, P., Field, C., Valentini, R., Heimann, M., Richey, J., et al. (2004).

The vulnerability of the carbon cycle in the 21st century: an assessment of carbon-climate-human interactions. In C. B. Field & M. R. Raupach (Eds.), *Toward CO2 Stabilization: Issues, Strategies, and Consequences* (pp. 45–76). Washington, DC: Island Press.

Guay, C. K. H., & Falkner, K. K. (1997). Barium as a tracer of Arctic halocline and river waters. *Deep-Sea Research Part II: Topical Studies in Oceanography*, *44*(8), 1543–1559. https://doi.org/10.1016/S0967-0645(97)00066-0

Guay, C. K. H., & Falkner, K. K. (1998). A survey of dissolved barium in the estuaries of major Arctic rivers and adjacent seas. *Continental Shelf Research*, *18*(8), 859–882. https://doi.org/10.1016/S0278-4343(98)00023-5

Guay, C. K. H., McLaughlin, F. A., & Yamamoto-Kawai, M. (2009). Differentiating fluvial components of upper Canada Basin waters on the basis of measurements of dissolved barium combined with other physical and chemical tracers. *Journal of Geophysical Research*, *114*(C1), C00A09. https://doi.org/10.1029/2008JC005099

Guéguen, C., McLaughlin, F. A., Carmack, E. C., Itoh, M., Narita, H., & Nishino, S. (2012). The nature of colored dissolved organic matter in the southern Canada Basin and East Siberian Sea. *Deep-Sea Research Part II: Topical Studies in Oceanography*, *81–84*, 102–113. https://doi.org/10.1016/j.dsr2.2011.05.004

Guieu, C., Huang, W. W., Martin, J.-M., & Yong, Y. Y. (1996). Outflow of trace metals into the Laptev Sea by the Lena River. *Marine Chemistry*, *53*(3–4), 255–267. https://doi.org/10.1016/0304-4203(95)00093-3

Hammerschmidt, C. R., & Fitzgerald, W. F. (2006). Methylmercury cycling in sediments on the continental shelf of southern New England. *Geochimica et Cosmochimica Acta*, *70*(4), 918–930. https://doi.org/10.1016/j.gca.2005.10.020

Hansell, D. A. (2005). Dissolved Organic Carbon Reference Material Program. *Eos, Transactions American Geophysical Union*, *86*(35), 318. https://doi.org/10.1029/2005EO350003

Hansell, D. A., Kadko, D., & Bates, N. R. (2004). Degradation of Terrigenous Dissolved Organic Carbon in the Western Arctic Ocean. *Science*, *304*(5672), 858–861. https://doi.org/10.1126/science.1096175

Hatta, M., Measures, C. I., Wu, J., Roshan, S., Fitzsimmons, J. N., Sedwick, P., & Morton, P. (2015). An overview of dissolved Fe and Mn distributions during the 2010-2011 U.S. GEOTRACES north Atlantic cruises: GEOTRACES GA03. *Deep-Sea Research Part II: Topical Studies in Oceanography*, *116*, 117–129.

https://doi.org/10.1016/j.dsr2.2014.07.005

Hayes, C. T., Anderson, R. F., Fleisher, M. Q., Serno, S., Winckler, G., & Gersonde, R. (2013). Quantifying lithogenic inputs to the North Pacific Ocean using the long-lived thorium isotopes. *Earth and Planetary Science Letters*, *383*, 16–25. https://doi.org/10.1016/J.EPSL.2013.09.025

Heimbürger, L. E., Sonke, J. E., Cossa, D., Point, D., Lagane, C., Laffont, L., et al. (2015). Shallow methylmercury production in the marginal sea ice zone of the central Arctic Ocean. *Scientific Reports*, *5*(1), 10318. https://doi.org/10.1038/srep10318

Hirose, K., & Tanoue, E. (2001). Strong ligands for thorium complexation in marine bacteria. *Marine Environmental Research*, *51*(2), 95–112. https://doi.org/10.1016/S0141-1136(00)00031-3

Ho, P., Resing, J. A., & Shiller, A. M. (2019). Processes controlling the distribution of dissolved Al and Ga along the U.S. GEOTRACES East Pacific Zonal Transect (GP16). *Deep-Sea Research Part I: Oceanographic Research Papers*, *147*, 128–145. https://doi.org/10.1016/j.dsr.2019.04.009

Hölemann, J. A., Schirmacher, M., & Prange, A. (2005). Seasonal variability of trace metals in the Lena River and the southeastern Laptev Sea: Impact of the spring freshet. *Global and Planetary Change*, *48*(1–3), 112–125. https://doi.org/10.1016/J.GLOPLACHA.2004.12.008

Hollweg, T. A., Gilmour, C. C., & Mason, R. P. (2010). Mercury and methylmercury cycling in sediments of the mid-Atlantic continental shelf and slope. *Limnology and Oceanography*, *55*(6), 2703–2722. https://doi.org/10.4319/lo.2010.55.6.2703

Holmes, R. M., McClelland, J. W., Peterson, B. J., Tank, S. E., Bulygina, E., Eglinton, T. I., et al. (2012). Seasonal and Annual Fluxes of Nutrients and Organic Matter from Large Rivers to the Arctic Ocean and Surrounding Seas. *Estuaries and Coasts*, *35*(2), 369–382. https://doi.org/10.1007/s12237-011-9386-6

Holmes, R. M., McClelland, J. W., Tank, S. E., Spencer, R. G. M., & Shiklomanov, A. I. (2019). Arctic Great Rivers Observatory. Water Quality Dataset, Version 20190904. Retrieved from https://arcticgreatrivers.org/data

Hood, E. M., Sabine, C. L., & Sloyan, B. M. (Eds.). (2010). *The GO-SHIP Repeat Hydrography Manual: A Collection of Expert Reports and Guidelines*. IOCCP Report Number 14, ICPO Publication Series Number 134. Retrieved from http://www.go-ship.org/HydroMan.html

Hsieh, Y.-T., Henderson, G. M., & Thomas, A. L. (2011). Combining seawater 232Th and

230Th concentrations to determine dust fluxes to the surface ocean. *Earth and Planetary Science Letters*, *312*(3–4), 280–290. https://doi.org/10.1016/J.EPSL.2011.10.022

Hunkins, K., & Whitehead, J. A. (1992). Laboratory simulation of exchange through Fram Strait. *Journal of Geophysical Research*, *97*(C7), 299–310. https://doi.org/10.1029/92JC00735

Ilina, S. M., Poitrasson, F., Lapitskiy, S. A., Alekhin, Y. V., Viers, J., & Pokrovsky, O. S. (2013). Extreme iron isotope fractionation between colloids and particles of boreal and temperate organic-rich waters. *Geochimica et Cosmochimica Acta*, *101*, 96–111. https://doi.org/10.1016/J.GCA.2012.10.023

Jacquet, S. H. M., Dehairs, F., Cardinal, D., Navez, J., & Delille, B. (2005). Barium distribution across the Southern Ocean frontal system in the Crozet-Kerguelen Basin. *Marine Chemistry*, *95*(3–4), 149–162. https://doi.org/10.1016/j.marchem.2004.09.002

Jakobsson, M. (2002). Hypsometry and volume of the Arctic Ocean and its constituent seas. *Geochemistry, Geophysics, Geosystems*, *3*(5), 1–18. https://doi.org/10.1029/2001GC000302

Jensen, L. T., Wyatt, N. J., Twining, B. S., Rauschenberg, S., Landing, W. M., Sherrell, R. M., & Fitzsimmons, J. N. (2019). Biogeochemical Cycling of Dissolved Zinc in the Western Arctic (Arctic GEOTRACES GN01). *Global Biogeochemical Cycles*, *33*(3), 343–369. https://doi.org/10.1029/2018GB005975

Ji, R., Jin, M., & Varpe, Ø. (2013). Sea ice phenology and timing of primary production pulses in the Arctic Ocean. *Global Change Biology*, *19*(3), 734–741. https://doi.org/10.1111/gcb.12074

John, S. G., Mendez, J., Moffett, J., & Adkins, J. (2012). The flux of iron and iron isotopes from San Pedro Basin sediments. *Geochimica et Cosmochimica Acta*, *93*, 14–29. https://doi.org/10.1016/J.GCA.2012.06.003

Jones, D. G. (2001). Development and application of marine gamma-ray measurements: A review. *Journal of Environmental Radioactivity*, *53*(3), 313–333. https://doi.org/10.1016/S0265-931X(00)00139-9

Jones, E. M., & Ulfsbo, A. (2017). Seawater carbonate chemistry (TA, DIC, pH) measured on water bottle samples during POLARSTERN cruise PS94 (ARK-XXIX/3). https://doi.org/10.1016/S0304-4203(99)00020-1

Jones, E. P., & Anderson, L. G. (1986). On the origin of the chemical properties of the Arctic Ocean halocline. *Journal of Geophysical Research*, *91*(C9), 10759. https://doi.org/10.1029/JC091iC09p10759

Jones, E. P., & Anderson, L. G. (2008). Is the global conveyor belt threatened by arctic ocean fresh water outflow? In *Arctic-Subarctic Ocean Fluxes: Defining the Role of the Northern Seas in Climate* (pp. 385–404). Dordrecht: Springer Netherlands. https://doi.org/10.1007/978-1-4020-6774-7_17

Jones, E. P., Swift, J. H., Anderson, L. G., Lipizer, M., Civitarese, G., Falkner, K. K., et al. (2003). Tracing Pacific water in the North Atlantic Ocean. *Journal of Geophysical Research*, *108*(C4), 3116. https://doi.org/10.1029/2001JC001141

Juhls, B., Paul Overduin, P., Hölemann, J., Hieronymi, M., Matsuoka, A., Heim, B., & Fischer, J. (2019). Dissolved organic matter at the fluvial-marine transition in the Laptev Sea using in situ data and ocean colour remote sensing. *Biogeosciences*, *16*(13), 2693–2713. https://doi.org/10.5194/bg-16-2693-2019

Kadko, D., Millero, F., Woosley, R., Hansel, D., Swift, J., Landing, W., et al. (2016). Carbon Dioxide, Hydrographic, and Chemical Data Obtained During the R/V Healy Cruise ARC01 in the Arctic Ocean (9 August - 12 October, 2015). https://doi.org/10.3334/CDIAC/OTG.CLIVAR_ARC01_33HQ20150809

Kadko, D., Galfond, B., Landing, W. M., & Shelley, R. U. (2016). Determining the pathways, fate, and flux of atmospherically derived trace elements in the arctic ocean/ice system. *Marine Chemistry*, *182*, 38–50. https://doi.org/10.1016/j.marchem.2016.04.006

Kadko, D., Aguilar-Islas, A., Bolt, C., Buck, C. S., Fitzsimmons, J. N., Jensen, L. T., et al. (2019). The residence times of trace elements determined in the surface Arctic Ocean during the 2015 US Arctic GEOTRACES expedition. *Marine Chemistry*, *208*, 56–69. https://doi.org/10.1016/j.marchem.2018.10.011

Kaiser, K., Canedo-Oropeza, M., McMahon, R., & Amon, R. M. W. (2017). Origins and transformations of dissolved organic matter in large Arctic rivers. *Scientific Reports*, *7*(1), 13064. https://doi.org/10.1038/s41598-017-12729-1

Kaiser, K., Benner, R., & Amon, R. M. W. (2017). The fate of terrigenous dissolved organic carbon on the Eurasian shelves and export to the North Atlantic. *Journal of Geophysical Research: Oceans*, *122*(1), 4–22. https://doi.org/10.1002/2016JC012380

Kienast, S. S., Winckler, G., Lippold, J., Albani, S., & Mahowald, N. M. (2016). Tracing dust input to the global ocean using thorium isotopes in marine sediments: ThoroMap. *Global Biogeochemical Cycles*, *30*(10), 1526–1541. https://doi.org/10.1002/2016GB005408

Kipp, L. E., Charette, M. A., Moore, W. S., Henderson, P. B., & Rigor, I. G. (2018). Increased fluxes of shelf-derived materials to the central Arctic Ocean. *Science*

Advances, *4*(1), 1–10. https://doi.org/10.1126/sciadv.aao1302

Kipp, L. E., Kadko, D. C., Pickart, R. S., Henderson, P. B., Moore, W. S., & Charette, M. A. (2019). Shelf-basin interactions and water mass residence times in the Western Arctic Ocean: insights provided by radium isotopes. *Journal of Geophysical Research: Oceans*, *124*(5), 2019JC014988. https://doi.org/10.1029/2019JC014988

Kipp, L. E., Henderson, P. B., Wang, Z. A., & Charette, M. A. (2020). Deltaic and estuarine controls on Mackenzie River solute fluxes to the Arctic Ocean. *Estuaries and Coasts*. https://doi.org/10.1007/s12237-020-00739-8

Kirchman, D. L., Malmstrom, R. R., & Cottrell, M. T. (2005). Control of bacterial growth by temperature and organic matter in the Western Arctic. *Deep Sea Research Part II: Topical Studies in Oceanography*, *52*(24–26), 3386–3395. https://doi.org/10.1016/J.DSR2.2005.09.005

Klunder, M. B., Laan, P., Middag, R., de Baar, H. J. W., & Bakker, K. (2012). Dissolved iron in the Arctic Ocean: Important role of hydrothermal sources, shelf input and scavenging removal. *Journal of Geophysical Research: Oceans*, *117*(C4), n/a-n/a. https://doi.org/10.1029/2011JC007135

Klunder, M. B., Bauch, D., Laan, P., de Baar, H. J. W., van Heuven, S., & Ober, S. (2012). Dissolved iron in the Arctic shelf seas and surface waters of the central Arctic Ocean: Impact of Arctic river water and ice-melt. *Journal of Geophysical Research: Oceans*, *117*(C1), 1–18. https://doi.org/10.1029/2011JC007133

Köhler, H., Meon, B., Gordeev, V. V., Spitzy, A., & Amon, R. M. W. (2003). Dissolved organic matter (DOM) in the estuaries of Ob and Yenisei and the adjacent Kara Sea. In R. Stein, K. Fahl, D. K. Fütterer, E. M. Galimov, & O. V. Stepanets (Eds.), *Siberian River Run-Off in the Kara Sea: Characterization, Quantification,Variability and Environmental Significance* (pp. 281–308). Amsterdam: Proceedings in Marine Science, Elsevier.

Kondo, Y., Obata, H., Hioki, N., Ooki, A., Nishino, S., Kikuchi, T., & Kuma, K. (2016). Transport of trace metals (Mn, Fe, Ni, Zn and Cd) in the western Arctic Ocean (Chukchi Sea and Canada Basin) in late summer 2012. *Deep Sea Research Part I: Oceanographic Research Papers*, *116*, 236–252. https://doi.org/10.1016/J.DSR.2016.08.010

Krumpen, T., Belter, H. J., Boetius, A., Damm, E., Haas, C., Hendricks, S., et al. (2019). Arctic warming interrupts the Transpolar Drift and affects long-range transport of sea ice and ice-rafted matter. *Scientific Reports*, *9*(1), 5459. https://doi.org/10.1038/s41598-019-41456-y

Laglera, L. M., Sukekava, C., Slagter, H. A., Downes, J., Aparicio-Gonzalez, A., & Gerringa, L. J. A. (2019). First Quantification of the Controlling Role of Humic Substances in the Transport of Iron across the Surface of the Arctic Ocean. *Environmental Science and Technology*, *53*(22), 13136–13145. https://doi.org/10.1021/acs.est.9b04240

Lam, P. J., Lee, J. M., Heller, M. I., Mehic, S., Xiang, Y., & Bates, N. R. (2018). Size-fractionated distributions of suspended particle concentration and major phase composition from the U.S. GEOTRACES Eastern Pacific Zonal Transect (GP16). *Marine Chemistry*, *201*, 90–107. https://doi.org/10.1016/j.marchem.2017.08.013

Lamborg, C. H., Hammerschmidt, C. R., Gill, G. A., Mason, R. P., & Gichuki, S. (2012). An intercomparison of procedures for the determination of total mercury in seawater and recommendations regarding mercury speciation during GEOTRACES cruises. *Limnology and Oceanography: Methods*, *10*, 90–100. https://doi.org/10.4319/lom.2012.10.90

Lammers, R. B., Shiklomanov, A. I., Vörösmarty, C. J., Fekete, B. M., & Peterson, B. J. (2001). Assessment of contemporary Arctic river runoff based on observational discharge records. *Journal of Geophysical Research Atmospheres*, *106*(D4), 3321–3334. https://doi.org/10.1029/2000JD900444

Landing, W. M., Cutter, G., & Kadko, D. C. (2019a). Bottle data from the CTD-ODF carousel on the GEOTRACES Arctic Section cruise (HLY1502) from August to October 2015 (U.S. GEOTRACES Arctic project). *Biological and Chemical Oceanography Data Management Office (BCO-DMO)*. https://doi.org/10.1575/1912/bco-dmo.646825.4

Landing, W. M., Cutter, G., & Kadko, D. C. (2019b). Bottle data from the GEOTRACES Clean Carousel sampling system (GTC) on the Arctic Section cruise (HLY1502) from August to October 2015 (U.S. GEOTRACES Arctic project). *Biological and Chemical Oceanography Data Management Office (BCO-DMO)*. https://doi.org/10.1575/1912/bco-dmo.647259.4

Laukert, G., Frank, M., Bauch, D., Hathorne, E. C., Gutjahr, M., Janout, M., & Hölemann, J. (2017). Transport and transformation of riverine neodymium isotope and rare earth element signatures in high latitude estuaries: A case study from the Laptev Sea. *Earth and Planetary Science Letters*, *477*, 205–217. https://doi.org/10.1016/J.EPSL.2017.08.010

Letscher, R. T., Hansell, D. A., & Kadko, D. (2011). Rapid removal of terrigenous dissolved organic carbon over the Eurasian shelves of the Arctic Ocean. *Marine Chemistry*,

123(1–4), 78–87. https://doi.org/10.1016/J.MARCHEM.2010.10.002

Little, S. H., Vance, D., Walker-Brown, C., & Landing, W. M. (2014). The oceanic mass balance of copper and zinc isotopes, investigated by analysis of their inputs, and outputs to ferromanganese oxide sediments. *Geochimica et Cosmochimica Acta*, *125*, 673–693. https://doi.org/10.1016/j.gca.2013.07.046

Mackin, J. E., & Aller, R. C. (1984). Processes affecting the behavior of dissolved aluminum in estuarine waters. *Marine Chemistry*, *14*(3), 213–232. https://doi.org/10.1016/0304-4203(84)90043-4

Marsay, C. M., Aguilar-Islas, A., Fitzsimmons, J. N., Hatta, M., Jensen, L. T., John, S. G., et al. (2018). Dissolved and particulate trace elements in late summer Arctic melt ponds. *Marine Chemistry*, *204*, 70–85. https://doi.org/10.1016/J.MARCHEM.2018.06.002

Mathis, J. T., Hansell, D. A., Kadko, D., Bates, N. R., & Cooper, L. W. (2007). Determining net dissolved organic carbon production in the hydrographically complex western Arctic Ocean. *Limnology and Oceanography*, *52*(5), 1789–1799. https://doi.org/10.4319/lo.2007.52.5.1789

Matsuoka, A., Boss, E., Babin, M., Karp-Boss, L., Hafez, M., Chekalyuk, A., et al. (2017). Pan-Arctic optical characteristics of colored dissolved organic matter: Tracing dissolved organic carbon in changing Arctic waters using satellite ocean color data. *Remote Sensing of Environment*, *200*, 89–101. https://doi.org/10.1016/j.rse.2017.08.009

McAlister, J. A., & Orians, K. J. (2012). Calculation of river-seawater endmembers and differential trace metal scavenging in the Columbia River plume. *Estuarine, Coastal and Shelf Science*, *99*, 31–41. https://doi.org/10.1016/J.ECSS.2011.12.013

McAlister, J. A., & Orians, K. J. (2015). Dissolved gallium in the Beaufort Sea of the Western Arctic Ocean: A GEOTRACES cruise in the International Polar Year. *Marine Chemistry*, *177*, 101–109. https://doi.org/10.1016/j.marchem.2015.05.007

McClelland, J. W., Holmes, R. M., Peterson, B. J., & Stieglitz, M. (2004). Increasing river discharge in the Eurasian Arctic: Consideration of dams, permafrost thaw, and fires as potential agents of change. *Journal of Geophysical Research*, *109*(D18), D18102. https://doi.org/10.1029/2004JD004583

McClelland, J. W., Holmes, R. M., Peterson, B. J., Raymond, P. A., Striegl, R. G., Zhulidov, A. V., et al. (2016). Particulate organic carbon and nitrogen export from major Arctic rivers. *Global Biogeochemical Cycles*, *30*(5), 629–643. https://doi.org/10.1002/2015GB005351

McLaughlin, F. A., Carmack, E. C., Macdonald, R. W., & Bishop, J. K. B. (1996). Physical

and geochemical properties across the Atlantic/Pacific water mass front in the southern Canadian Basin. *Journal of Geophysical Research: Oceans*, *101*(C1), 1183–1197. https://doi.org/10.1029/95JC02634

Measures, C. I. (1999). The role of entrained sediments in sea ice in the distribution of aluminium and iron in the surface waters of the Arctic Ocean. *Marine Chemistry*, *68*(1–2), 59–70. https://doi.org/10.1016/S0304-4203(99)00065-1

Measures, C. I., Hatta, M., Fitzsimmons, J., & Morton, P. (2015). Dissolved Al in the zonal N Atlantic section of the US GEOTRACES 2010/2011 cruises and the importance of hydrothermal inputs. *Deep-Sea Research Part II: Topical Studies in Oceanography*, *116*, 176–186. https://doi.org/10.1016/j.dsr2.2014.07.006

Middag, R., de Baar, H. J. W., Laan, P., & Bakker, K. (2009). Dissolved aluminium and the silicon cycle in the Arctic Ocean. *Marine Chemistry*, *115*(3–4), 176–195. https://doi.org/10.1016/J.MARCHEM.2009.08.002

Middag, R., de Baar, H. J. W., Laan, P., & Klunder, M. B. (2011). Fluvial and hydrothermal input of manganese into the Arctic Ocean. *Geochimica et Cosmochimica Acta*, *75*(9), 2393–2408. https://doi.org/10.1016/J.GCA.2011.02.011

Middag, R., Séférian, R., Conway, T. M., John, S. G., Bruland, K. W., & de Baar, H. J. W. (2015). Intercomparison of dissolved trace elements at the Bermuda Atlantic Time Series station. *Marine Chemistry*, *177*, 476–489. https://doi.org/10.1016/j.marchem.2015.06.014

Middelboe, M., & Lundsgaard, C. (2003). Microbial activity in the Greenland Sea: Role of DOC lability, mineral nutrients and temperature. *Aquatic Microbial Ecology*, *32*(2), 151–163. https://doi.org/10.3354/ame032151

Millero, F., Woosley, R., DiTrolio, B., & Waters, J. (2009). Effect of Ocean Acidification on the Speciation of Metals in Seawater. *Oceanography*, *22*(4), 72–85. https://doi.org/10.5670/oceanog.2009.98

Moore, R. M. (1981). Oceanographic distributions of zinc, cadmium, copper and aluminium in waters of the central arctic. *Geochimica et Cosmochimica Acta*, *45*(12), 2475–2482. https://doi.org/10.1016/0016-7037(81)90099-5

Moran, M. A., Sheldon, W. M., & Zepp, R. G. (2000). Carbon loss and optical property changes during long-term photochemical and biological degradation of estuarine dissolved organic matter. *Limnology and Oceanography*, *45*(6), 1254–1264. https://doi.org/10.4319/lo.2000.45.6.1254

Morford, J. L., & Emerson, S. (1999). The geochemistry of redox sensitive trace metals in

sediments. *Geochimica et Cosmochimica Acta*, *63*(11–12), 1735–1750. https://doi.org/10.1016/S0016-7037(99)00126-X

Morison, J., Steele, M., Kikuchi, T., Falkner, K., & Smethie, W. (2006). Relaxation of central Arctic Ocean hydrography to pre-1990s climatology. *Geophysical Research Letters*, *33*(17), L17604. https://doi.org/10.1029/2006GL026826

Morison, J., Kwok, R., Peralta-Ferriz, C., Alkire, M., Rigor, I., Andersen, R., & Steele, M. (2012). Changing Arctic Ocean freshwater pathways. *Nature*, *481*(7379), 66–70. https://doi.org/10.1038/nature10705

Muench, R. D., Gunn, J. T., Whitledge, T. E., Schlosser, P., & Smethie, W. (2000). An Arctic Ocean cold core eddy. *Journal of Geophysical Research: Oceans*, *105*(C10), 23997–24006. https://doi.org/10.1029/2000jc000212

Murray, H., Meunier, G., Van Den Berg, C. M. G., Cave, R. R., & Stengel, D. B. (2014). Voltammetric characterisation of macroalgae-exuded organic ligands (L) in response to Cu and Zn: A source and stimuli for L. *Environmental Chemistry*, *11*(2), 100–113. https://doi.org/10.1071/EN13085

Mysak, L. A. (2001). Patterns of Arctic Circulation. *Science*, *293*(5533), 1269–1270.

Newton, B., Tremblay, L. B., Cane, M. A., & Schlosser, P. (2006). A simple model of the Arctic Ocean response to annular atmospheric modes. *Journal of Geophysical Research: Oceans*, *111*(9), C09019. https://doi.org/10.1029/2004JC002622

Newton, J. L., Aagaard, K., & Coachman, L. K. (1974). Baroclinic eddies in the Arctic Ocean. *Deep Sea Research and Oceanographic Abstracts*, *21*(9), 707–719. https://doi.org/10.1016/0011-7471(74)90078-3

Newton, R., Schlosser, P., Mortlock, R., Swift, J., & MacDonald, R. (2013). Canadian Basin freshwater sources and changes: Results from the 2005 Arctic Ocean Section. *Journal of Geophysical Research: Oceans*, *118*(4), 2133–2154. https://doi.org/10.1002/jgrc.20101

Newton, R., Pfirman, S., Tremblay, B., & DeRepentigny, P. (2017). Increasing transnational sea-ice exchange in a changing Arctic Ocean. *Earth's Future*, *5*(6), 633–647. https://doi.org/10.1002/2016EF000500

Nicolaus, M., Katlein, C., Maslanik, J., & Hendricks, S. (2012). Changes in Arctic sea ice result in increasing light transmittance and absorption. *Geophysical Research Letters*, *39*(24), 2012GL053738. https://doi.org/10.1029/2012GL053738

Nishimura, S., Kuma, K., Ishikawa, S., Omata, A., & Saitoh, S.-I. (2012). Iron, nutrients, and humic-type fluorescent dissolved organic matter in the northern Bering Sea shelf, Bering Strait, and Chukchi Sea. *Journal of Geophysical Research*, *117*(C02025), 1–13.

https://doi.org/10.1029/2011JC007355

Noble, A. E., Ohnemus, D. C., Hawco, N. J., Lam, P. J., & Saito, M. A. (2017). Coastal sources, sinks and strong organic complexation of dissolved cobalt within the US North Atlantic GEOTRACES transect GA03. *Biogeosciences*, *14*(11), 2715–2739. https://doi.org/10.5194/bg-14-2715-2017

Ober, S., Rijkenberg, M. J. A., & Gerringa, L. J. A. (2016a). Physical oceanography measured with ultra clean CTD/Water sampler-system during POLARSTERN cruise PS94 (ARK-XXIX/3). *Royal Netherlands Institute for Sea Research, Texel*. PANGEA. https://doi.org/10.1594/PANGAEA.859560

Ober, S., Rijkenberg, M. J. A., & Gerringa, L. J. A. (2016b, April 13). Physical oceanography measured on water bottle samples with ultra clean CTD/Water sampler-system during POLARSTERN cruise PS94 (ARK-XXIX/3). *Royal Netherlands Institute for Sea Research, Texel*. PANGAEA. https://doi.org/10.1594/PANGAEA.859561

Opsahl, S., Benner, R., & Amon, R. M. W. (1999). Major flux of terrigenous dissolved organic matter through the Arctic Ocean. *Limnology and Oceanography*, *44*(8), 2017–2023. https://doi.org/10.4319/lo.1999.44.8.2017

Orians, K. J., & Bruland, K. W. (1988). The marine geochemistry of dissolved gallium: A comparison with dissolved aluminum. *Geochimica et Cosmochimica Acta*, *52*(12), 2955–2962. https://doi.org/10.1016/0016-7037(88)90160-3

Orr, J. C., Epitalon, J. M., Dickson, A. G., & Gattuso, J. P. (2018). Routine uncertainty propagation for the marine carbon dioxide system. *Marine Chemistry*, *207*, 84–107. https://doi.org/10.1016/j.marchem.2018.10.006

Osborne, E., Richter-Menge, J., & Jeffries, M. (2018). *Arctic Report Card 2018*. Retrieved from https://www.arctic.noaa.gov/Report-Card

Outridge, P. M., Macdonald, R. W., Wang, F., Stern, G. A., & Dastoor, A. P. (2008). A mass balance inventory of mercury in the Arctic Ocean. *Environmental Chemistry*, *5*(2), 89. https://doi.org/10.1071/EN08002

Pasqualini, A., Schlosser, P., Newton, R., & Koffman, T. N. (2017). U.S. GEOTRACES Arctic Section Ocean Water Hydrogen and Oxygen Stable Isotope Analyses (Version 1.0) [Data set]. *Interdisciplinary Earth Data Alliance (IEDA)*. https://doi.org/https://doi.org/10.1594/ieda/100633

Pavlov, A. K., Granskog, M. A., Stedmon, C. A., Ivanov, B. V., Hudson, S. R., & Falk-Petersen, S. (2015). Contrasting optical properties of surface waters across the Fram Strait and its potential biological implications. *Journal of Marine Systems*, *143*, 62–72.

https://doi.org/10.1016/j.jmarsys.2014.11.001

Peterson, B. J., Holmes, R. M., McClelland, J. W., Vörösmarty, C. J., Lammers, R. B., Shiklomanov, A. I., et al. (2002). Increasing river discharge to the Arctic Ocean. *Science*, *298*(5601), 2171–2173. https://doi.org/10.1126/science.1077445

Pfirman, S. L., Kögeler, J. W., & Rigor, I. (1997). Potential for rapid transport of contaminants from the Kara Sea. *Science of The Total Environment*, *202*(1–3), 111–122. https://doi.org/10.1016/S0048-9697(97)00108-3

Pickart, R. S., Weingartner, T. J., Pratt, L. J., Zimmermann, S., & Torres, D. J. (2005). Flow of winter-transformed Pacific water into the Western Arctic. *Deep Sea Research Part II: Topical Studies in Oceanography*, *52*(24–26), 3175–3198. https://doi.org/10.1016/J.DSR2.2005.10.009

Pickart, R. S., Spall, M. A., & Mathis, J. T. (2013). Dynamics of upwelling in the Alaskan Beaufort Sea and associated shelf–basin fluxes. *Deep Sea Research Part I: Oceanographic Research Papers*, *76*, 35–51. https://doi.org/10.1016/J.DSR.2013.01.007

Planquette, H., & Sherrell, R. M. (2012). Sampling for particulate trace element determination using water sampling bottles: Methodology and comparison to in situ pumps. *Limnology and Oceanography: Methods*, *10*(5), 367–388. https://doi.org/10.4319/lom.2012.10.367

Pokrovsky, O. S., Manasypov, R. M., Loiko, S., Shirokova, L. S., Krickov, I. A., Pokrovsky, B. G., et al. (2015). Permafrost coverage, watershed area and season control of dissolved carbon and major elements in western Siberian rivers. *Biogeosciences*, *12*(21), 6301–6320. https://doi.org/10.5194/bg-12-6301-2015

Polyakov, I. V., Pnyushkov, A. V., Alkire, M. B., Ashik, I. M., Baumann, T. M., Carmack, E. C., et al. (2017). Greater role for Atlantic inflows on sea-ice loss in the Eurasian Basin of the Arctic Ocean. *Science*, *356*(6335), 285–291. https://doi.org/10.1126/SCIENCE.AAI8204

Porcelli, D., Andersson, P. S., Baskaran, M., Frank, M., Björk, G., & Semiletov, I. (2009). The distribution of neodymium isotopes in Arctic Ocean basins. *Geochimica et Cosmochimica Acta*, *73*(9), 2645–2659. https://doi.org/10.1016/J.GCA.2008.11.046

Proshutinsky, A. Y., & Johnson, M. A. (1997). Two circulation regimes of the wind-driven Arctic Ocean. *Journal of Geophysical Research: Oceans*, *102*(C6), 12493–12514. https://doi.org/10.1029/97JC00738

Proshutinsky, A. Y., Krishfield, R., Timmermans, M.-L., Toole, J., Carmack, E., McLaughlin, F., et al. (2009). Beaufort Gyre freshwater reservoir: State and variability

from observations. *Journal of Geophysical Research*, *114*, C00A10. https://doi.org/10.1029/2008JC005104

Pyle, K. M., Hendry, K. R., Sherrell, R. M., Legge, O., Hind, A. J., Bakker, D., et al. (2018). Oceanic fronts control the distribution of dissolved barium in the Southern Ocean. *Marine Chemistry*, *204*, 95–106. https://doi.org/10.1016/j.marchem.2018.07.002

Pyle, K. M., Hendry, K. R., Sherrell, R. M., Legge, O., Hind, A. J., Bakker, D., et al. (2019). Corrigendum to Oceanic fronts control the distribution of dissolved barium in the Southern Ocean. *Marine Chemistry*, *210*, 72. https://doi.org/10.1016/j.marchem.2018.09.004

Rabe, B., Karcher, M., Schauer, U., Toole, J. M., Krishfield, R. A., Pisarev, S., et al. (2011). An assessment of Arctic Ocean freshwater content changes from the 1990s to the 2006-2008 period. *Deep-Sea Research Part I: Oceanographic Research Papers*, *58*(2), 173–185. https://doi.org/10.1016/j.dsr.2010.12.002

Rabe, B., Karcher, M., Kauker, F., Schauer, U., Toole, J. M., Krishfield, R. A., et al. (2014). Arctic Ocean basin liquid freshwater storage trend 1992-2012. *Geophysical Research Letters*, *41*(3), 961–968. https://doi.org/10.1002/2013GL058121

Rabe, B., Schauer, U., Ober, S., Horn, M., Hoppmann, M., Korhonen, M., et al. (2016a, April 13). Physical oceanography during POLARSTERN cruise PS94 (ARK-XXIX/3). *Alfred Wegener Institute, Helmholtz Centre for Polar and Marine Research, Bremerhaven*. PANGAEA. https://doi.org/10.1594/PANGAEA.859558

Rabe, B., Schauer, U., Ober, S., Horn, M., Hoppmann, M., Korhonen, M., et al. (2016b, April 13). Physical oceanography measured on water bottle samples during POLARSTERN cruise PS94 (ARK-XXIX/3). *Alfred Wegener Institute, Helmholtz Centre for Polar and Marine Research, Bremerhaven*. PANGAEA. https://doi.org/10.1594/PANGAEA.859559

Raymond, P. A., McClelland, J. W., Holmes, R. M., Zhulidov, A. V., Mull, K., Peterson, B. J., et al. (2007). Flux and age of dissolved organic carbon exported to the Arctic Ocean: A carbon isotopic study of the five largest arctic rivers. *Global Biogeochemical Cycles*, *21*(4), GB4011. https://doi.org/10.1029/2007GB002934

Rigor, I. G., Wallace, J. M., & Colony, R. L. (2002). Response of Sea Ice to the Arctic Oscillation. *Journal of Climate*, *15*(18), 2648–2663. https://doi.org/10.1175/1520-0442(2002)015<2648:ROSITT>2.0.CO;2

Rijkenberg, M. J. A., Middag, R., Laan, P., Gerringa, L. J. A., van Aken, H. M., Schoemann, V., et al. (2014). The Distribution of Dissolved Iron in the West Atlantic Ocean. *PLoS*

ONE, *9*(6), e101323. https://doi.org/10.1371/journal.pone.0101323

Rijkenberg, M. J. A., Slagter, H. A., van der Loeff, M. R., van Ooijen, J., & Gerringa, L. J. A. (2018). Dissolved Fe in the deep and upper Arctic Ocean with a focus on Fe Limitation in the Nansen Basin. *Frontiers in Marine Science*, *5*, 88. https://doi.org/10.3389/fmars.2018.00088

Robinson, L. F., Noble, T. L., & McManus, J. F. (2008). Measurement of adsorbed and total 232Th/230Th ratios from marine sediments. *Chemical Geology*, *252*(3–4), 169–179. https://doi.org/10.1016/J.CHEMGEO.2008.02.015

Roeske, T., Bauch, D., Rutgers V.D. Loeff, M., & Rabe, B. (2012). Utility of dissolved barium in distinguishing North American from Eurasian runoff in the Arctic Ocean. *Marine Chemistry*, *132–133*, 1–14. https://doi.org/10.1016/J.MARCHEM.2012.01.007

Rudels, B. (2009). Arctic Ocean Circulation. *Encyclopedia of Ocean Sciences*, 211–225. https://doi.org/10.1016/B978-012374473-9.00601-9

Rudels, B. (2015). Arctic Ocean circulation, processes and water masses: A description of observations and ideas with focus on the period prior to the International Polar Year 2007-2009. *Progress in Oceanography*, *132*, 22–67. https://doi.org/10.1016/j.pocean.2013.11.006

Rudels, B., Larsson, A. M., & Sehlstedt, P. I. (1991). Stratification and water mass formation in the Arctic Ocean: some implications for the nutrient distribution. *Polar Research*, *10*(1), 19–32. https://doi.org/10.1111/j.1751-8369.1991.tb00631.x

Rudels, B., Jones, E. P., Anderson, L. G., & Kattner, G. (1994). On the Intermediate Depth Waters of the Arctic Ocean. In *The Polar Oceans and Their Role in Shaping the Global Environment* (Vol. 85, pp. 33–46). American Geophysical Union. https://doi.org/10.1029/gm085p0033

Rudnick, R. L., & Gao, S. (2003). Composition of the Continental Crust. In *Treatise on Geochemistry* (pp. 1–64). Pergamon. https://doi.org/10.1016/B0-08-043751-6/03016-4

Rutgers van der Loeff, M., Kühne, S., Wahsner, M., Höltzen, H., Frank, M., Ekwurzel, B., et al. (2003). 228Ra and226Ra in the Kara and Laptev seas. *Continental Shelf Research*, *23*(1), 113–124. https://doi.org/10.1016/S0278-4343(02)00169-3

Rutgers van der Loeff, M., Kipp, L., Charette, M. A., Moore, W. S., Black, E., Stimac, I., et al. (2018). Radium Isotopes Across the Arctic Ocean Show Time Scales of Water Mass Ventilation and Increasing Shelf Inputs. *Journal of Geophysical Research: Oceans*, *123*(7), 4853–4873. https://doi.org/10.1029/2018JC013888

Saito, M. A., & Goepfert, T. J. (2008). Zinc-cobalt colimitation of *Phaeocystis antarctica*.

Limnology and Oceanography, *53*(1), 266–275. https://doi.org/10.4319/lo.2008.53.1.0266

Schlitzer, R., Anderson, R. F., Dodas, E. M., Lohan, M., Geibert, W., Tagliabue, A., et al. (2018). The GEOTRACES Intermediate Data Product 2017. *Chemical Geology*, *493*, 210–223. https://doi.org/10.1016/J.CHEMGEO.2018.05.040

Schlosser, P., Bauch, D., Fairbanks, R., & Bönisch, G. (1994). Arctic river-runoff: mean residence time on the shelves and in the halocline. *Deep Sea Research Part I: Oceanographic Research Papers*, *41*(7), 1053–1068. https://doi.org/10.1016/0967-0637(94)90018-3

Schlosser, P., Newton, R., Ekwurzel, B., Khatiwala, S., Mortlock, R., & Fairbanks, R. (2002). Decrease of river runoff in the upper waters of the Eurasian Basin, Arctic Ocean, between 1991 and 1996: Evidence from δ18O data. *Geophysical Research Letters*, *29*(9), 3-1-3–4. https://doi.org/10.1029/2001gl013135

Scholz, F., Hensen, C., Noffke, A., Rohde, A., Liebetrau, V., & Wallmann, K. (2011). Early diagenesis of redox-sensitive trace metals in the Peru upwelling area – response to ENSO-related oxygen fluctuations in the water column. *Geochimica et Cosmochimica Acta*, *75*(22), 7257–7276. https://doi.org/10.1016/J.GCA.2011.08.007

Scholz, F., Siebert, C., Dale, A. W., & Frank, M. (2017). Intense molybdenum accumulation in sediments underneath a nitrogenous water column and implications for the reconstruction of paleo-redox conditions based on molybdenum isotopes. *Geochimica et Cosmochimica Acta*, *213*, 400–417. https://doi.org/10.1016/j.gca.2017.06.048

Schuster, P. F., Schaefer, K. M., Aiken, G. R., Antweiler, R. C., Dewild, J. F., Gryziec, J. D., et al. (2018). Permafrost Stores a Globally Significant Amount of Mercury. *Geophysical Research Letters*, *45*(3), 1463–1471. https://doi.org/10.1002/2017GL075571

Schuur, E. A. G., McGuire, A. D., Schädel, C., Grosse, G., Harden, J. W., Hayes, D. J., et al. (2015). Climate change and the permafrost carbon feedback. *Nature*, *520*, 171–179. https://doi.org/10.1038/nature14338

Semiletov, I., Pipko, I., Gustafsson, Ö., Anderson, L. G., Sergienko, V., Pugach, S., et al. (2016). Acidification of East Siberian Arctic Shelf waters through addition of freshwater and terrestrial carbon. *Nature Geoscience*, *9*(5), 361–365. https://doi.org/10.1038/ngeo2695

Serreze, M. C., & Barrett, A. P. (2011). Characteristics of the Beaufort Sea high. *Journal of Climate*, *24*(1), 159–182. https://doi.org/10.1175/2010JCLI3636.1

Serreze, M. C., Barrett, A. P., Slater, A. G., Woodgate, R. A., Aagaard, K., Lammers, R. B.,

et al. (2006). The large-scale freshwater cycle of the Arctic. *Journal of Geophysical Research: Oceans*, *111*(11), C11010. https://doi.org/10.1029/2005JC003424

Serreze, M. C., Holland, M. M., & Stroeve, J. (2007). Perspectives on the Arctic's shrinking sea-ice cover. *Science*, *315*(5818), 1533–6. https://doi.org/10.1126/science.1139426

Severmann, S., Johnson, C. M., Beard, B. L., & McManus, J. (2006). The effect of early diagenesis on the Fe isotope compositions of porewaters and authigenic minerals in continental margin sediments. *Geochimica et Cosmochimica Acta*, *70*(8), 2006–2022. https://doi.org/10.1016/J.GCA.2006.01.007

Severmann, S., McManus, J., Berelson, W. M., & Hammond, D. E. (2010). The continental shelf benthic iron flux and its isotope composition. *Geochimica et Cosmochimica Acta*, *74*(14), 3984–4004. https://doi.org/10.1016/J.GCA.2010.04.022

Shaw, T. J., Moore, W. S., Kloepfer, J., & Sochaski, M. A. (1998). The flux of barium to the coastal waters of the southeastern USA: the importance of submarine groundwater discharge. *Geochimica et Cosmochimica Acta*, *62*(18), 3047–3054. https://doi.org/10.1016/S0016-7037(98)00218-X

Shen, Y., Benner, R., Robbins, L. L., & Wynn, J. G. (2016). Sources, distributions, and dynamics of dissolved organic matter in the Canada and Makarov Basins. *Frontiers in Marine Science*, *3*, 198. https://doi.org/10.3389/fmars.2016.00198

Shiller, A. M. (1996). The effect of recycling traps and upwelling on estuarine chemical flux estimates. *Geochimica et Cosmochimica Acta*, *60*(17), 3177–3185. https://doi.org/10.1016/0016-7037(96)00159-7

Shiller, A. M. (1998). Dissolved gallium in the Atlantic Ocean. *Marine Chemistry*, *61*(1–2), 87–99. https://doi.org/10.1016/S0304-4203(98)00009-7

Shiller, A. M., & Frilot, D. M. (1996). The geochemistry of gallium relative to aluminum in Californian streams. *Geochimica et Cosmochimica Acta*, *60*(8), 1323–1328. https://doi.org/10.1016/0016-7037(96)00002-6

Sholkovitz, E. R. (1976). Flocculation of dissolved organic and inorganic matter during the mixing of river water and seawater. *Geochimica et Cosmochimica Acta*, *40*(7), 831–845. https://doi.org/10.1016/0016-7037(76)90035-1

Slagter, H. A., Reader, H. E., Rijkenberg, M. J. A., Rutgers van der Loeff, M., de Baar, H. J. W., & Gerringa, L. J. A. (2017). Organic Fe speciation in the Eurasian Basins of the Arctic Ocean and its relation to terrestrial DOM. *Marine Chemistry*, *197*, 11–25. https://doi.org/10.1016/J.MARCHEM.2017.10.005

Slagter, H. A., Laglera, L. M., Sukekava, C., & Gerringa, L. J. A. (2019). Fe-Binding

Organic Ligands in the Humic-Rich TransPolar Drift in the Surface Arctic Ocean Using Multiple Voltammetric Methods. *Journal of Geophysical Research: Oceans*, *124*(3), 1491–1508. https://doi.org/10.1029/2018JC014576

Soerensen, A. L., Jacob, D. J., Schartup, A. T., Fisher, J. A., Lehnherr, I., St Louis, V. L., et al. (2016). A mass budget for mercury and methylmercury in the Arctic Ocean. *Global Biogeochemical Cycles*, *30*(4), 560–575. https://doi.org/10.1002/2015GB005280

Sonke, J. E., & Heimbürger, L. E. (2012, July). Environmental science: Mercury in flux. *Nature Geoscience*. https://doi.org/10.1038/ngeo1508

Sonke, J. E., Teisserenc, R., Heimbürger-Boavida, L.-E., Petrova, M. V, Marusczak, N., Le Dantec, T., et al. (2018). Eurasian river spring flood observations support net Arctic Ocean mercury export to the atmosphere and Atlantic Ocean. *Proceedings of the National Academy of Sciences*, *115*(50), E11586–E11594. https://doi.org/10.1073/pnas.1811957115

Spencer, R. G. M., Mann, P. J., Dittmar, T., Eglinton, T. I., McIntyre, C., Holmes, R. M., et al. (2015). Detecting the signature of permafrost thaw in Arctic rivers. *Geophysical Research Letters*, *42*(8), 2830–2835. https://doi.org/10.1002/2015GL063498

Stedmon, C. A., Amon, R. M. W., Rinehart, A. J., & Walker, S. A. (2011). The supply and characteristics of colored dissolved organic matter (CDOM) in the Arctic Ocean: Pan Arctic trends and differences. *Marine Chemistry*, *124*(1–4), 108–118. https://doi.org/10.1016/J.MARCHEM.2010.12.007

Stedmon, C. A., Granskog, M. A., & Dodd, P. A. (2015). An approach to estimate the freshwater contribution from glacial melt and precipitation in East Greenland shelf waters using colored dissolved organic matter (CDOM). *Journal of Geophysical Research: Oceans*, *120*(2), 1107–1117. https://doi.org/10.1002/2014JC010501

Steele, M., Morison, J., Ermold, W., Rigor, I., & Ortmeyer, M. (2004). Circulation of summer Pacific halocline water in the Arctic Ocean. *Journal of Geophysical Research*, *109*(C2), C02027. https://doi.org/10.1029/2003JC002009

de Steur, L., Steele, M., Hansen, E., Morison, J., Polyakov, I., Olsen, S. M., et al. (2013). Hydrographic changes in the Lincoln Sea in the Arctic Ocean with focus on an upper ocean freshwater anomaly between 2007 and 2010. *Journal of Geophysical Research: Oceans*, *118*(9), 4699–4715. https://doi.org/10.1002/jgrc.20341

Stevenson, E. I., Fantle, M. S., Das, S. B., Williams, H. M., & Aciego, S. M. (2017). The iron isotopic composition of subglacial streams draining the Greenland ice sheet. *Geochimica et Cosmochimica Acta*, *213*, 237–254. https://doi.org/10.1016/J.GCA.2017.06.002

Stoffyn, M., & Mackenzie, F. T. (1982). Fate of dissolved aluminum in the oceans. *Marine Chemistry*, *11*(2), 105–127. https://doi.org/10.1016/0304-4203(82)90036-6

Tank, S. E., Raymond, P. A., Striegl, R. G., McClelland, J. W., Holmes, R. M., Fiske, G. J., & Peterson, B. J. (2012). A land-to-ocean perspective on the magnitude, source and implication of DIC flux from major Arctic rivers to the Arctic Ocean. *Global Biogeochemical Cycles*. https://doi.org/10.1029/2011GB004192

Tank, S. E., Striegl, R. G., McClelland, J. W., & Kokelj, S. V. (2016). Multi-decadal increases in dissolved organic carbon and alkalinity flux from the Mackenzie drainage basin to the Arctic Ocean. *Environmental Research Letters*, *11*(5), 054015. https://doi.org/10.1088/1748-9326/11/5/054015

Torres-Valdés, S., Tsubouchi, T., Bacon, S., Naveira-Garabato, A. C., Sanders, R., McLaughlin, F. A., et al. (2013). Export of nutrients from the Arctic Ocean. *Journal of Geophysical Research: Oceans*, *118*(4), 1625–1644. https://doi.org/10.1002/jgrc.20063

Trefry, J. H., & Metz, S. (1989). Role of hydrothermal precipitates in the geochemical cycling of vanadium. *Nature*, *342*(6249), 531–533. https://doi.org/10.1038/342531a0

Tréguer, P. J., & De La Rocha, C. L. (2013). The World Ocean Silica Cycle. *Annual Review of Marine Science*, *5*(1), 477–501. https://doi.org/10.1146/annurev-marine-121211-172346

Tremblay, J.-É., & Gagnon, J. (2009). The effects of irradiance and nutrient supply on the productivity of Arctic waters: a perspective on climate change. In *Influence of Climate Change on the Changing Arctic and Sub-Arctic Conditions* (pp. 73–93). Dordrecht: Springer Netherlands. https://doi.org/10.1007/978-1-4020-9460-6_7

Tria, J., Butler, E. C. V., Haddad, P. R., & Bowie, A. R. (2007). Determination of aluminium in natural water samples. *Analytica Chimica Acta*, *588*(2), 153–165. https://doi.org/10.1016/J.ACA.2007.02.048

Uher, G., Hughes, C., Henry, G., & Upstill-Goddard, R. C. (2001). Non-conservative mixing behavior of colored dissolved organic matter in a humic-rich, turbid estuary. *Geophysical Research Letters*, *28*(17), 3309–3312. https://doi.org/10.1029/2000GL012509

Ulfsbo, A., Jones, E. M., Casacuberta, N., Korhonen, M., Rabe, B., Karcher, M., & van Heuven, S. M. A. C. (2018). Rapid Changes in Anthropogenic Carbon Storage and Ocean Acidification in the Intermediate Layers of the Eurasian Arctic Ocean: 1996-2015. *Global Biogeochemical Cycles*, *32*(9), 1254–1275. https://doi.org/10.1029/2017GB005738

Valk, O., Rutgers van der Loeff, M. M., Geibert, W., Gdaniec, S., Moran, S. B., Lepore, K., et al. (2019). Circulation changes in the Amundsen Basin from 1991 to 2015 revealed from distributions of dissolved 230Th. *Ocean Science Discussions*, 1–27. https://doi.org/10.5194/os-2019-49

Vancoppenolle, M., Bopp, L., Madec, G., Dunne, J., Ilyina, T., Halloran, P. R., & Steiner, N. (2013). Future Arctic Ocean primary productivity from CMIP5 simulations: Uncertain outcome, but consistent mechanisms. *Global Biogeochemical Cycles*, *27*(3), 605–619. https://doi.org/10.1002/gbc.20055

Vieira, L. H., Achterberg, E. P., Scholten, J., Beck, A. J., Liebetrau, V., Mills, M. M., & Arrigo, K. R. (2019). Benthic fluxes of trace metals in the Chukchi Sea and their transport into the Arctic Ocean. *Marine Chemistry*, *208*, 43–55. https://doi.org/10.1016/j.marchem.2018.11.001

Walvoord, M. A., Voss, C. I., & Wellman, T. P. (2012). Influence of permafrost distribution on groundwater flow in the context of climate-driven permafrost thaw: Example from Yukon Flats Basin, Alaska, United States. *Water Resources Research*, *48*(7), W07524. https://doi.org/10.1029/2011WR011595

Wang, F., Macdonald, R. W., Armstrong, D. A., & Stern, G. A. (2012). Total and Methylated Mercury in the Beaufort Sea: The Role of Local and Recent Organic Remineralization. *Environmental Science & Technology*, *46*(21), 11821–11828. https://doi.org/10.1021/es302882d

Wang, K., Munson, K. M., Beaupré-Laperrière, A., Mucci, A., Macdonald, R. W., & Wang, F. (2018). Subsurface seawater methylmercury maximum explains biotic mercury concentrations in the Canadian Arctic. *Scientific Reports*, *8*(1), 14465. https://doi.org/10.1038/s41598-018-32760-0

Wehrli, B., & Stumm, W. (1989). Vanadyl in natural waters: Adsorption and hydrolysis promote oxygenation. *Geochimica et Cosmochimica Acta*, *53*(1), 69–77. https://doi.org/10.1016/0016-7037(89)90273-1

Wheeler, P. A., Watkins, J. M., & Hansing, R. L. (1997). Nutrients, organic carbon and organic nitrogen in the upper water column of the Arctic Ocean: implications for the sources of dissolved organic carbon. *Deep Sea Research Part II: Topical Studies in Oceanography*, *44*(8), 1571–1592. https://doi.org/10.1016/S0967-0645(97)00051-9

Whitmore, L. M., Morton, P. L., Twining, B. S., & Shiller, A. M. (2019). Vanadium cycling in the Western Arctic Ocean is influenced by shelf-basin connectivity. *Marine Chemistry*, *216*, 103701. https://doi.org/10.1016/j.marchem.2019.103701

Williams, W. J., & Carmack, E. C. (2015). The “interior” shelves of the Arctic Ocean: Physical oceanographic setting, climatology and effects of sea-ice retreat on cross-shelf exchange. *Progress in Oceanography*, *139*, 24–41. https://doi.org/10.1016/j.pocean.2015.07.008

Woodgate, R. A., Aagaard, K., & Weingartner, T. J. (2005). A year in the physical oceanography of the Chukchi Sea: Moored measurements from autumn 1990-1991. *Deep-Sea Research Part II: Topical Studies in Oceanography*, *52*(24–26), 3116–3149. https://doi.org/10.1016/j.dsr2.2005.10.016

Woosley, R. J., Millero, F. J., & Takahashi, T. (2017). Internal consistency of the inorganic carbon system in the Arctic Ocean. *Limnology and Oceanography: Methods*, *15*(10), 887–896. https://doi.org/10.1002/lom3.10208

Wynn, J. G., Robbins, L. L., & Anderson, L. G. (2016). Processes of multibathyal aragonite undersaturation in the Arctic Ocean. *Journal of Geophysical Research: Oceans*, *121*(11), 8248–8267. https://doi.org/10.1002/2016JC011696

Yamamoto-Kawai, M., McLaughlin, F. A., Carmack, E. C., Nishino, S., & Shimada, K. (2009). Aragonite undersaturation in the Arctic Ocean: effects of ocean acidification and sea ice melt. *Science*, *326*(5956), 1098–100. https://doi.org/10.1126/science.1174190

Yang, R., & Van Den Berg, C. M. G. (2009). Metal complexation by humic substances in seawater. *Environmental Science and Technology*, *43*(19), 7192–7197. https://doi.org/10.1021/es900173w

Yeats, P. A. (1988). Manganese, nickel, zinc and cadmium distributions at the Fram 3 and Cesar ice camps in the Arctic Ocean. *Oceanologica Acta*, *11*(4), 383–388. Retrieved from https://pdfs.semanticscholar.org/20b3/e00752ee569963853a95680e910268eeeee5.pdf?_ga=2.86163096.183395914.1563981265-1646889259.1563981265

Yeats, P. A., & Westerlund, S. (1991). Trace metal distributions at an Arctic Ocean ice island. *Marine Chemistry*, *33*(3), 261–277. https://doi.org/10.1016/0304-4203(91)90071-4

Zhang, R., John, S. G., Zhang, J., Ren, J., Wu, Y., Zhu, Z., et al. (2015). Transport and reaction of iron and iron stable isotopes in glacial meltwaters on Svalbard near Kongsfjorden: From rivers to estuary to ocean. *Earth and Planetary Science Letters*, *424*, 201–211. https://doi.org/10.1016/j.epsl.2015.05.031

Zhang, R., Jensen, L. T., Fitzsimmons, J. N., Sherrell, R. M., & John, S. (2019). Dissolved cadmium and cadmium stable isotopes in the western Arctic Ocean. *Geochimica et*

Cosmochimica Acta, *258*, 258–273. https://doi.org/10.1016/J.GCA.2019.05.028

Zhang, Y., Jacob, D. J., Dutkiewicz, S., Amos, H. M., Long, M. S., & Sunderland, E. M. (2015). Biogeochemical drivers of the fate of riverine mercury discharged to the global and Arctic oceans. *Global Biogeochemical Cycles*, *29*(6), 854–864. https://doi.org/10.1002/2015GB005124

Zimmermann, B., Porcelli, D., Frank, M., Andersson, P. S., Baskaran, M., Lee, D.-C., & Halliday, A. N. (2009). Hafnium isotopes in Arctic Ocean water. *Geochimica et Cosmochimica Acta*, *73*(11), 3218–3233. https://doi.org/10.1016/J.GCA.2009.02.028

Table 1. Endmember parameter values for the water mass analysis linear mixing model.

Water Mass	Salinity	$\delta^{18}O$ [‰]	Arctic N:P [a, b]
Atlantic Water	34.92	+0.3	0
Pacific Water	32.50	-1.1	1
Meteoric Water	0	-19	0
Sea-Ice Meltwater	4	Surf. + 2.6 ‰	Surface

(a) (Newton et al., 2013)

(b) Pacific Water: slope =14; intercept = -11; Atlantic Water: slope = 17; intercept = -2.

Table 2. Linear curve fit data and statistics for the TEI vs. meteoric water relationship plots.

Property	slope	y-int	r2	p
Alk [uM]	-14.1788	2365.40	0.53	0.000
CDOM [V]	0.0038	0.08	0.59	0.000
cFe (dFe-sFe) [nM]	0.0924	-0.83	0.88	0.000
d232Th [pM]	0.0941	-0.56	0.83	0.000
dAl [nM]	0.0501	0.55	0.23	0.093
dBa [nM]	1.1597	41.61	0.68	0.000
dCd [nM]	0.0117	0.05	0.66	0.000
dCo [pM]	7.9853	55.78	0.54	0.000
dCo_labile [pM]	2.6214	-19.11	0.61	0.008
dCu [nM]	0.2881	1.25	0.96	0.000
del_114Cd [permil]	0.0077	0.38	0.10	0.319
del_56Fe [permil]	0.0504	-0.82	0.51	0.009
del_66Zn [permil]	0.0220	0.08	0.14	0.227
dEr [pM]	0.2492	7.34	0.49	0.000
dFe [nM]	0.1960	-0.33	0.67	0.000
dGa [pM]	-0.3859	14.93	0.58	0.000
DIC [uM]	-11.4712	2240.12	0.43	0.000
dMn [nM]	0.1509	1.31	0.41	0.000
dNd [pM]	0.9532	24.73	0.54	0.000
dNi [nM]	0.2750	3.09	0.91	0.000
DOC [uM]	3.9774	52.91	0.88	0.000
dPb [nM]	-0.0005	0.01	0.59	0.000
dV [nM]	-0.6114	25.70	0.65	0.001
dZn [nM]	0.0525	0.28	0.36	0.001
total Hg [pM]	0.0061	1.15	0.01	0.600
total MeHg [pM]	-0.0055	0.16	0.28	0.007
Nitrate [uM]	-0.2432	4.97	0.48	0.000
pAl [nM]	-0.6779	23.08	0.01	0.521
pFe [nM]	-0.1068	4.96	0.01	0.613
Phosphate [uM]	0.0124	0.46	0.13	0.000
pMn [nM]	-0.0062	1.84	0.00	0.895
Ra226 [dpm/100L]	0.2523	5.79	0.49	0.000
Ra228 [dpm/100L]	0.9614	1.10	0.81	0.000
sFe (<0.02um) [nM]	0.1778	-1.22	0.79	0.000
Silicate [uM]	0.4576	3.35	0.30	0.000
POC	0.0188	0.20	0.18	0.342
d13C POC [permil]	0.0912	-31.10	0.04	0.665
p bSi [uM]	0.0027	-0.02	0.40	0.128

Table 3. Fluxes to the central Arctic Ocean in association with the Transpolar Drift. The endmember TEI concentrations are derived from the linear curve fits with meteoric water at a 20% meteoric water value.

Dissolved Species	Concentration*	Units	Flux (mol/y)	Error
Fe	3.6	nmol L^{-1}	1.0E+08	5.1E+07
Cu	7.0	nmol L^{-1}	2.0E+08	9.9E+07
Ni	8.6	nmol L^{-1}	2.4E+08	1.2E+08
^{232}Th	1.3	pmol L^{-1}	3.5E+04	1.8E+04
DOC	132	µmol L^{-1}	3.7E+15	1.9E+15
Nd	44	pmol L^{-1}	1.2E+06	6.2E+05

*at 20% meteoric water

Methods Appendix

The methods for TEIs already published can be found in the papers listed in Table A1 below. For the determination of DIC and TA concentrations, methods are previously published in Ulfsbo et al. (2018) and Woosley et al. (2017). However, the joint description of the two cruises and the uncertainty analysis was not previously discussed. The precision from replicate sample analyses was estimated to be better than 2 µmol L^{-1} for both DIC and TA during GN04 (Jones & Ulfsbo, 2017) and better than 2.5 µmol L^{-1} and 2 µmol L^{-1} for DIC and TA, respectively, during GN01 (Kadko et al., 2016). The accuracy of DIC and TA was determined by routine analyses of Certified Reference Materials (CRM) provided by A.G. Dickson, Scripps Institution of Oceanography, USA. Deep water (> 2000 m) mean concentrations for both cruises at the cross-over station (GN04-101 and GN01-31) agree within the uncertainty of the measurements. Uncertainty propagation for the carbonate system variables was performed according to Orr et al. (2018). Based on input variables from Table 1 of Orr et al. (2018) with two of the carbonate system parameters, the combined relative uncertainty for the third measured parameter was calculated using standard uncertainties in the dissociation constants and total boron to salinity ratio given by Orr et al. (2018). The propagated combined standard uncertainty was 3.3 µmol L^{-1}, 3.2 µmol L^{-1}, and 0.012 units for DIC, TA, and pH, respectively.

DOC was determined by high temperature combustion on a Shimadzu TOC-L, as described by Dickson et al. (2007). Consensus Reference Waters were analyzed as a regular check on the quality and reliability of the measurements (Hansell, 2005). The DOC measurements from both cruises (GN01 and GN04) were done in the same lab and were consistent at the crossover stations.

Fluorescent components of chromophoric DOM (CDOM) were measured in situ using two Dr. Haardt fluorometers with backscatter fluorescence sensors that excite at 350-460 nm and emit at 550 nm. The light source and settings in the two sensors were slightly different on the GN01 and GN04 cruises, so the two fluorometers were intercalibrated using a polynomial fit of the data collected at a crossover station to ensure comparability. The correlation coefficient for the polynomial function was r^2=0.994.

As noted in the Methods section, certain TEI data (dFe, dZn, dCd, dMn; Table A1) are presented as the average of data collected from multiple laboratories and different analytical methods (e.g. Flow Injection Analysis vs. Inductively Coupled Plasma Mass Spectrometry); therefore, the data for these TEIs used in this paper cannot be found on any of the online

databases. Please refer to the provided supplementary data file for the average values as well as the original data sources used to create the averages.

There was good agreement between the ^{228}Ra and ^{226}Ra measurements made on the GN01 and GN04 transects. At the crossover station, ^{228}Ra activities measured on GN04 were 14.9 ± 1.0 dpm $100L^{-1}$ at 10 m and those measured on GN01 were 16.2 ± 0.6 dpm $100L^{-1}$ and 17.2 ± 0.6 dpm $100L^{-1}$ at 2 m and 24 m, respectively. The ^{226}Ra activities measured at 10 m on GN04 were 9.1 ± 0.5 dpm $100L^{-1}$, while those measured on GN01 were 11.2 ± 0.2 dpm $100L^{-1}$ and 10.9 ± 0.4 dpm $100L^{-1}$ at 2 m and 24 m, respectively.

The REE data collected at the crossover station (stations HLY1502-30 and PS94-101) within 14 days compare well especially below 500 m water depth, where they are within 1 pmol L^{-1} for Nd and 0.5 pmol L^{-1} for Er. Given the typical analytical uncertainties of ±0.4 pmol L^{-1} for Nd and ±0.2 pmol L^{-1} for Er (GN04), the agreement between the two datasets is excellent. Moreover, both laboratories participated in a small inter-laboratory comparison of dissolved REE in seawater aliquots from 3000 m water depth at SAFe North Pacific station. The results of all four participating labs agreed within 3.3 % RSD for all REE except Ce, Gd, and Lu (Behrens et al., 2016).

The GN01 and GN04 Hg species data were intercalibrated at the crossover station. Total Hg concentrations agreed well for the majority of sampling depths. The tHg and MeHg data have been intercalibrated and validated by the GEOTRACES standards & intercalibration committee.

The GN01 and GN04 expeditions collected and analyzed thorium samples from the crossover station in the Makarov Basin and are well-intercalibrated with the exception of a few outliers, which are likely due to the uncertainty in ^{232}Th blank-corrections in the GN04 dataset. Th analyses were shared among 4 groups: LDEO and U. Minnesota for GN01, AWI (Valk et al., 2019) and LSCE (Gdaniec et al., 2020)for GN04. These 4 groups had participated in the GEOTRACES intercalibration exercise on Th isotopes (R. F. Anderson et al., 2012). A new intercalibration paper based on this Arctic work and focusing in particular on shallow samples is in preparation.

Table A1. References from which data was drawn for use in this TPD synthesis paper or from which methods were used to generate previously unpublished data. Refer to the publication for the sample handling and analytical methods pertaining to the TEI of interest.

TEI	Reference(s)
Hydrography, inorganic nutrients (NO_3^-, PO_4^{3-}, SiO_4)	(Cutter et al., 2014)
$\delta^{18}O$	(Pasqualini et al., 2017)
Total alkalinity, dissolved inorganic carbon	(Dickson et al., 2007; Kadko, Millero, et al., 2016)
DOC	(Hansell, 2005)
Ra isotopes	(Kipp et al., 2018, 2019; Rutgers van der Loeff et al., 2018)
dBa	(Ho et al., 2019; Jacquet et al., 2005)
POC, bSi, $\delta^{13}C$-POC	(Lam et al., 2018)
pFe, pAl, pmol L^{-1}n, pBa	(Lam et al., 2018; Planquette & Sherrell, 2012)
dFe (GN01 is average of Fitzsimmons, John & Hatta; PS94 is average of Gerringa ICP-MS and FIA analysis)	(Conway et al., 2013; Hatta et al., 2015; Jensen et al., 2019; Middag et al., 2015; Rijkenberg et al., 2014)
dMn (GN01 is average of Fitzsimmons & Hatta)	(Hatta et al., 2015; Jensen et al., 2019)
dCd, dZn (GN01 is average of Fitzsimmons & John)	(Conway et al., 2013; Jensen et al., 2019)
dNi, dCu, dPb	(Conway et al., 2013; Jensen et al., 2019; Middag et al., 2015)
Soluble and colloidal Fe ultrafiltration	(Fitzsimmons & Boyle, 2014; Hatta et al., 2015)
Fe-binding organic ligands	(Slagter et al., 2017)
dAl	(Measures et al., 2015)
dCo, LCo	(Hawco et al., 2016)
$\delta^{56}Fe$, $\delta^{66}Zn$, $\delta^{114}Cd$	(Conway et al., 2013)
dGa	(Ho et al., 2019)
dV	(Whitmore et al., 2019)

Hg species	(Agather et al., 2019; Heimbürger et al., 2015; Lamborg et al., 2012)
dNd, dEr	(Behrens et al., 2016)
^{232}Th	(Anderson et al., 2012)

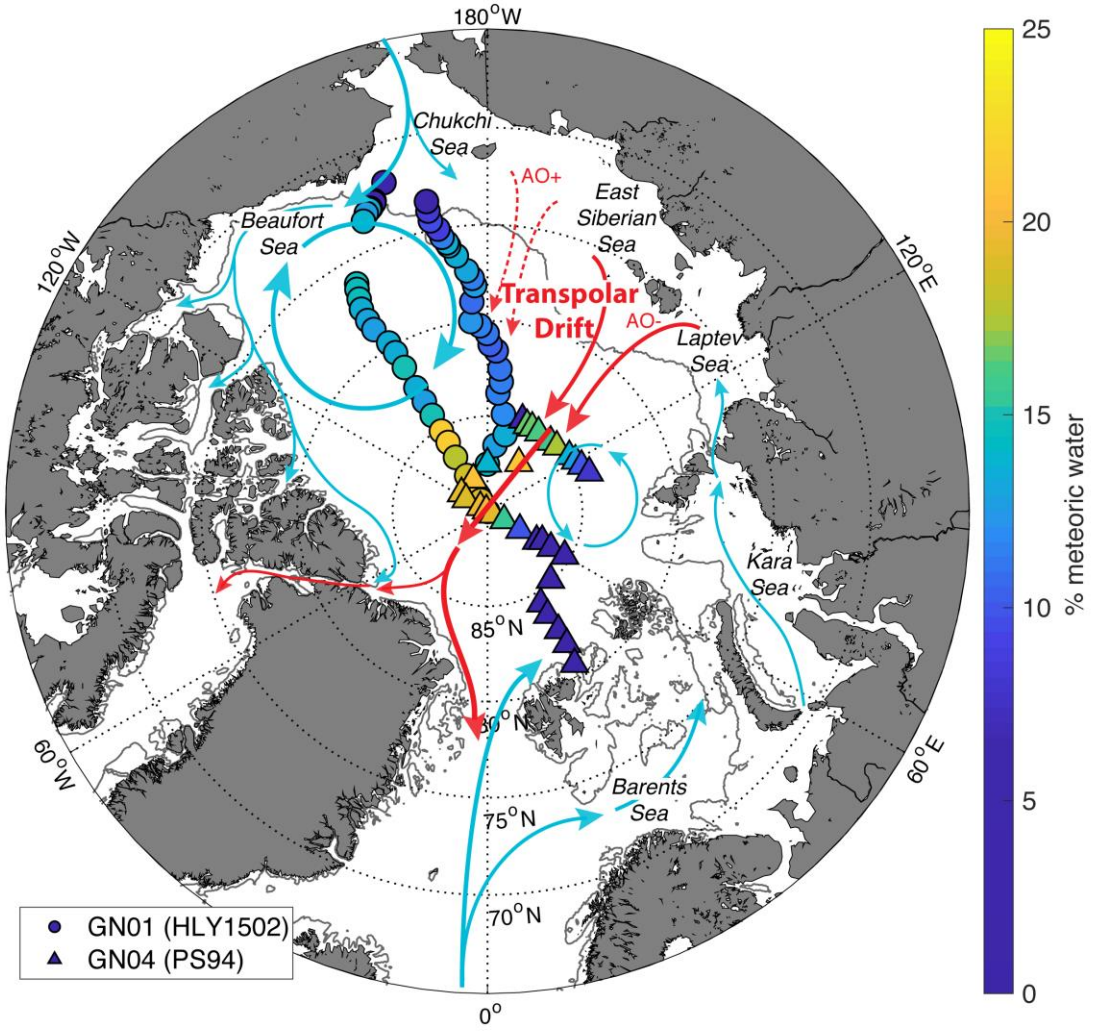

Figure 1. Map of the Arctic Ocean with the major upper ocean circulation features (blue arrows) as well as the Transpolar Drift (TPD; red arrows). The symbols indicate the station locations for the two GEOTRACES cruises GN01 (circles) and GN04 (triangles). The symbol colors denote the meteoric water fraction at each station. Also shown is the approximate location of the TPD origin for the positive (AO+) and negative (AO-) modes of the Arctic Oscillation (AO). The 200m isobath is shown in grey.

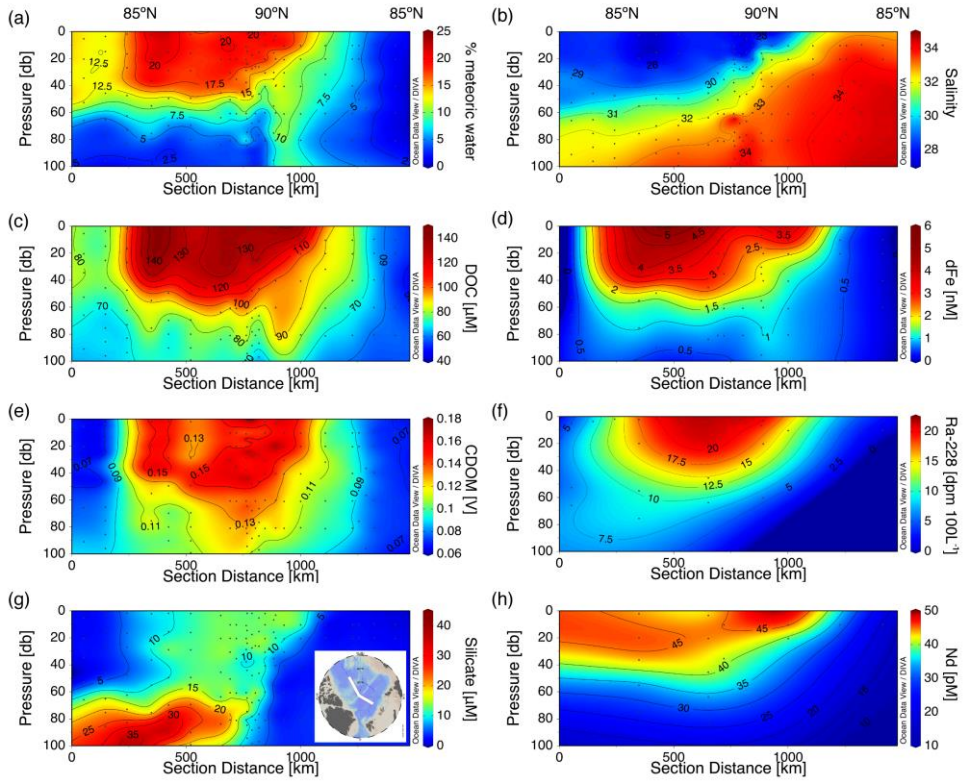

Figure 2. Section plots for key trace element and isotope concentrations along a transect that spans two GEOTRACES cruises and bisects the Transpolar Drift. The stations included in the contour plots is shown on the map inset for (g) and the distance is relative to a station located at 82°N, 150°W.

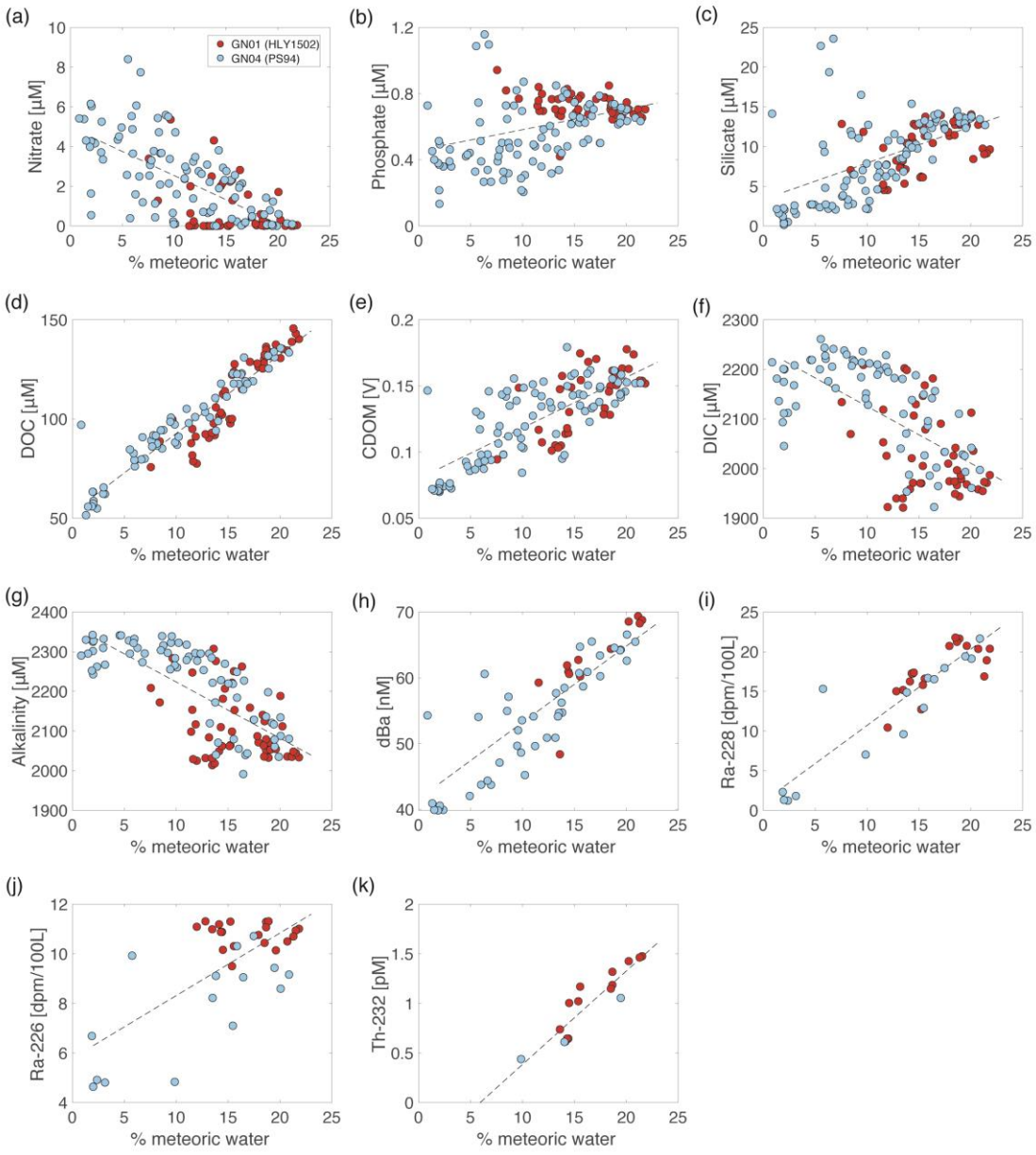

Figure 3. Trace element and isotope concentrations as a function of the meteoric water percentage at stations from the GEOTRACES GN01 (red circles) and GN04 (blue circles) cruises. Data are restricted to 0-50 m for stations north of 84°N. Regression lines are shown for variables with significant ($p<0.05$) relationships with meteoric water.

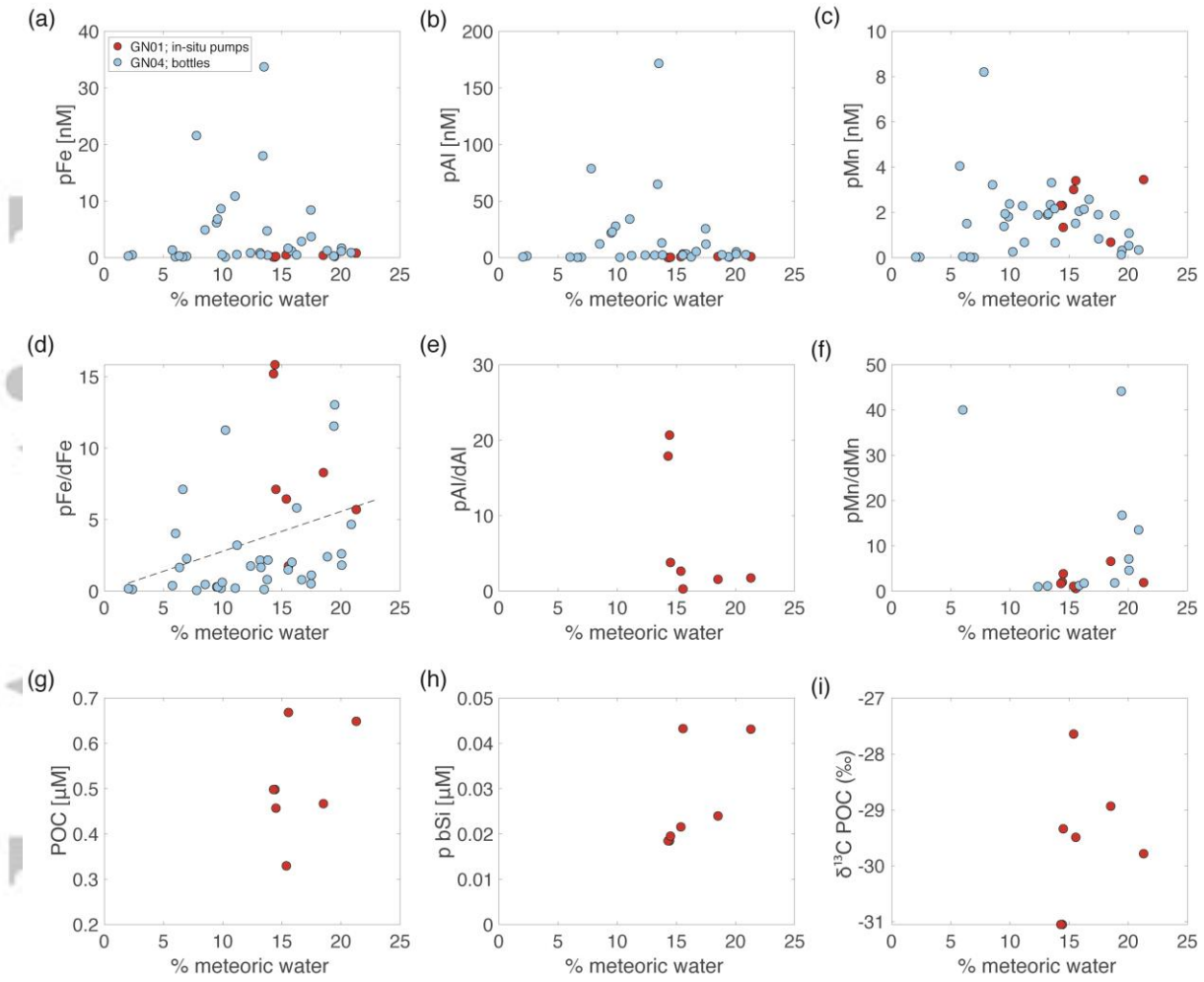

Figure 4. Particulate trace element and isotope concentrations as a function of the meteoric water percentage at stations from the GEOTRACES GN01 (red circles) and GN04 (blue circles) cruises. Data are restricted to 0-50 m for stations north of 84°N. The GN01 data are from the small size fraction (1-51 µm) in situ pump filters, while the GN04 samples were bottle collected on 0.45 µm filters. Regression lines are shown for variables with significant ($p<0.05$) relationships with meteoric water.

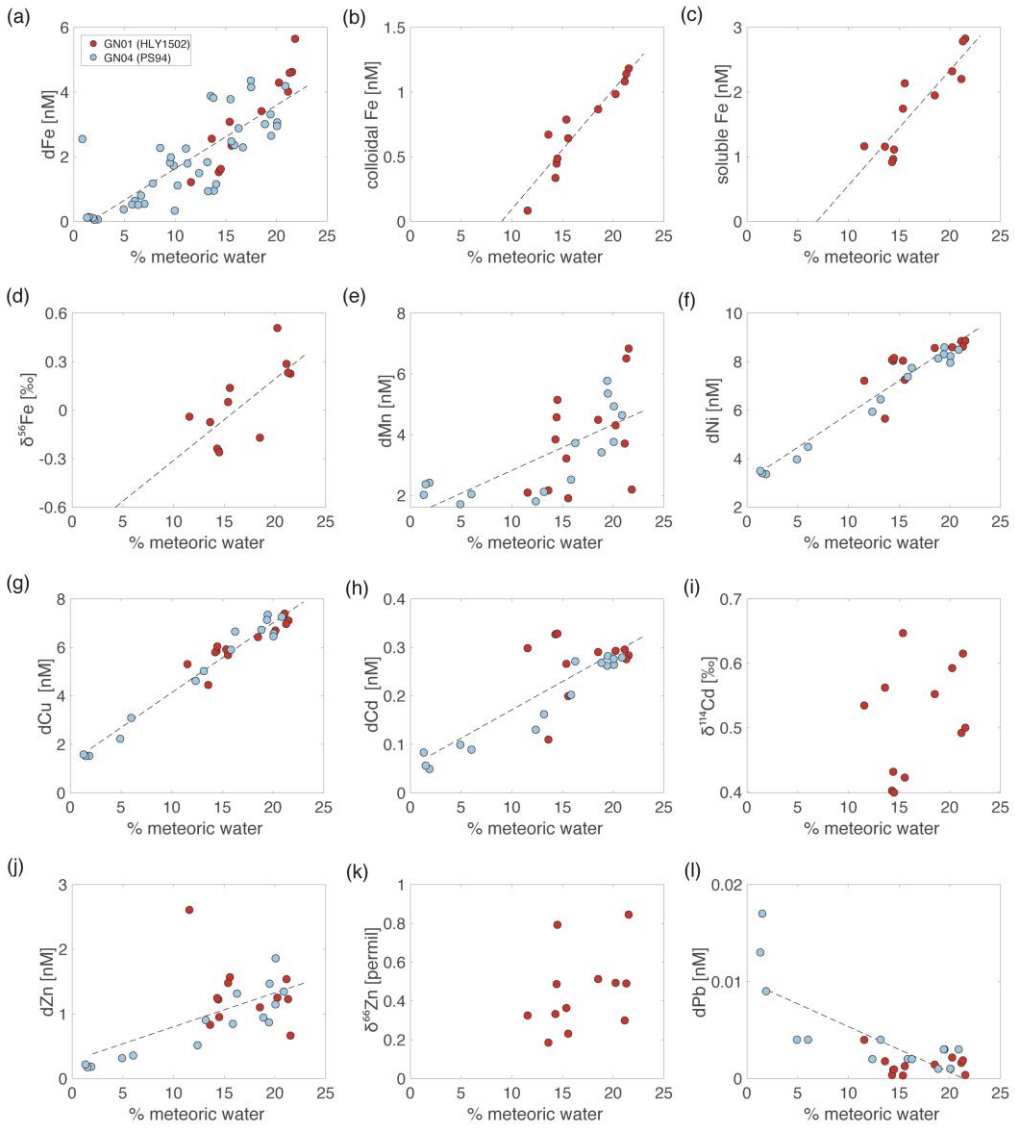

Figure 5. Trace element and isotope concentrations as a function of the meteoric water percentage at stations from the GEOTRACES GN01 (red circles) and GN04 (blue circles) cruises. Data are restricted to 0-50 m for stations north of 84°N. Regression lines are shown for variables with significant ($p<0.05$) relationships with meteoric water.

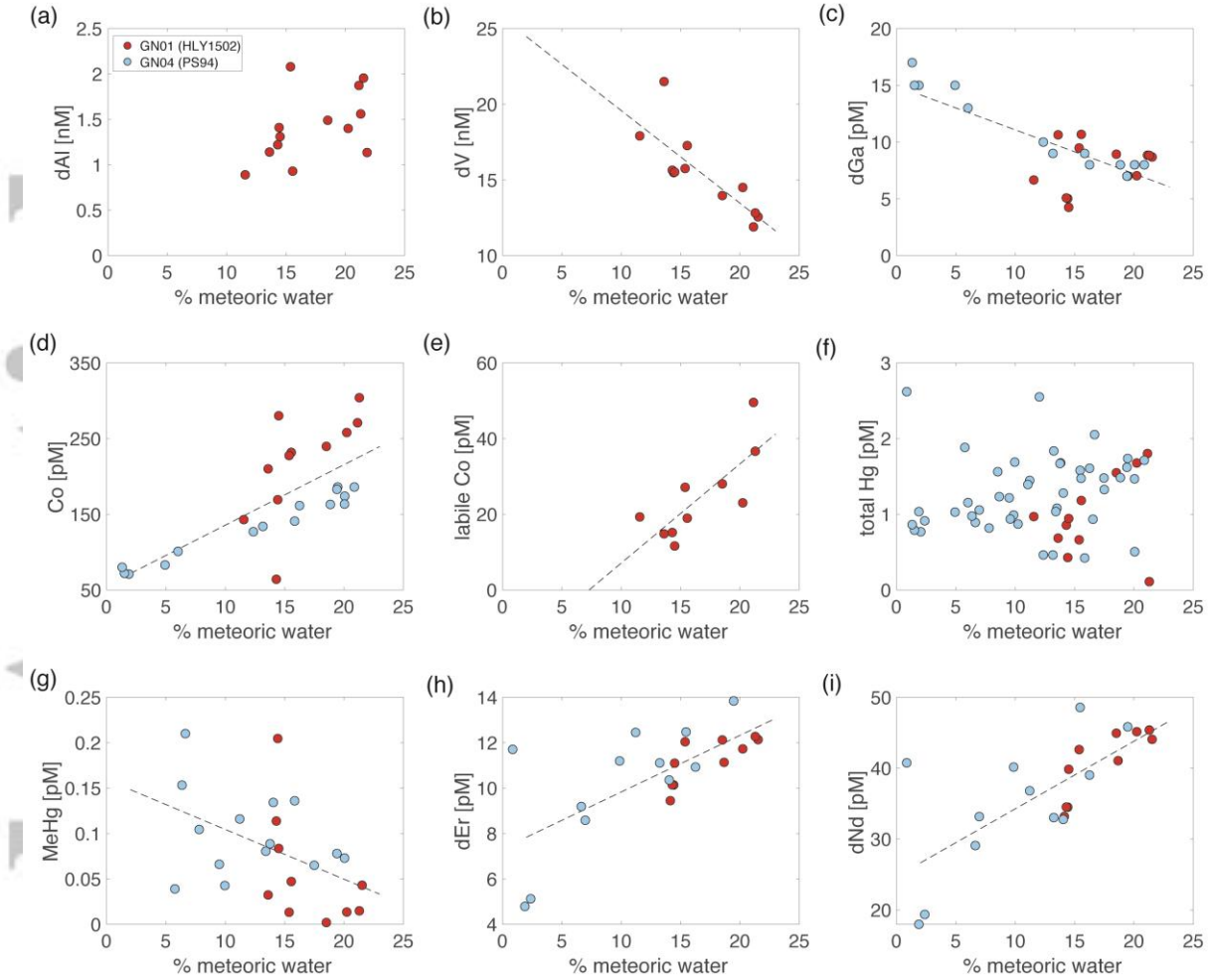

Figure 6. Trace element and isotope concentrations as a function of the meteoric water percentage at stations from the GEOTRACES GN01 (red circles) and GN04 (blue circles) cruises. Data are restricted to 0-50 m for stations north of 84°N. Regression lines are shown for variables with significant ($p<0.05$) relationships with meteoric water.

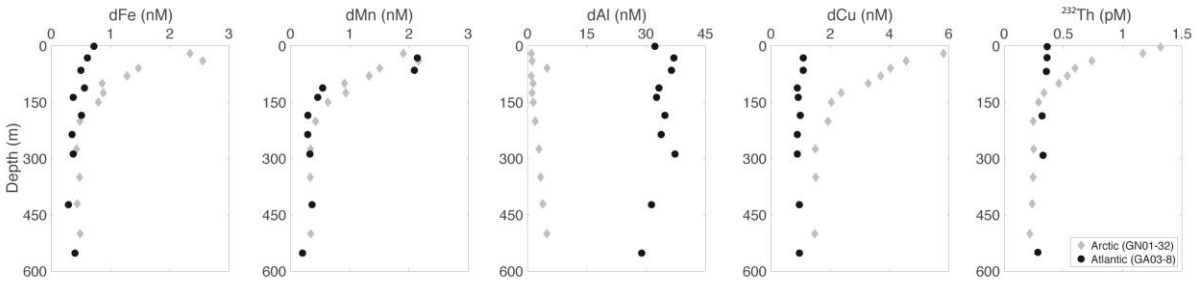

Figure 7. Surface to 600 m trace element and isotope concentration profiles for Arctic GEOTRACES GN01 station 32 (90°N; grey diamonds) as compared to Atlantic GEOTRACES GA03 station 8 (35.4°N, 66.5°W; black circles).